Manipulation of Composition, Morphology, and Surface Chemistry of Semiconductor Quantum Dots for Enhanced Photophysics

by

Barbara K. Hughes

B.A., Colorado State University, 2005

A thesis submitted to the

Faculty of the Graduate School of the

University of Colorado in partial fulfillment

of the requirements for the degree of

Doctor of Philosophy

Department of Chemistry and Biochemistry

This thesis entitled:

Manipulation of Composition, Morphology, and Surface Chemistry of Semiconductor Quantum Dots for Enhanced Photophysics

written by Barbara K. Hughes

has been approved for the Department of Chemistry and Biochemistry by

_____

Arthur J. Nozik

_____

David M. Jonas

Date: _____

The final copy of this thesis has been examined by the signatories, and we find that both the content and the form meet acceptable presentation standards of scholarly work in the above mentioned discipline.

Hughes, Barbara K. (Ph.D. Chemistry)

Manipulation of Composition, Morphology, and Surface Chemistry of Semiconductor Quantum Dots for Enhanced Photophysics

Thesis Directed by Professor Arthur J. Nozik and Professor David Jonas

Semiconductor quantum dots (QDs) are an interesting class of materials in that they exhibit unique physical properties when compared to their bulk counterparts. These unique properties and the breadth of tunability which they possess have made QD research a major field of study for more than 20 years for technologies such as catalysis, bio-imaging, solid-state lighting, and solar energy conversion. The primary concern for the application of semiconductor QDs in any field is not only to be able to precisely control physical properties (i.e., optical, electrical, magnetic) but also to understand how to achieve increased stability in these materials. A greater understanding of the chemistry of QD growth, surface construction, and composition are necessary to realize these goals. This thesis explores each of these areas of QD chemistry and the subsequent effects on their photophysical properties. Through manipulation of QD morphology, we have prepared PbSe QD dimers, which has allowed for a better understanding of electronic structure in quantum confined systems. Specifically we have observed a new absorption feature in the

1st exciton QD-dimer spectra, which we assign to a splitting of the 8-fold degenerate 1S level upon fusion of two monomer species. Surface treatment of PbSe QDs with a newly synthesized alkylselenide ligand has led to higher air stability, unique temperature dependent PL properties and the observation of a new surface-related trap level. Alongside producing more stable QDs, the nature of the strong $Pb_{surface}$ to Se-R bond may also have implications for affecting kinetic processes like carrier relaxation, which could facilitate production of materials that show enhanced multiple exciton generation (MEG) yields. Finally, substitutional doping of PbSe QDs has allowed for modulation of QD compositions and in turn tuning of the dominant carrier type in both solution and in QD films. Although just a small contribution to the larger reservoir of work in this area, these results provide promise for improving stability and efficiency of QD devices for solar energy conversion.

To my parents, for bringing me into this world and giving endless love and support.

Acknowledgements

First and foremost I'd like to thank you Art for allowing/encouraging me to finish my PhD in your group. After I left Berkeley, I was certain that I was finished with graduate school, but this has been one of the best decisions of my life, and I appreciate the encouragement that I've received from both you and your lovely wife Rhoda. I feel so lucky to have had the opportunity to work in your group, and to know you. To Mr. B (a.k.a. the Beard, a.k.a. Matt Beard): Working with you for the last 6 years has been such a blessing! I have been very lucky to work for someone who is not only intelligent and creative, but who also has such a big heart. Research is tough and pretty much makes you want to quit on a daily basis, but your door was always open, and you were there to help me work through things. Thank you for helping me to achieve my goals, for setting your expectations high for me, and for pushing me to reach my full potential.

To Justin Johnson (JJ), Joey Luther (Joseph), Jeff Blackburn (Jeffrey's), and Dan Ruddy (DRudd): I can't believe I was allowed to have so many wonderful mentors! You have each contributed so greatly to making my experience in grad school amazing and to making me a better scientist through your support and guidance. I'd like to thank each of you for your advice and friendship. Encyclopedia JJ, I think your random knowledge of EVERYTHING might just rival The Google! You've pretty much picked me up out of every rut, pep talked me through every trial, and commiserated with me about every experiment that has ever gone awry for the last 6 years. I want to be just like you when I grow up! Joseph! Thank you for selflessly giving of your time in lab, in editing papers, and in listening to me gripe on our long runs. And thank you for allowing me to hone in my vegan baking

skills…that kind of knowledge is priceless. Jeffrey's, you're my go-to guy for beer and chocolate…enough said.

To the rest of the my grad school buddies and QD group, especially Hazmatt, Kevo, Rebs, Crispy, Mr. Midgett, and Tavo, I love you guys dearly, and you made each and every day better. Also I 'd like to give a little shout out to PV Power, the best softball team in Arvada, CO (that is for co-ed, lower division, softball), but the best nevertheless!

Finally to the padres, my support and my best friends: Thank you guys for being the best! In my whole life, I only strive to have a heart as big as yours, patience as endless, and faith as strong as you both have shown me, my whole life. Your belief in me has never let me fail, even when I have had very little myself. Thank you, and I love you forever. Pj-ster Dj-ster, don't think I forgot about the best brother in the world…love your guts too!

Contents

Chapter 3: Control of PbSe Quantum Dot Surface Chemistry and Photophysics Using an Alkylselenide Ligand

Chapter 4: Electronic Impurity Doping of PbSe QDs

Chapter 5 Conclusions

Tables

Figures

Chapter 1:
Introduction

1.I. Semiconductor Quantum Dots

Semiconductor quantum structures are inorganic nanocrystals (NCs) composed of a few thousand atoms or less that experience quantum confinement in at least one dimension. That is to say, a quantum confined nanostructure approaches and then becomes smaller than the exciton Bohr radius, a natural length scale that characterizes the average separation between electrons and holes in a bulk semiconductor. Quantum dots (QDs) are inorganic nanocrystals that experience quantum confinement in 3-dimensions, quantum rods (QRs) in -2 dimensions, and quantum plates or sheets experience confinement in only one dimension. As a result of quantum confinement, semiconductor NCs show electronic structure somewhere intermediate between molecules and bulk semiconductors and can exhibit dramatic size-dependent properties. These materials characteristics have made semiconductor quantum dots an intense area of research for more than a decade for chemists, physicists, and materials scientists alike.

Nanoscale colloidal semiconductor structures, with at least one dimension small enough to experience quantum confinement-effects, have captured the imagination and

attention of scientists interested in controlling various chemical and photophysical processes. Aside from desirable quantum confinement properties, colloidal nanocrystals are attractive because they are often synthesized in a low-temperature, low-cost and potentially easily scalable manner using a simple bench-top reaction bath. Considerable progress in producing a variety of shapes, compositions, and complex structures has been achieved. However, there are challenges to overcome in order for these novel materials to gain their full potential and become a new driver for industrial applications. The final shape, composition, nanocrystal-ligand structure, and size can depend on a delicate interplay of precursors, surface ligands, and other compounds that may or may not participate in the reaction. In this thesis, a detailed description of our efforts to better understand how to manipulate composition, morphology, and surface chemistry of PbSe semiconductor quantum dots will be discussed as well as the observed effects on photophysical properties.

1.II. The Subtle Chemistry of Colloidal, Quantum-Confined Semiconductor Nanostructures

'Bottom-up' nanocrystals and nanostructures offer numerous advantages over their bulk and thin film counterparts, such as higher and tunable catalytic activity, control over bandgap and energy levels, and favorable excited-state carrier relaxation dynamics. Perhaps their greatest advantage is the prospect of synthesizing complex nanostructures that have tailored and synergistic properties employing simple bench top synthetic

methods. This work will focus primarily on how these materials can be manipulated synthetically to exploit these desirable properties. In order for quantum confined nanostructures to have the largest technological impact, we must continually seek to move beyond basic challenges of reproducibility and growth mechanisms to a deeper understanding of obtaining precise control over nanocrystal formation that will enable further engineering of nanostructures with unique and desirable properties. There are, therefore, research opportunities with regard to achieving fine control over nanocrystal monodispersity, structure, composition, and defects related to surface states. In the following chapters, efforts to control morphology (PbSe QD dimers), ligand-quantum dot structure (novel surface ligands), and QD composition (doping of PbSe QDs) will be presented. A brief discussion of the state-of-art in understanding how synthetic precursors can be manipulated to effect such change is warranted here.

Currently, there are three major solution-based approaches to synthesize semiconductor nanostructures: hot injection,[1] the heating-up method, [2,3] and the reduction method. [3-5] Inherent to each of these methodologies is a certain amount of parameter space that can be explored and manipulated not only in the form of reaction conditions, but also important are elemental and molecular precursors, solvents, terminating ligands and even chemical impurities which have been shown to play an important role in the end product. [5,6] These synthetic "knobs," when turned, allow for distinct control over composition and architecture, though they are at times subtle and their mechanisms not fully understood.

The crystalline and thus faceted nature of nanocrystals opens a door to controlled nanoparticle shape design mediated through surface ligand protecting groups, which

energetically favor particular surface facets. [7,8] Surface ligands aid in stabilizing and isolating nanoparticles in aqueous or organic solvents, acting to reduce the surface energies through bonding, in most cases, with surface metals to reduce surface charge. The ligand-nanoparticle interface is highly dynamic and its structure depends on temperature, binding strength of ligand functional groups to the nanocrystal surface, as well as factors, such as, steric hindrance, and ligand-solvent interactions. Even at room temperature, ligands are in dynamic equilibrium between bound and unbound states as surface-bound ligands continually exchange with neutral ligands with a rate that is inversely proportional to the binding strength, and increases substantially as heat is applied to the system. During nanoparticle growth, kinetics can dominate over thermodynamics, and therefore, the binding strength, and thus, the time constant at which ligands self-exchange at the surface affects the growth rates of individual facets. Surfaces to which ligands are strongly bound exhibit hindered growth in their respective crystal directions. As a result, the addition of various surface selective ligands to the reaction mixture alters growth kinetics along different axes, allowing for nanocrystal shape control. This kind of ligand-assisted shape control has been exploited in CdSe nanostructures where strongly binding ligands, such as alkyl phosphonic acids, allow for well-controlled nanoscale dimensions in CdSe rods, whereas with alkyl phosphonic oxides alone, large, irregularly-shaped rods result. [9]

A wealth of unique properties result from such shape control in nanostructures, however, in many cases the precise application of these anisotropic shaped nanostructures are still to be uncovered and exploited. One particular application that has seen many beneficial attributes from quasi 1-D (i.e. “rod-like”) nanocrystals is solar photoconversion.

For photovoltaics (electricity from sunlight), nanorods of CdSe show improved electron transport properties compared to spherical crystals in solar cells where the nanocrystals are blended with light-absorbing, hole-conducting polymers. [10] For photoelectrochemistry (chemical fuels from sunlight), complex heterostructured nanorods consisting of a small CdSe QD embedded in a CdS nanorod with a Pt catalyst grown on the tip, provide the unique advantage of being able to control the separation distance between the photogenerated electron and hole by changing the rod length. [11] Another enticing avenue of research involves exploring the phenomenon of multiple exciton generation (MEG) as a function of nanocrystal shape. MEG has shown to benefit not only from quantum confinement (QDs more efficiently undergo MEG than bulk crystals),[12] but further enhancement is also observed upon 1-D shape manipulation. [13]Enhancement of MEG in 1-D structures occurs due to the larger Coulomb interaction in anisotropic systems over isotropic structures.[14] Further increases in the MEG efficiency are needed to have the largest impact on solar photoconversion, and shape control may be a critical 'knob' for enhancing this process.

The high level of complexity achieved for CdX (X=S, Se, Te) has allowed researchers to build an arsenal of tools for creating unique nanostructures, and these tools have in turn been used as a basis for synthetic shape control in other material systems. However, the same techniques do not always translate, and shape control has become a new challenge in systems with greater symmetry such as the rock salt crystal lattice. The lead chalcogenides, which will be the focus of this work, serve as a particularly good model system for understanding unique quantum confinement effects because they possess very large bulk

Bohr exciton radii, thus are under extreme confinement when their dimensions are reduced to less than 20 nm.[15] For example, although bulk PbSe has a bandgap of 0.279 eV, high quality nanocrystals of PbSe are easily synthesized which can exhibit a bandgap as high as 2.0 eV. Unlike the II-VI materials, however; where a unique crystallographic direction lends itself to a high level of structural complexity, the crystal structure of the Pb-chalcogenides is highly symmetric, and thus symmetrically shaped crystals (quasi-spherical to cube-like crystals) are favored during growth. For the IV-VI materials, not only do ligand-QD interactions play a role in deliberate shape control, but also QD-QD, ligand-ligand, and ligand-solvent interactions are likely important factors that must be considered.

In much the same way that ligand-assisted shape control can be achieved in the II-VI system, the surface growth in PbX salts can likewise be tuned. For instance, selective strong binding of aliphatic primary amines to the {111}[16] facets of PbSe leads to the formation of octahedral particles due to growth of the {100} faces.[17] Amines also play an important role in the formation of PbSe 1-D structures. Koh et al. find that incorporating tris(diethylamino) phosphine selenide in place of TOP-Se, but otherwise under similar reaction conditions produced 1-D structures rather than isotropic structures.[18] While the role of the amine is unclear it likely plays a role in hindering growth in certain crystal directions. However, the kinetics and mechanism must be quite different than in the CdSe system, as simply blocking one face over another will not lead to anisotropic growth in the isotropic PbSe system. Therefore, the mechanism must include some component of QD-QD or ligand-ligand interaction that is generally termed ‘oriented attachment’.

In the oriented attachment mechanism, isotropic QDs form first and then fuse along a specific crystallographic direction during the reaction, which has been recorded in real-time by Yuk et al. with Pt nanocrystals.[19] Oriented attachment is quite distinct from continued growth along a specific crystallographic axis and is a powerful tool that has been invoked in the preparation of complex PbSe structures such as nanowires, rings, and other complex anisotropic structures. Oriented attachment will be discussed in greater detail in Chapter 2.

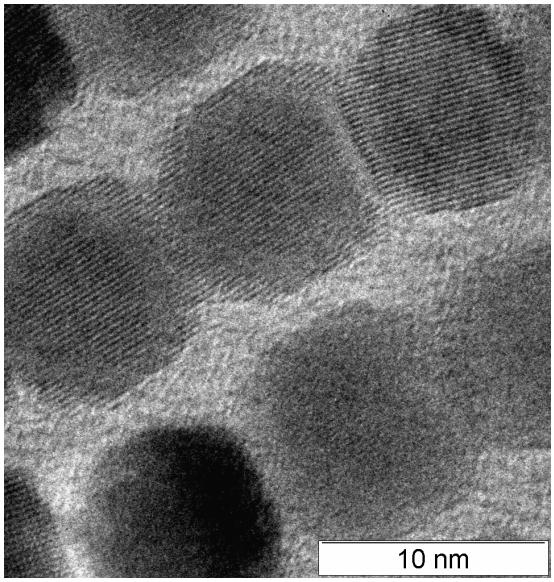

Figure 1.1. Strings of PbSe "pearls"
The early stages of PbSe nanowire formation showing oriented attachment of individual QDs along a single axis. In this way, nanoparticles with rocksalt crystal structures can form elongated structures. Particles will eventually fuse and exhibit continuous lattice fringes.

Just as changing QD size and morphology can affect electrical and optical properties, likewise adjustments to composition and the innate QD stoichiometry can have significant consequences. Chemical doping of semiconductor QDs, as in their bulk counterparts, could

lead to better control over many desirable electrical and optical properties such as photoluminescence quantum yields, charge-carrier mobilities for QD-films, and enhanced MEG. QD doping can be achieved though both control of the QD stoichiometry and through intentional impurity doping of colloidal QDs The stoichiometry and the introduction of dopant atoms can be tailored by post-introduction of the desired dopant or surface atoms. In Chapter 3, it is shown that the elemental composition of PbSe quantum dots can be altered via surface modifications in order to produce a more anion-rich QD. Here, the effects of introducing a novel surface ligand on shape, composition and photophysics will be discussed. Finally, in Chapter 4, a study will be presented on the more traditional route towards QD doping, through the addition of electronic impurity atoms.

1.III. Optical Properties of PbSe QDs

In this section, an overview of the relevant optical properties for quasi-spherical PbSe QDs is provided. More in-depth discussions can be found in the various references cited throughout this thesis. Here, we follow and use the notation of Bartnik et al.[20] and Kang and Wise.[21] In bulk PbSe, valence band maxima and conduction band minimum occur at 4 equivalent L points in the first Brillouin zone. Therefore, neglecting spin, these states are 4-fold degenerate. From a molecular viewpoint, states near the valence band maximum consists primarily of Se-p orbitals with minor contribution from Pb-s, while the conduction band has Pb-p character with minor contribution from Se-s orbitals. Kang and Wise applied a four band **k.p** approximation to describe the electronic wavefunctions

within PbSe and PbS QDs, where the band structure near the L-point was considered to be isotropic. [21] Tudury et al. incorporated the anisotropy at the L point for PbSe and PbTe QDs within this **k.p** approximation. [22] Later, this theory was extended to PbSe quantum rods by Bartnik et al. [20] The states are labeled as nL_J^{π}, where n is the primary quantum number, L is the orbital angular momentum, while J is the total angular momentum, and π is the parity. The states are labeled according to their orbital angular momentum as S(L=0), P(L=1), D(L=2), etc.

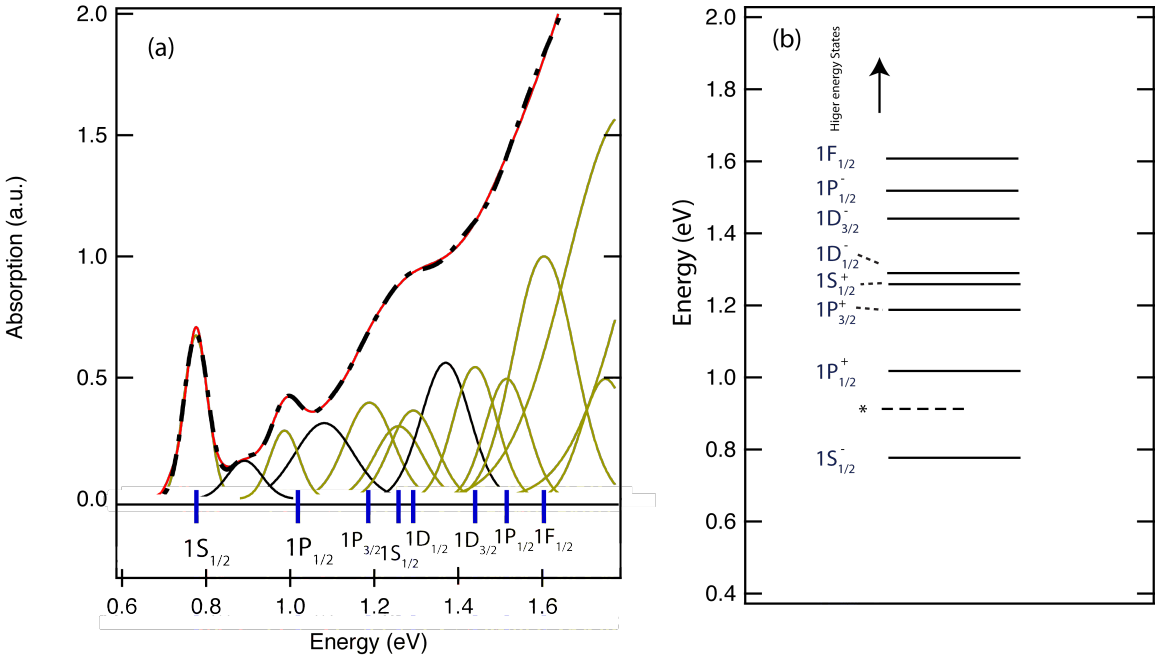

Figure 1.2. Optical Density of PbSe QDs and Observed Transitions
(a) Optical density of PbSe QDs with first exciton absorption at 0.777 eV. The red-dashed line is a best fit of a sum of Gaussians with center positions given by the Bartnik et al. transitions (blue lines). The green/tan lines are for the Bartnik et al. centered transitions while the black lines are apparent transitions not identified as exciton transitions, but are included here to improve the modeling (one such transition is marked with an a* in Figure b). **(b)** Optical transitions for PbSe QDs.

Figure 1.2a displays a typical absorption spectrum of PbSe QDs with $1S_{1/2}$ transition ($1S_h$ to $1S_e$) at 0.78 eV. Three clear features are seen in the spectra. Employing typical spectral deconvolution techniques, in this case using a combination of 2nd derivative analysis and non-linear least squares fitting, 8 distinct features can be clearly identified. These states have been assigned to various excitonic transitions (shown in Fig 1.2b). A sum of Gaussian functions is used to model the data. A Gaussian function is centered on a transition determined from Bartnik et al. and is incorporated with the linewidth of each transition held to be the same. Three Gaussians (black lines) were added to improve the model, however, because they are not obviously associated with exciton transitions, their origin is not yet clear and may warrant further investigation beyond the scope of this thesis. The fit also reproduces the second derivative of the absorption spectra (red-dashed line). A complete discussion and description of the optical selection rules can be found elsewhere and will not be reproduced here. [20,21,23,24] The first three transitions are important for this presentation and consist of the $1S^h_{1/2} - 1S^e_{1/2}$, and the $1P^h_{1/2} - 1P^e_{1/2}$ which is split by the band anisotropy from the $1P^h_{3/2} - 1P^e_{3/2}$.

1.IV. Sizing Curve and Size-distribution

In Figure. 1.3 a series of absorption spectra for various sizes of PbSe QDs is shown (data has been offset in the vertical direction for clarity). The relationship between the size of the QD and the lowest energy transition (labeled here as the $1S_{1/2}$) has been reported to be

$$E_{S_{1/2}} = 0.278 + \frac{1}{0.016d^2+0.209d+0.45} \qquad [1.1]$$

by Moreels and co-workers, where d is the QD diameter. [25] In our laboratory we have verified, via TEM analysis, Equation 1.1 and it is shown in Figure 1.3 as the red-dashed line, with the squares being determined by TEM and UV-vis spectroscopy. As seen in Figure 1.3, the bandgap of semiconductor QDs is highly sensitive to changes in QD diameter or the number of atoms that compose the QD. A significant decrease in the first energy transition is observed for only a 3 Å difference in diameter, giving QD size measurement essentially monolayer sensitivity. In light of these results, it is easy to see how optical properties can readily be manipulated using materials engineering. Changing the structure, morphology and chemical composition can all be employed to achieve desirable optical properties.

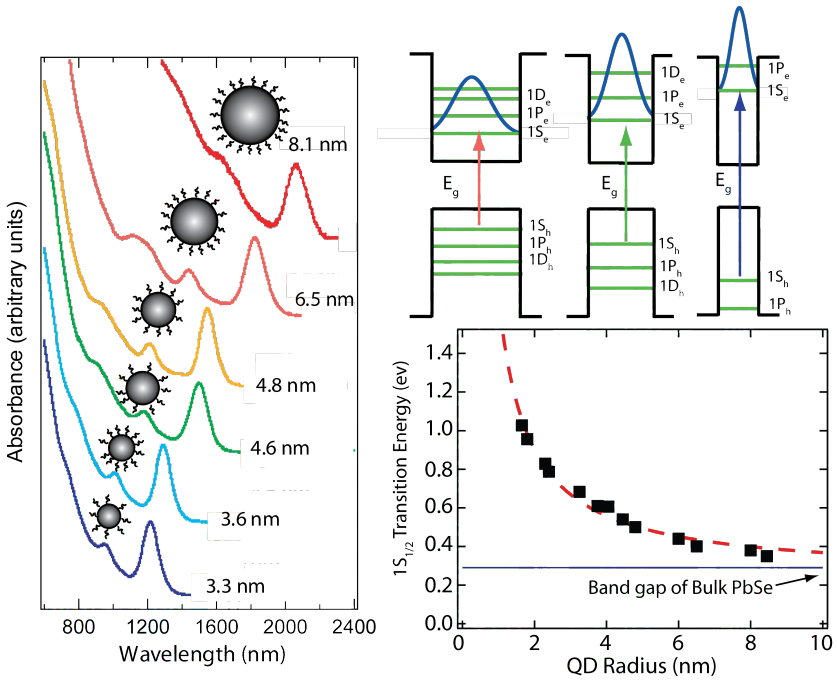

Figure 1.3. Size-dependent Bandgap of PbSe QDs
Absorption spectra of PbSe QDs spanning the range from 3.3 nm to 8.1 nm show strong quantum-confined $1S_{1/2}$ exciton shifted absorption. As the size of a semiconductor nanocrystal decreases below the bulk semiconductor's Bohr exciton radius, the exciton experiences increasingly strong confinement effects which significantly alter the allowed energy levels and result in a size-dependent and increasingly discrete electronic structure. The interband transition energies increase, and their widths narrow, resulting in optical absorption spectra that reveal structure indicative of discrete transitions with gaps between transitions reaching several hundred meV. (reproduced from Semonin et al.[26])

Equation 1.1 can easily be inverted to find, for any given $1S_{1/2}$ transition energy, a corresponding diameter. The absorption spectra of QDs is inhomogeneously broadened by the distribution of sizes and shapes within the ensemble of QDs. Knowing the sizing curve and the lineshape of the $1S_{1/2}$ we can calculate the size-distribution, and for the QDs in Figure 1.2, this is shown in Figure 1.4. For this particular sample the size-distribution is roughly Gaussian with a mean size of 2.5 nm (radius) and standard deviation of ~ 5%.

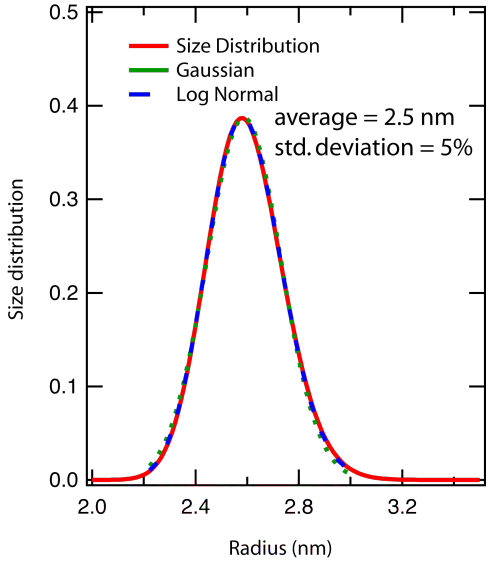

Figure 1.4. Size distribution of QD samples in Figure. 1.1
The green dotted line is for a Gaussian distribution while the blue dotted line is for a Log Normal distribution. The log-normal is slightly better than the Gaussian.

1.V. Absorption Coefficient and QD Concentration

The last concept concerning the optical properties of PbSe QDs that will be important for the remainder of this thesis is the determination of QD concentration from the absorption spectrum as well as how to compare the oscillator strength of the first exciton transition. The absorption cross section per particle, $\sigma_a(\omega)$, in the high energy regime is,

$$\sigma_a(\omega) = \frac{4}{3}\pi R^3 \frac{n_1}{n_2}|f(\omega)|^2 \alpha_b(\omega), \qquad [1.2]$$

where R is the radius, n_1 and n_2 are the refractive indices of the semiconductor and the solvent, $f(\omega)$ is a local-field correction factor, and α_b is the bulk absorption coefficient.[27] Equation 1.2 implies that at high energy the absorption per unit of PbSe is independent of

the QD size and resembles that of bulk PbSe. Those states near the band edges are most affected by quantum size effects and do not obey Equation 1.2. The absorption properties of colloidal QDs differ from bulk or thin film absorption due to the frequency-dependent local field correction factor, $f(\omega)$, which accounts for the different dielectric constants of the high dielectric PbSe and the surrounding low dielectric solvent. σ_a has been determined for a variety of QDs, including PbSe, using analytical techniques. One can independently determine $\sigma_a(\omega)$ and verify Equation 1.2. The absorption cross section per dot can be used to determine the number density (N, number of QDs per cubic cm) of QDs in solution through the following equation,

$$N = \frac{2.303(OD)}{\sigma_a \cdot l} \qquad [1.3]$$

where OD is the optical density measured through a pathlength, l.[27] The total oscillator strength of the 1st exciton transition can be determined in the presence of inhomogeneous broadening by integrating over the transition. This is important when comparing two QD samples that have undergone some chemical treatment that may either change the size-distribution or their optical properties.

1.VI. Applications for Semiconductor QDs: Multiple Exciton Generation

Among the many advantageous properties of semiconductor QDs is that they more efficiently undergo Auger processes such as impact ionization than their bulk counterparts. For bulk semiconductors, absorption of a photon with energy $E_g \leq h\nu$ results in the creation

of an electron-hole pair, or exciton. When $E_g < h\nu$, both the electron and the hole have energy in excess of their respective band edges. Primarily, however, this excess energy above the bandgap is lost as heat to the crystal lattice. Hot charge carriers interact with the crystal lattice and lose energy through inelastic optical phonon scattering. If either carrier (e^- or h^+) is sufficiently energized, it is also possible, but less probable, that this excess energy can be scattered with a valence band electron and result in the creation of an additional e^-/h^+ pair. This process is known as impact ionization in bulk. Due to the constraints that both energy and momentum must be conserved, the minimum energy required for a bulk crystals to undergo impact ionization is often greater than $2E_g$. [28] In addition to the need for high-energy photons, impact ionization in the bulk does not occur with a sufficiently high rate to compete with carrier cooling through phonon scattering and is therefore not the dominant cooling process for bulk semiconductor crystals.

Semiconductor QDs benefit from their electronic structures marked by discrete energy levels as opposed to the continuous bands in bulk semiconductors. Due to this splitting between energy levels, or intraband gaps (which can be on the order of 100 meV), simultaneous emission of multiple optical phonons (energies on the order of~30 meV) are required for efficient cooling to the lowest exciton energy level. This impedance to cooling due to the requirement of multiple phonon-electron scattering events is known as the phonon bottleneck. Retarded cooling by phonon scattering allows for competition from alternate relaxation pathways such as multiple exciton generation (MEG) in QDs. MEG is the process by which absorption of a single photon with energy of at least 2x the bandgap results in the creation of more than one e^-/h^+ pair (See Figure 1.5).

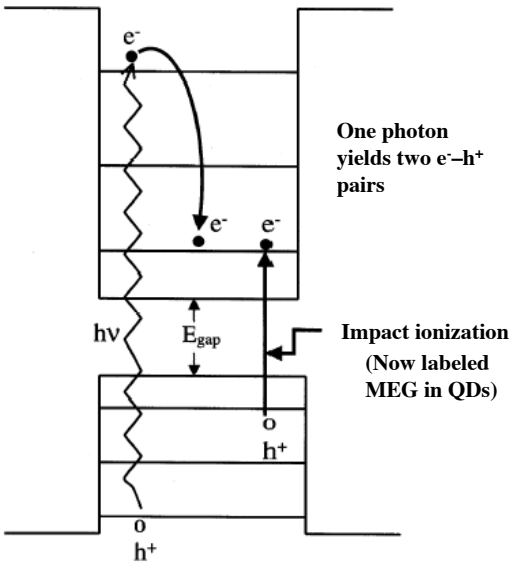

Figure 1.5. Mechanism for multiple exciton generation (MEG) in QDs
The process of multiple exciton generation depicted here involves the absorption of a single high-energy photon to create "hot charge carriers", which instead of cooling to the band edge and losing excess energy to heat, utilize this excess energy to produce an additional electron/hole pair. (Reproduced from Nozik-Quantum Dot Solar Cells[29])

This process, while still competing with other cooling routes, is also enhanced in QDs in light of increased carrier interactions due to their small volumes. Theoretically, for an ideal MEG yield of unity, each additional bandgap of energy possessed by an absorbed photon should result in the creation of an additional exciton, giving rise to a staircase function plot of the MEG quantum yield in Figure 1.6.

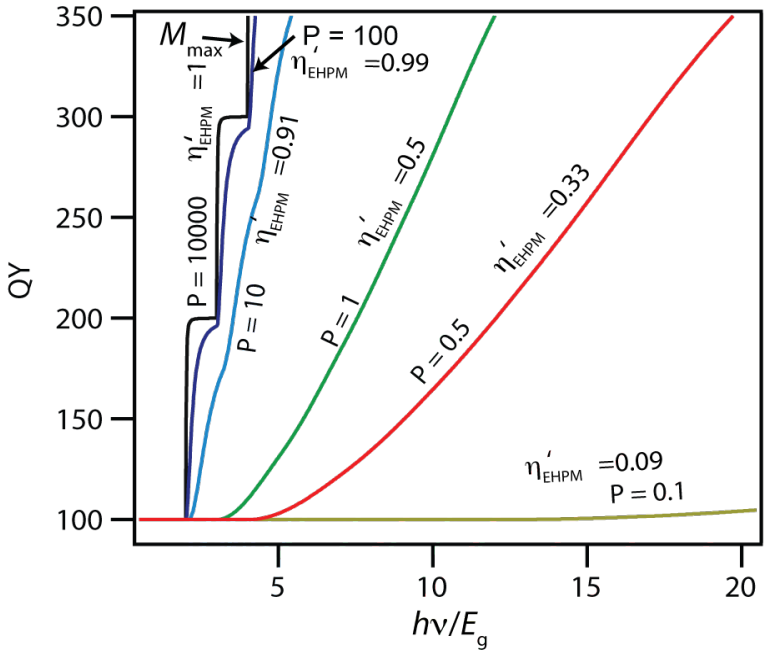

Figure 1.6. Percent Quantum Yield Plot as a Function of Normalized Bandgap
The above plot of quantum yield (QY) as a function of the normalized bandgap shows the MEG efficiency (slope = η'_{EHPM}) of a given system. *P* is threshold parameter that determines whether MEG onset is hard, electron-hole pair multiplication (EHPM) begins at exactly $2E_g$ (P>>1) or soft (P<1). The percent quantum yield is defined as the [(#e^-/h^+ pairs)/(single absorbed photon)] × 100. For the idealized case (black line), for every additional bandgap of energy possessed by the photon, an additional e^-/h^+ pair is created. (Reproduced from Beard et al. [12])

MEG has been observed in QDs of Si, CdSe, InAs, PbSe, PbS, and PbTe. [30] While the MEG onset for the Pb-chalcogenides has not yet been observed at photon energies as low as $2E_g$, the MEG process has definitely been determined to occur more efficiently in semiconductor QDs of PbSe as compared to bulk PbSe (shown in Figure 1.7).

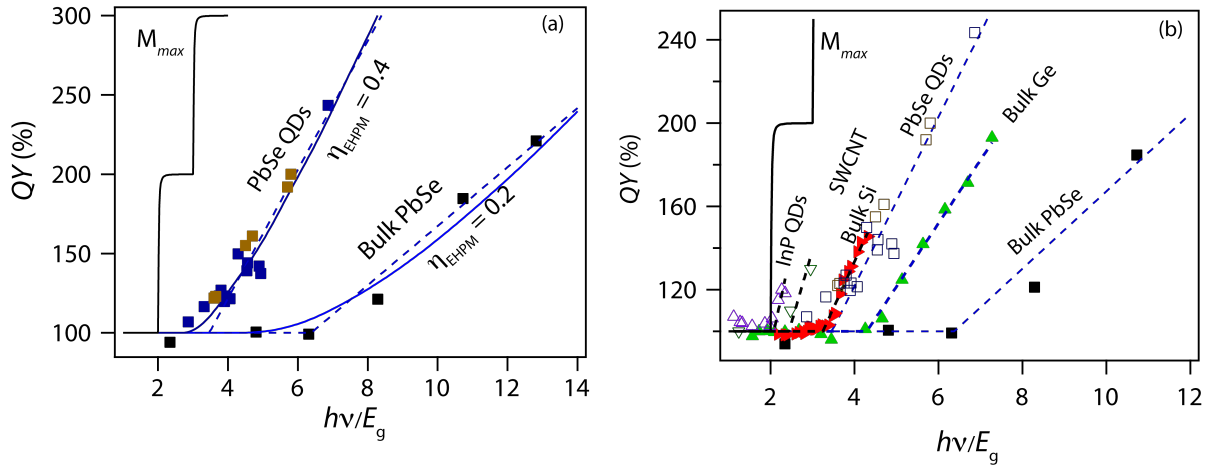

Figure 1.7. Quantum Yield Plot Comparing MEG Efficiency in Multiple Materials
(a) Quantum yield plot illustrating the improvement of MEG for PbSe QDs compared to bulk PbSe. (b) Quantum yield plot of MEG for various materials. The staircase function representing maximum MEG efficiency is shown in both plots. (Reproduced from Beard et al.[31])

While MEG has been shown to be more efficient in QDs than in bulk semiconductors, there is still work to be done in the area of lowering the energy required for MEG onset. Once again, the field stands to gain from purposeful manipulation of QD materials properties. Synthesis of novel materials, which either slow cooling or enhance the MEG onset, are desired. Synthetic achievements described in this thesis provide a basis towards increasing our understanding of how such structures may be built.

References

(1) Yin, Y.; Alivisatos, P.,Colloidal Nanocrystal Synthesis and the Organic-Inorganic Interface. *Nature* **2005**, *437*, 664-670.

(2) Joo, J.; Na, H. B.; Yu, T.; Yu, J. H.; Kim, Y. W.; Wu, F. X.; Zhang, J. Z.; Hyeon, T.,Generalized and facile synthesis of semiconducting metal sulfide nanocrystals. *Journal of the American Chemical Society* **2003**, *125*, 11100-11105.

(3) Kwon, S. G.; Hyeon, T.,Colloidal Chemical Synthesis and Formation Kinetics of Uniformly Sized Nanocrystals of Metals, Oxides, and Chalcogenides. *Accounts of Chemical Research* **2008**, *41*, 1696-1709.

(4) Krylova, G.; Giovanetti, L. J.; Requejo, F. G.; Dimitrijevic, N. M.; Prakapenka, A.; Shevchenko, E. V.,Study of Nucleation and Growth Mechanism of the Metallic Nanodumbbells. *Journal of the American Chemical Society* **2012**, *134*, 4384-4392.

(5) Ruddy, D. A.; Johnson, J. C.; Smith, E. R.; Neale, N. R.,Size and Bandgap Control in the Solution-Phase Synthesis of Near-Infrared-Emitting Germanium Nanocrystals. *Acs Nano* **2010**, *4*, 7459-7466.

(6) Millstone, J. E.; Wei, W.; Jones, M. R.; Yoo, H.; Mirkin, C. A.,Iodide ions control seed-mediated growth of anisotropic gold nanoparticles. *Nano Letters* **2008**, *8*, 2526-2529.

(7) Bealing, C. R.; Baumgardner, W. J.; Choi, J. J.; Hanrath, T.; Hennig, R. G.,Predicting Nanocrystal Shape through Consideration of Surface-Ligand Interactions. *Acs Nano* **2012**, *6*, 2118-2127.

(8) Puzder, A.; Williamson, A. J.; Zaitseva, N.; Galli, G.; Manna, L.; Alivisatos, A. P.,The effect of organic ligand binding on the growth of CdSe nanoparticles probed by Ab initio calculations. *Nano Letters* **2004**, *4*, 2361-2365.

(9) Yin, Y.; Alivisatos, A. P.,Colloidal nanocrystal synthesis and the organic-inorganic interface. *Nature* **2005**, *437*, 664-670.

(10) Huynh, W. U.; Dittmer, J. J.; Alivisatos, A. P.,Hybrid nanorod-polymer solar cells. *Science* **2002**, *295*, 2425-2427.

(11) Amirav, L.; Alivisatos, A. P.,Photocatalytic Hydrogen Production with Tunable Nanorod Heterostructures. *Journal of Physical Chemistry Letters* **2010**, *1*, 1051-1054.

(12) Beard, M. C.; Midgett, A. G.; Hanna, M. C.; Luther, J. M.; Hughes, B. K.; Nozik, A. J.,Comparing Multiple Exciton Generation in Quantum Dots To Impact Ionization in Bulk Semiconductors: Implications for Enhancement of Solar Energy Conversion. *Nano Letters* **2010**, *10*, 3019-3027.

(13) Cunningham, P. D.; Boercker, J. E.; Foos, E. E.; Lumb, M. P.; Smith, A. R.; Tischler, J. G.; Melinger, J. S.,Enhanced Multiple Exciton Generation in Quasi-One-Dimensional Semiconductors. *Nano Letters* **2011**, *11*, 3476-3481.

(14) Bartnik, A. C.; Efros, A. L.; Koh, W. K.; Murray, C. B.; Wise, F. W.,Electronic States and Optical Properties of PbSe Nanorods and Nanowires. *Physical Review B* **2010**, *82*, 195313.

(15) Wise, F. W.,Lead salt quantum dots: The limit of strong quantum confinement. *Accounts of Chemical Research* **2000**, *33*, 773-780.

(16) Evans, C. M.; Evans, M. E.; Krauss, T. D.,Mysteries of TOPSe Revealed: Insights into Quantum Dot Nucleation. *Journal of the American Chemical Society* **2010**, *132*, 10973-10975.

(17) Cho, K. S.; Talapin, D. V.; Gaschler, W.; Murray, C. B.,Designing PbSe Nanowires and Nanorings Through Oriented Attachment of Nanoparticles. *Journal of the American Chemical Society* **2005**, *127*, 7140-7147.

(18) Koh, W.-k.; Yoon, Y.; Murray, C. B.,Investigating the Phosphine Chemistry of Se Precursors for the Synthesis of PbSe Nanorods. *Chemistry of Materials* **2011**, *23*, 1825-1829.

(19) Yuk, J. M.; Park, J.; Ercius, P.; Kim, K.; Hellebusch, D. J.; Crommie, M. F.; Lee, J. Y.; Zettl, A.; Alivisatos, A. P.,High-Resolution EM of Colloidal Nanocrystal Growth Using Graphene Liquid Cells. *Science* **2012**, *336*, 61-64.

(20) Bartnik, A. C.; Efros, A. L.; Koh, W. K.; Murray, C. B.; Wise, F. W.,Electronic states and optical properties of PbSe nanorods and nanowires. *Physical Review B* **2010**, *82*.

(21) Kang, I.; Wise, F. W.,Electronic structure and optical properties of PbS and PbSe quantum dots. *Journal of the Optical Society of America B-Optical Physics* **1997**, *14*, 1632-1646.

(22) Tudury, G. E.; Marquezini, M. V.; Ferreira, L. G.; Barbosa, L. C.; Cesar, C. L.,Effect of band anisotropy on electronic structure of PbS, PbSe, and PbTe quantum dots. *Physical Review B* **2000**, *62*, 7357-7364.

(23) Goupalov, S. V.,Selection rules for optical transitions in PbSe nanocrystal quantum dots: Drastic effect of structure inversion asymmetry. *Physical Review B* **2009**, *79*.

(24) An, J. M.; Franceschetti, A.; Dudiy, S. V.; Zunger, A.,The peculiar electronic structure of PbSe quantum dots. *Nano Letters* **2006**, *6*, 2728-2735.

(25) Moreels, I.; Lambert, K.; De Muynck, D.; Vanhaecke, F.; Poelman, D.; Martins, J. C.; Allan, G.; Hens, Z.,Composition and size-dependent extinction coefficient of colloidal PbSe quantum dots. *Chem Mater* **2007**, *19*, 6101-6106.

(26) Semonin, O. E.; Luther, J. M.; Beard, M. C.,Quantum dots for next-generation photovoltaics. *Materials Today* **2012**, *15*, 508-515.

(27) Yu, P. R.; Beard, M. C.; Ellingson, R. J.; Ferrere, S.; Curtis, C.; Drexler, J.; Luiszer, F.; Nozik, A. J.,Absorption cross-section and related optical properties of colloidal InAs quantum dots. *Journal of Physical Chemistry B* **2005**, *109*, 7084-7087.

(28) Smith, A.; Dutton, D.,Behavior of Lead Sulfide Photocells in the Ultraviolet. *J. Opt. Soc. Am. B.* **1958**, *48*.

(29) Nozik, A. J., Quantum dot solar cells. *Physica E: Low-dimensional Systems and Nanostructures* **2002**, *14*, 115-120.

(30) Beard, M. C.; Ellingson, R. J.,Multiple exciton generation in semiconductor nanocrystals: Toward efficient solar energy conversion. *Laser & Photonics Reviews* **2008**, *2*, 22.

(31) Beard, M. C.,Multiple Exciton Generation in Semiconductor Quantum Dots. *Journal of Physical Chemistry Letters* **2011**, *2*, 7.

CHAPTER 2:

Dimers: Novel Heterostructures of the Lead Chalcogenides

Abstract

We have studied the synthesis of Pb-chalcogenide dimer structures (fused pairs of quantum dots) via microwave synthetic techniques. Dimers ranging in length from 6-15 nm were produced by oriented attachment of single nanocrystals with diameters of 3.1-7.8 nm. While smaller nanoparticles likely contain more higher energy surfaces, monomers with diameters exceeding about 5 nm appear to have the greatest affinity for dimer formation, and therefore, gave the greatest yields of fused structures. We find a new absorption feature in the 1st exciton dimer spectra and assign this to a splitting of the 8-fold degenerate 1st exciton band. The 1st exciton band is split by ~ 50 meV in the dimers produced from smaller monomers. We have also explored dimers produced by fusing two QDs of different size to form PbSe heterostructures.

2.I. Introduction

Multiple exciton generation (MEG) is enhanced in QDs compared to impact ionization in bulk semiconductors.[1] However, MEG must be further optimized if these unique materials are to have a significant impact on solar energy conversion technologies. There are two basic lines of attack in order to further increase MEG yields. Increase the rate of MEG over competing relaxation pathways or decrease the influence of competing relaxation channels. We propose that the only way to address these issues is through directed synthesis of nanostructures in which it would be possible to observe competing relaxation channels. Control over morphology and composition can allow for tailoring desirable quantum-size effects such as exciton delocalization, charge-transfer, and multiple exciton generation (MEG).

MEG is a process that occurs in quantum-confined semiconductor nanocrystals where upon absorption of a single high-energy photon of light more than one exciton, or electron-hole-pair, can be produced. Absorption of a photon within a semiconductor produces a hole in the valence band and a corresponding electron in the conduction band. If the energy of the absorbed photon is at least twice that of the band gap (E_g), then the excess kinetic energy contained in the newly created hot-exciton can be used to boost an additional valence band electron into the conduction band, producing another exciton. Experimentally, Pb-chalcogenide QDs are known to exhibit MEG and exhibit a photo-energy threshold, photon-energy for which multiple-excitons begin to be produced, of approximately 3-times E_g. [2-4]

Semiconductor nano-heterostructures are unique chemical systems in which carrier dynamics such as charge separation, carrier lifetime, and energy relaxation pathways can be controlled through the manipulation of QD composition, surface and/or internal structure, and geometry or shape. Each of these factors can have significant effects on carrier dynamics as have been observed in mixed chemical systems in the cadmium salt family. Previous work has been reported on energy transfer studies in heterostructures of CdSe/CdS as well as CdSe/CdTe of different morphologies. [5-8] For the CdSe/CdS system, manipulation of the different sizes, compositions, and morphologies resulted in the ability to tune between Type I, Type II, and quasi Type II structures (See Figure 1).

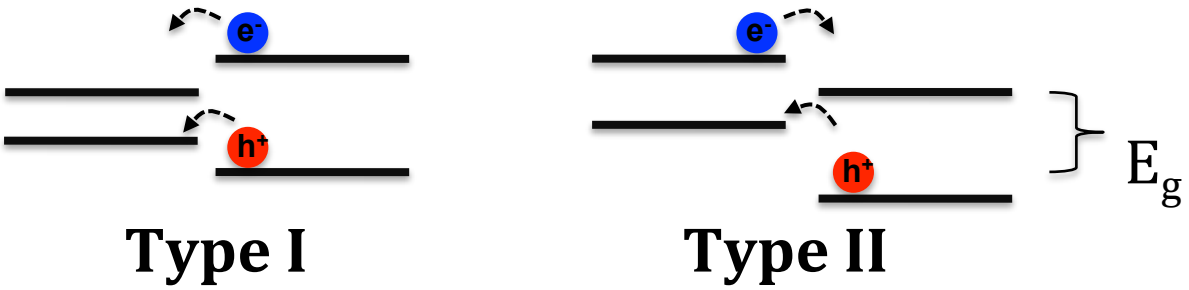

Figure 2.1. Type I/II Band Offsets
Typical band offsets for Type I and Type II architectures. This type of band structure can be engineered by manipulating nanoparticle sizes, compositions, and morphologies.

In the idealized Type II band alignment, researchers have observed efficient charge separation where the photo-excited electron resides in one component while the hole localizes in the other component, whereas in a quasi-Type II band alignment intrinsic energetic barriers to charge separation were discovered due to lattice mismatch for specific QD structures resulting in one of carriers being localized in one of the components

but the other carrier remaining delocalized across the entire nano-heterostructure. [9-13] These cadmium compounds have been extensively studied, and are model systems for how photo-physical properties such as electron/hole cooling rates can be manipulated by internal structure and nanoscale architecture. In one of the more striking examples, Pandey et al. designed a structure to significantly slow down carrier cooling in a CdSe/ZnSe/CdS heterostructure, and they provide some of the basic motivations for exploring other semiconductor heterostructure materials such as the Pb-salt systems. [8]

There are important implications for the rational design of QD systems that show interesting photophysics which will potentially allow for greater understanding of carrier dynamics and processes such as MEG. It is our goal to perform directed synthesis of both Type I and Type II structures by combining quantum dots in dumbbell or peanut-shaped structures as opposed to the typical core/shell or nanorod–type architectures that have been investigated extensively in previous studies. Here, we are developing the synthetic foundation that allows for purposeful manipulation of size and composition with the intent of producing interesting light harvesting systems.

2.II. Building PbSe QD Dimers

PbSe QD-dimer structures can affect carrier relaxation pathways so as to increase MEG yields via either a decrease in surface mediated cooling that results from a larger volume-to-surface ratio, and/or increase the MEG rate due to the larger Coulomb interaction of 1-dimension structures vs spherical QDs. QRods and QDs have similar E_g

where the short axis of the rod is equal to the diameter of the QD, indicating that quantum-confinement effects are conserved. The elongated nanocrystal could stabilize additional charger carriers arising from MEG while reducing recombination due to electrostatic interactions between charges and surface traps. Furthermore, PbSe QD dimers produced from various sizes of starting monomer and Pb-chalcogenide heterodimers could then be used to investigate energy flow in Type I (PbSe/PbSe) and Type II (PbSe/PbS) structures.

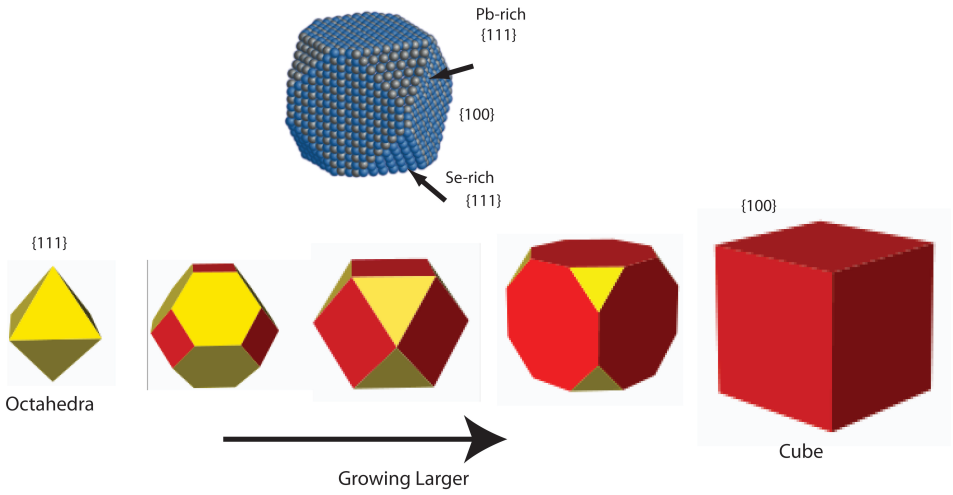

Figure 2.2. Evolution of Nanocrystal Shapes/Faceting as a Function of Size
Top panel shows a faceted PbSe QD with {100} and {111} faces exposed. The {100} faces are non-polar containing alternating Pb and Se atoms, while the {111} faces are either all terminated with Pb or Se atoms. Bottom panel shows how the PbSe QD morphology and surface structure evolves as the QD grows. Smaller QDs are dominated by the {111} surfaces and are octahedral or cubooctahedra while larger QDs are dominated by the {100} faces becoming truncated cubes or cubic.

A first goal towards building PbSe dimers is an understanding of how particle fusion occurs, at the heart of which is an understanding of the nanoparticle surface, composition,

and structure. In 2009, Murray et al. reported the preparation of PbSe nanowires by fusion of PbSe monomers in a process called oriented attachment. [14] Oriented attachment is a process where two nanoparticles fuse along a particular crystal axis and has been observed and studied in a variety of nanocrystal systems. In the case of PbSe QDs, oriented attachment was postulated to proceed as a result of large dipole moments that form due to the faceted nature of the NC. While {100} crystal faces are composed of stoichiometric Pb and Se atoms, and are therefore non-polar, the idealized {111} faces can be composed entirely of either Pb or Se. In the particular case where the top half of {111} faces are all Pb or all Se, a large dipole moment arises within the NCs which can then facilitate alignment of particles and eventual fusion. (There are 8 {111} faces in a truncated octahedron). However, multiple groups have now reported on the non-stoichiometric nature of PbSe NCs. [15-17] Apparently Pb^{2+} completely dominates the crystal surface. Furthermore, recent modeling studies investigating the energetics of NC surfaces determined that oriented attachment via dipole-dipole interaction is not likely due to the fully polar {111} surfaces once predicted, but rather to nano polar domains on the surface, which are then energetically stabilized by capping ligands. [18] This then raises the question of whether or not PbSe QDs could be made anion-rich as well, and whether or not a mixture of the two would facilitate dimer fusion.

2.II.a. Manipulation of the Surface of PbSe QDs

Dipole-dipole interactions, to some extent, could help the alignment and eventual fusion of precursor nanoparticles. Since intrinsic dipole moments of a Pb-salt nanocrystal is to a large extent governed by the surface stoichiometry, if a portion of the starting NCs could be made anion-rich or partially anion-rich and then allowed to react with the cation-rich particles, this could facilitate dimer formation through alignment of those particles that exhibit different nanopolar domains, if for no other reason than to lower the surface energy of the Se-terminated dots. The implications for anion-rich NCs extend beyond dimer formation, however. A layer-by-layer approach to building NCs, first cation then anion-rich, with successive surface treatments, means better control over NC morphology and composition. Anion-rich particles may also exhibit unique opto-electronic properties in solution, which have previously only been studied in films. These suppositions for the possibility of synthesizing a stable, anion-terminated PbSe nanoparticle will be discussed further in Chapter 3.

Here, we detail a solution-based methodology for preparing PbSe dimer structures in which the yield of dimer formation from monomers is strongly controlled by reaction conditions (temperature/reaction time), the concentration of surface ligands and the as-prepared monomer particle size. In our studies, we did not achieve yields greater than ~40%, and therefore, we developed an organic density gradient coupled with ultracentrifugation to separate dimers from monomers and larger oligomeric materials, and were successful on small scales. Spectroscopic characterization of dimer samples reveal the appearance of new absorbance and emission bands.

2.II.b. Materials

Selenium (99.99%), oleic acid (90%), 1-octadecene (ODE, 90%), trioctylphosphine (TOP 90%), diphenylphosphine (DPP, 98%), anhydrous ethanol, anhydrous hexane, and tetrachloroethylene (TCE, 99.9+%) were purchased from Aldrich and used as received. Lead Oxide (99.999%) was purchased from Alfa Aesar. For microwave experiments, a CEM Discover S-Class Microwave Reactor was employed.

2.II.c. PbSe Nanocrystal Synthesis

PbSe was synthesized according to previously reported procedures. [19] Using standard air-free techniques, 1.091 g PbO was dissolved by heating in 3.452 g oleic acid and 13.56 g of ODE. The reaction mixture was allowed to heat to 150 °C under N_2 with a vent needle for approximately 1 hour at which point the solution was clear. 0.096 g of DPP was then mixed with 15 mL of a 1 M solution of TOP-Se. This mixture was then quickly injected into the hot $Pb(oleate)_2$ solution, and the nanocrystals were allowed to grow for a time consistent with the production of the desired nanocrystal size.

2.II.d. General Synthesis of Pb-Chalcogenide Dimers

For a typical dimer synthesis, 50 mg of as-made QDs are first dispersed in a minimum amount of hexane. To this dispersion 5 mL 1-octadecene and 0.35 mL of one of

the following ligands; oleic acid, $Pb(oleate)_2$, or oleylamine, is added. Hexane is then removed by vacuum and gentle heating, and the remaining QD solution is heated to 150 °C for 1 hour under N_2, then cooled to room temperature and washed twice with Ethanol/Hexane. Standard air-free techniques are used throughout. TEM images show appreciable numbers of dimers in the sample depending on heating time and ligand concentration. Irrespective of ligand choice, excessive heating results in the growth of smaller QDs to make larger QDs as well as the formation of uncontrolled larger oligomeric material (trimers, tetramers etc.) rather than the desired dimers.

An alternative method for synthesizing dimers with reduced reaction times and comparable dimer yields involves the use of a microwave reactor. For a typical microwave reaction, the previously mentioned quantities of reactants are still employed. The reactants are loaded into the reaction vessel after hexane has been removed from the system. While monitoring both the temperature and the pressure, the reaction mixture is heated to 150 C under vigorous stirring conditions, at which point the temperature is held constant for 1 min 30 seconds prior to cooling to room temperature.

2.II.e. Characterization of Nanomaterials

Optical absorption data was collected on a Shimadzu UV-3600 spectrophotometer. Transmission electron microscopy (TEM) characterization was performed on a Philips CM200 Transmission Electron Microscope. Photoluminescence (PL) was measured on solution-QD samples dispersed in TCE, with excitation provided by a NIR-LED (emitting at

950). The emission and excitation spectra were fiber coupled to the emission monochromator of the fluorescence spectrometer and measured with a two-stage thermocouple-cooled InGaAs photodiode. The excitation LED is driven by a 15V square wave at 25 Hz using a Stanford Research Systems (SRS) DS335 function generator. The resulting InGaAs signal was amplified using a SRS SR530 lock-in amplifier, and spectra were corrected for detector efficiencies using a calibrated lamp.

2.III. Results and Discussion

Cho et al. first reported the synthesis of PbSe nanowires by oriented attachment in 2005.[14] Under optimized conditions, PbSe monomers fuse along similar exposed lattice planes to produce nanowires with lengths from 3-30 μm. Each nanowire, therefore, consists of hundreds of fused monomers. The lattice plane for which the monomers fuse can be manipulated depending on the choice of stabilizing surfactant leading to a variety of nanowires, such as, zig-zag, straight, and undulated. Fusion of just two particles appears to be the rate-limiting step with subsequent attachment to form wires occurring almost instantaneously. Therefore, modulation of growth time during nanowire synthesis has no effect on controlling nanowire length. In our efforts, we find that removing aliquots of the reaction mixture and quenching in cold ethanol immediately following hot injection/nucleation shows only QD monomers in solution. In contrast, the early precursors to nanowire formation, smaller oriented chains, have been observed in PbSe QD samples that have been allowed to age at room temperature. [14] Elongated PbSe oligomers

have also been purposefully synthesized by post-synthetically heating, as-prepared QDs in the presence of excess oleic acid, the stabilizing ligand. [14] Hanrath et al. found that treating oleic acid passivated PbSe QDs with pyridine also resulted in oligomeric PbSe networks. [20] The resulting morphology was found to be size-dependent and correlated to the exposed facets. In such reactions, PbSe oligomer chains can be produced, though no rational experimental design has been developed to fine tune the QD chain lengths. In this work we demonstrate that by controlling the growth time, temperature, and stabilizing ligand for the post-treatment of as-prepared nanocrystals, that the size of nanocrystal chains can be engineered to favor the formation of PbSe dimers as the predominant reaction product compared to larger oligomeric materials.

PbSe dimers have been prepared from solutions of QDs with diameters ranging from 3.1 nm to 7.8 nm. Analysis of TEM images confirms that dimer formation involves complete fusion of QD monomers. Lattice planes are observed to be continuous through the entire structure (see inset Figure 2.3). Dimer product yields are dependent on the size of the starting monomer. As the particle size increases, so too does the dimer yield for those particles synthesized using an excess of oleic acid. Figure 2.4c shows dimer yields as quantified by TEM analysis for QDs with starting diameters of 5.1, 5.9, and 7.8 nm. Upon heating at 150 C in excess ligand, these reactions give dimer yields of 17%, 23%, and 34% respectively. Yields were determined by averaging dimer populations versus other reaction products over multiple TEM images taken at random to give an unbiased account.

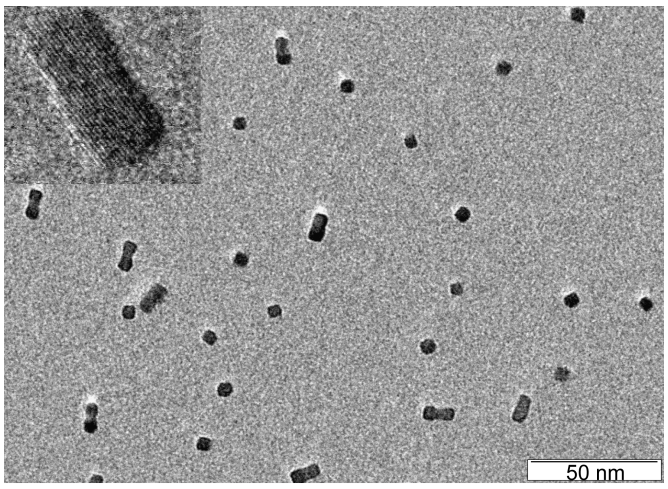

Figure 2.3. PbSe Dimers from 7.8 nm QDs
Dimers of PbSe prepared from 7.8 nm quantum dots in the presence of excess oleic acid. (Inset) Continuous lattice fringes show the single-crystalline dimer product.

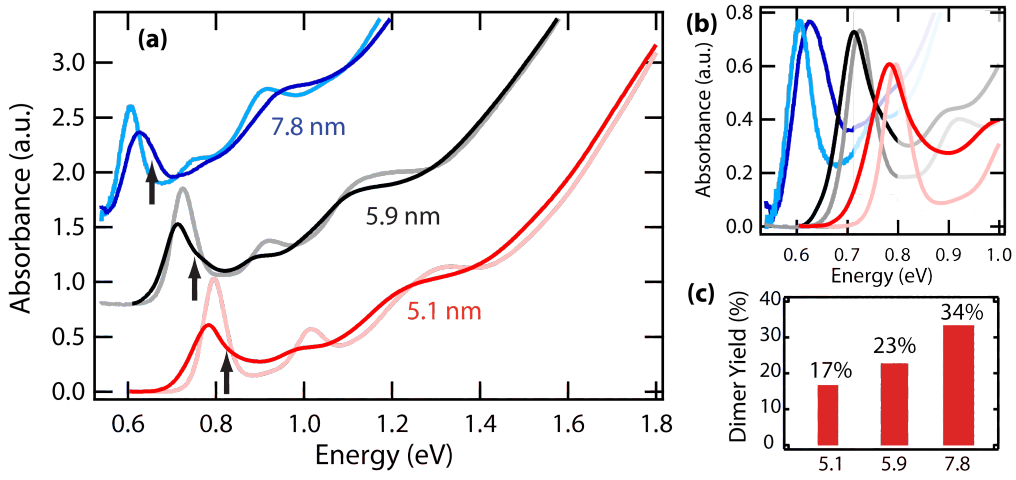

Figure 2.4. PbSe Dimer Absorbance and Yield as a Function of Size
(a). Absorbance spectra for 5.1, 5.9, and 7.8 nm QDs (shaded lines) and their corresponding dimer spectra (solid lines), showing characteristic broadening of the first exciton peak and the appearance of shoulder feature on the blue side of the $1S_{1/2}$. Spectra normalized at 3.1 eV. **(b)**Absorbance spectra from (a) normalized at the 1S band. **(c)** Dimer yields as a function of the original QD size as determined by analysis of TEM images.

Absorbance spectra (Figure 2.4) for dimer solutions differ markedly from those of as-prepared QDs. After a typical dimer synthesis, the first exciton peak red shifts approximately 20-40 nm on average, and there is an apparent broadening in the lowest energy transition. In Figure 2.4a and b we compare the absorption spectra of the starting monomers to that of the dimer containing solutions after the reaction. The spectra in Figure 2.4a are normalized at 3.1 eV where the absorption cross-section is independent of size or shape, while, in Figure 2.4b the data are normalized at the peak of 1S band. As previously mentioned, semiconductor QDs have a size dependent bandgap, which is shifted to lower energies as the apparent diameter is increased. Therefore, the presence of larger quantum confined materials (dimers and larger oligomers) accounts for the observed red shift in the absorption spectrum as well as contributing to an increase in the size distribution, resulting in broadening of the 1S absorption peak. In addition, to a shift towards lower energies and peak broadening, dimer solutions prepared from QDs with diameters in the range of 5-6 nm exhibit a shoulder peak, blue-shifted from the first exciton peak (see arrows in Figure 2.4a and Figure 2.4b) For particles approaching 8 nm, this blue-shifted shoulder appears only as a broadening of the 1S peak.

Dimer formation is sensitive to both reaction time and temperature, with higher occurrences of large oligomeric chains at higher temperatures and longer heating intervals. In addition to temperature and reaction time, the initial concentration of QDs appears to play a role in the ratio of dimers to larger oligomeric material. In the typical dimer reaction discussed above, 50 mg of QDs are dissolved in 5 mL 1-octadecene and then heated. However, when the starting material concentration is reduced to 10 mg, an increase of

about 6% is observed in dimer yields for reactions with 5.1 nm monomer QDs. The increase in dimer yield can likely be attributed to the inhibition of forming large PbSe oligomer chains by reducing particle-particle interactions, which make QD fusions less probable. In this case, single fusion events become more likely than extended chain growth and result in higher dimer yields and lower yields of extended-chain species.

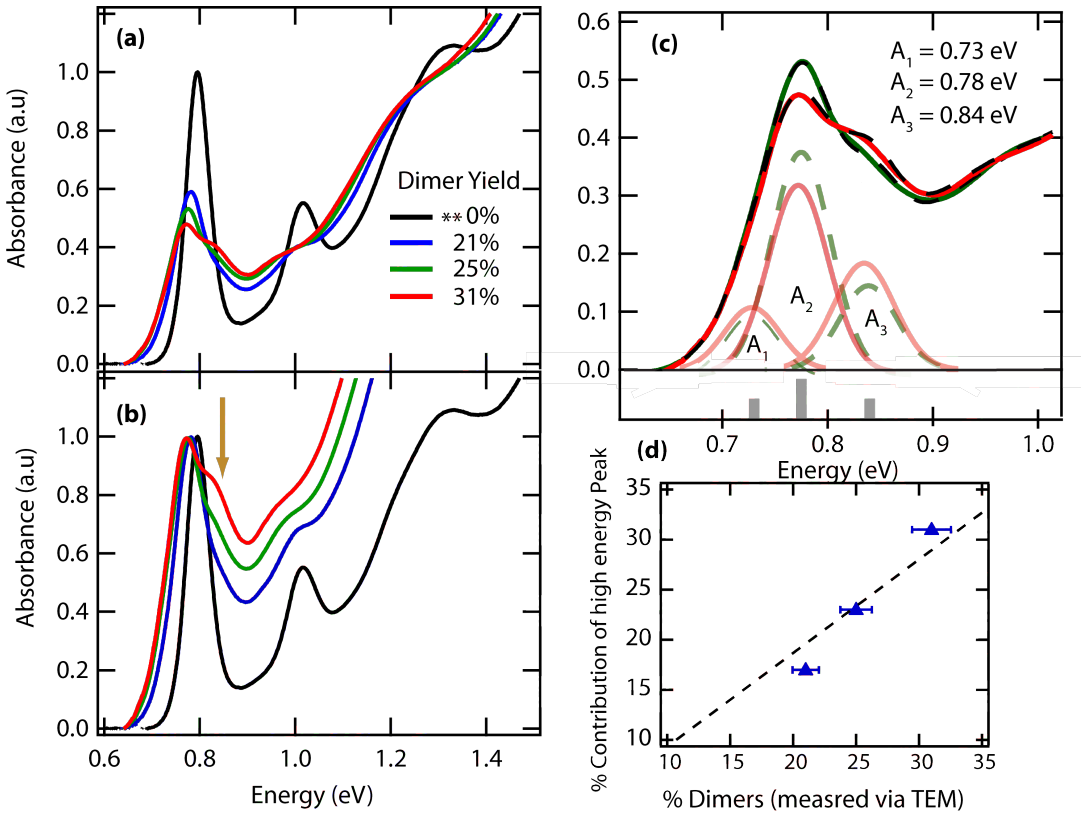

Figure 2.5. Analysis of Dimer Solutions from 5.1 nm Monomers
Absorbance spectra of PbSe dimer-containing solutions synthesized from 5.1 nm monomers showing the intensity change in the characteristic blue-shifted shoulder as dimer yield increases. In **(a)** spectra are normalized at high energy (3.1 eV) where the per PbSe absorption is independent of size or shape. In **(b)** spectra are normalized at the first exciton peak. Note the ** indicates the spectrum of the unreacted sample. Part **(c)** shows the spectral decomposition of the 1S peak for the 31% and 25% data shown in part (a). The 1S is decomposed into three Gaussian peaks labeled here as A_1, A_2, and A_3. The dashed green lines show the contribution of each peak to the 25% spectra while the pink lines are for the 31%. The major difference is a reduction of A_2 and increase in A_3. Part **(d)** shows contribution of A_3 to the 1S band as a function of dimer concentration.

In Figure 2.5 we display the spectra of dimer solutions that have been prepared from 5.1 nm monomers where the synthesis conditions have been varied to produce dimer yields of 21, 25 and 31%. In Figure 2.5a the data have been normalized at high photon energy. We have further verified that the integrated area of the 1S band is equal for the 4

spectra shown in Figure 2.5a, indicating that the oscillator strength remains constant for these samples. For comparison we show in Figure 2.5b the data normalized at the peak of the 1S band. In both Figure 2.5a and b the black line is the unreacted monomer spectra. The intensity of the blue-shifted shoulder increases with increasing dimer yield and is indicative of dimer species. We conclude that the absorption spectra contain contributions mainly from the unreacted monomers and the dimers from the following evidence; (1) TEM pictographs indicate that there are less than 5% larger oligomeric material; (2) A clear isosbestic point at around 0.82 eV (best seen in Figure 2.5a) results from a decrease in the monomer population concurrent with an increase in the dimer population. The presence of the isosbestic point indicates that monomers and dimers have distinct spectral features.

Spectral decomposition of the 1S band indicates that in the dimer-containing solutions there are three peaks, which we have labeled as A_1, A_2, and A_3, for the low, middle and high-energy peaks. In Figure 2.5c we show the spectral decomposition for the 25% (green dashed lines) and 31% (pink lines) containing dimers shown in Figure 2.5a. A_2 arises from unreacted monomers and its energetic position (0.78 eV) is roughly equal to that of the monomers (0.79 eV). Our data is consistent with a splitting of the 1S band into two peaks for the dimer spectra. A_1 and A_3 arise from the dimers and are roughly equally split by about 50-60 meV from the monomer peak. Figure 2.5d displays the contribution of the A_3 peak to the total absorbance of the 1S band plotted against the % dimers determined via TEM analysis, indicating that this peak is directly related to the amount of dimers in solution. An apparent isosbestic point appears at both the second and third energy transitions (which arise from the $1P^h_{1/2} - 1P^e_{1/2}$ and $1P^h_{3/2} - 1P^e_{3/2}$ transitions) as well.

However, closer inspection shows that these isosbestic points are actually an overall shift to lower energies (relative to the 1S level) of the 1P band as the dimer population increases. The 2nd and 3rd exciton result from splitting of the (3x8) degenerate 1P states into $1P_{1/2}$ and $1P_{3/2}$ due to the band anisotropy[21,22] and mixing of interband valence states.[23] Thus one possible explanation for A_3 is significantly larger splitting of the $1P_{3/2}$ band, so that these states merge with the 1S states. However, this hypothesis cannot account for the A_1 and E_1 bands.

Emission spectra confirm our peak assignments. Figure 2.6 shows the emission from two different dimer solutions with differing dimer yields. Spectral decomposition of both the absorbance and emission spectra are consistent with one another. In contrast to the absorption band, the emission band consists of only two peaks, one from each of the major species in solution. As in the case of the absorption spectra we labeled the two emission bands as E_1 and E_2 corresponding to the low and high energy bands. The dimers (E_1) only emit from the lowest energy transition corresponding to the A_1 band (see Figure. 2.6b inset) while the monomers emit at E_2 corresponding to the A_2 band. The splitting of the emission and absorbance bands are approximately the same. For example, in Figure. 2.6a, the absorbance bands show a splitting of 50-60 meV, while the emission is 60 meV. The Stokes Shift of monomers and dimers also appears roughly the same.

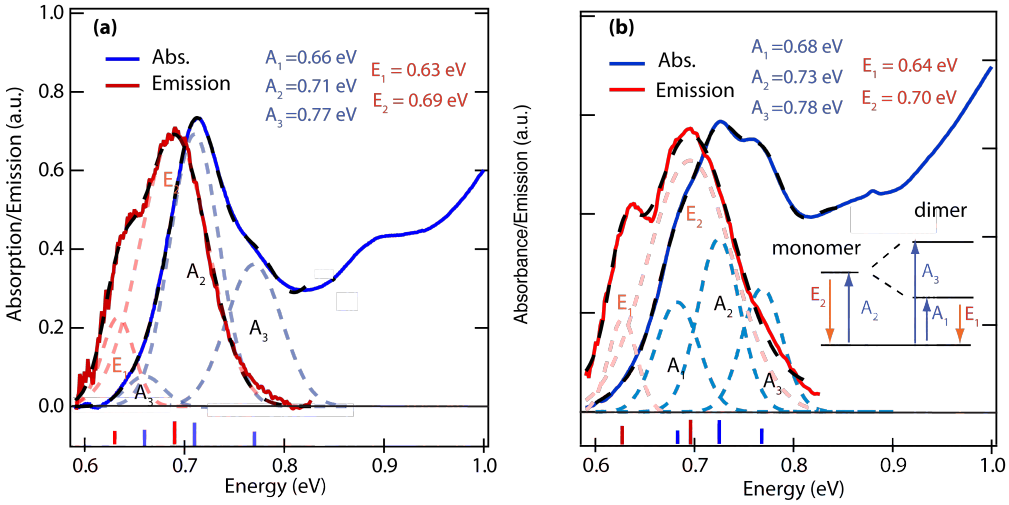

Figure 2.6. Absorbance and Emission Components From Dimer-Containing Solutions Absorbance spectra (blue) and emission spectra (red) of dimer-containing solutions prepared from **(a)** 6 nm PbSe QDs monomers and **(b)** 5.8 nm PbSe monomers. Absorbance spectra show 3 absorbance peaks while emission spectra display two.

We have analyzed the spectra of dimer solutions produced from 6 distinct starting monomer QD sizes, ranging from 3.1 to 7.2 nm and plot the observed splitting as a function of diameter in Figure 2.7. The splitting ranges from ~140 meV for the 3.1 nm to ~ 50 meV for the largest 7.2 nm monomers. There is an approximate 5% size-dispersion in the monomer solution and this results in an ~ 35-40 meV inhomogeneous broadening of the 1S band, and since the splitting for the larger QDs is on the same order of magnitude as the inhomogeneously broadened line, the larger dimers show only a broadened 1S band compared to the distinct peaks in the smaller QDs. There are several mechanisms that can contribute to splitting of the 1S exciton band and have been discussed by various authors. The most likely cause seems to be intervalley coupling. [23,24] Zunger et al. and Delerue et al. have calculated the splitting that results from the intervalley coupling for spherical PbSe QDs and find a size-dependent coupling that closely resembles the values measured here.

[23,24] The Delerue calculations are shown in Figure 2.7 as the red circles and blue squares for the conduction and valence band splitting. Zunger et al. calculated the splitting for small and large PbSe QD and found the splitting to increase with smaller size as observed here. Those calculations are for sphere where no or very small splittings are observed in experimental spectra, while the measurements here are for dimers.

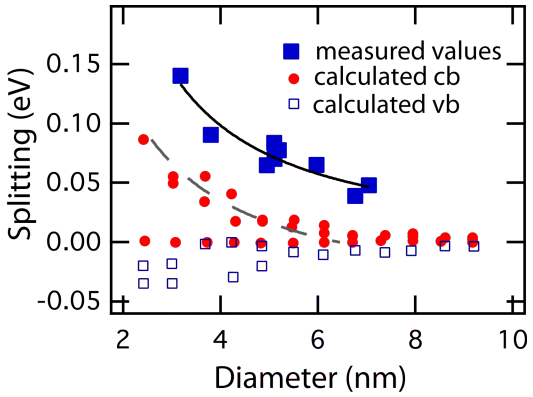

Figure 2.7. 1S Band Splitting for PbSe Dimers
Blue squares are the measured splitting of the bands from the monomer band for 5 sizes of QDs (the 5.1 nm monomers were measured three times). The red circles are the splitting calculated from for the conduction band while the blue squares are for the valence band. [24]

Varying the type of ligand and the ligand concentration has marked effects on dimer yield. For a sample of 5.9 nm QDs, we performed a side-by-side comparison of oleylamine ligands (Figure 2.8a) and oleic acid (Figure 2.8b) varying the concentrations of each ligand from 1.1 to 3.3 mmols. For those samples containing oleic acid, the appearance of the blue-shifted shoulder increases with increasing oleic acid concentration similar to what was discussed above. This is also true for the oleylamine–containing samples, however some striking differences are observed.

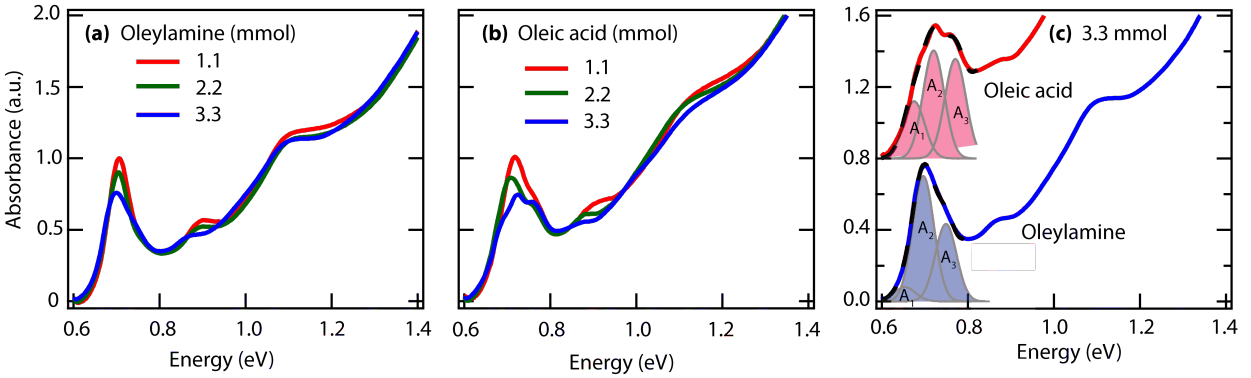

Figure 2.8. Dimers Prepared from Oleylamine *vs* Oleic Acid
Absorbance spectra for dimers prepared in **(a)** oleylamine and **(b)** oleic acid as a function of ligand concentration. Spectra are normalized at 3.1 eV. In **(c)** the spectral decomposition is shown for 3.3 mmol cases of Oleic acid (red) and oleylamine (blue).

For the oleylamine-containing samples, the first exciton peaks shift to lower energies than those in the oleic acid samples. Additionally, the appearance of the blue-shifted shoulder with increasing oleylamine is less pronounced. From TEM image analysis, the greatest point of contrast between the reaction products for these two samples is in the percentage of larger oligomeric material. While the percent oligomeric material ranges from 1-5% for the oleic acid-containing samples, samples using oleylamine produced as much as 44% oligomeric material with an oleylamine concentration of 3.3 mmol. This observation is consistent with that of Hanrath et al. who exposed PbSe QD solutions to pyridine and observed that mainly oligomeric PbSe networks form. [20] Furthermore, the dimer and oligomer species resulting from reactions with oleic acid undergo oriented attachment predominantly along the {111} facets as compared to those formed in the presence of oleylamine which seem to show no preference for facet-specific fusion. The absence of a strongly absorbing high-energy shoulder to the first exciton peak, for the

oleylamine-containing samples, may simply be a result of competing absorbances from multiple QD oligomer species.

It is worth noting that recent reports of PbSe nanorod formation show absorbance spectra closely resembling those that we see for dimer formation with significant first exciton peak broadening on the high-energy side when compared to QDs of similar diameter. In 2010 Murray et al. reported on the first synthesis of PbSe nanorods. [25] Repeating this experiment in our lab, we found that the reaction gives rise to elongated structures in quantitative yields (whether straight or branched), with no remaining monomer species. The absorbance spectrum observed for PbSe nanorods (shown in Figure 2.9) bares marked similarity to dimer-containing solutions, which also contain larger oligomeric species.

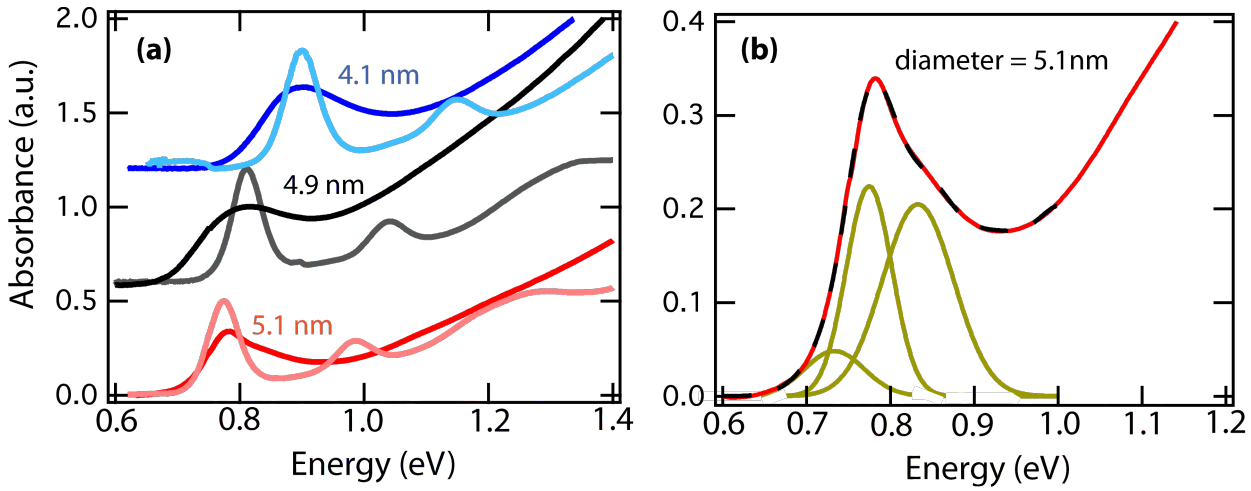

Figure 2.9. Absorbance for PbSe QDs and QRods with Similar 1st Exciton Transitions **(a)** Absorbance Spectrum for PbSe nanorods compared to QDs with similar first exciton transitions. (Offset for clarity). PbSe nanorods exhibit broadened first exciton peak with a high-energy shoulder, mirroring those observed in dimer-containing samples. **(b)** Spectral decomposition of PbSe QRod spectra similar to the dimer analysis, data corresponds to red trace in part (a).

The significant increase in oligomeric material observed when oleylamine is employed in excess, in lieu of oleic acid, suggests possible mechanisms for the role of excess capping reagent in dimer formation. Long-chain hydrocarbons with Lewis basic functional head groups are typically employed as surface stabilizers for Pb-chalcogenide QDs. These Lewis bases bind to surface Pb atoms with varying degrees of polarity depending on the nature of the functional head group and exposed crystal facets. Interactions between surface cations (Lewis acids) and stabilizing ligands (Lewis bases) can be characterized in terms of hard and soft acid/base interactions (HSAB). According to HSAB, hard acids and bases are compact and nonpolarizable while soft acids and bases are larger and more diffuse due to inner electrons shielding nuclear charge from the outer electrons making them more polarizable. The most stable adducts are formed from hard-hard and soft-soft interactions. Typical surface ligands for the Pb-chalcogenides include: carboxylic acids(R-CO_2^-), thiols (RS^-), (RNH_2)amines, and phosphonic acids (R-PO_3H^{2-}). The approximate order of increasing hardness of these ligands as Lewis bases is as follows: $RS^- > RNH_2 > R\text{-}CO_2^- \sim R\text{-}PO_3H_2$. Following this line of reasoning, with Pb^{2+} being a borderline to soft acid, soft to intermediate base-containing ligands such as oleylamine should form the most stable bond with the Pb^{2+} orbital at the PbSe QD surface. These interactions should in part explain the comparative differences in the occurrence of oriented attachment in samples containing oleic acid and oleylamine.

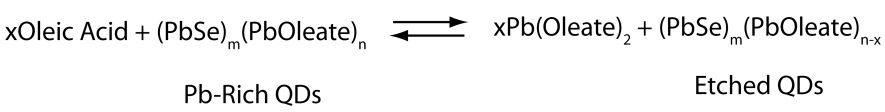

Given the structural nature of PbSe QDs as multifaceted crystals with a stoichiometric core and a terminating surface shell of surfactant-stabilized Pb atoms, the role of excess ligand may more accurately be described as one of removing or etching Pb from the QD surface. Moreels et al. observed that during storage of oleic acid-capped QDs under ambient conditions, some of the oleic acid ligands desorbed surface Pb to form an equilibrium between bound ligands and free $Pb(oleate)_2$ in solution. [26] As the free oleic acid concentration is increased, so too is the amount of desorbed Pb^{2+} forming additional free $Pb(oleate)_2$. Given that oleylamine should form a bond with Pb^{2+} that is covalent in nature, involving lone pairs on N, it must be at least as effective as oleate at stripping away surface Pb atoms, when present in excess, and exposing unpassivated surfaces. These bare surface sites are then less sterically hindered from undergoing fusion, and attach more efficiently. Fusion may also be driven by the need to decrease the surface energies of these bare surface sites. A second case to consider is that amines may not exhibit tight-binding to all of the crystal facets of PbSe. Cho et al. observe that addition of oleylamine to the PbSe reaction mixture induces the formation of octahedral PbSe nanoparticles. [14] This evidence suggests that oleylamine binds more efficiently to the {111} facets, which allows for faster growth of the {100} facets. In summary, oleylamine is very effective at removing Pb^{2+} from surfaces where tight binding occurs (like the {111}) and is in dynamic equilibrium undergoing exchange more readily at other surfaces (like the {100}). This dual interaction thus explains why oriented attachment is so efficient in reactions containing excess oleylamine.

Carboxylate, a hard acid, should form a more polar bond with surface Pb atoms. Given an excess of oleic acid, a protonated carboxylate, extraction of Pb must occur through a proton exchange at the surface. A possible mechanism for Pb extraction is one of $Pb(oleate)_2$ leaving behind a proton in the vacant Pb site at the QD surface. This process, like in the case of oleylamine, requires the breaking of a covalent Pb-Se bond, but now a proton transfer must occur to the PbSe surface to make a stable $Pb(oleate)_2$ molecule. Unlike amines that undergo fast exchange at the {100} surface, oleic acid must exhibit some kinetic hindrance to fusion associated with the proton transfer.

If dimer formation is viewed in light of this picture of exposed or ligand-free surfaces fusing, then our size-dependent dimer formation trends in the presence excess oleic acid also make sense. PbSe QDs are best modeled as truncated octahedra with 6-stochiometric {100} facets and 8-high energy {111} facets that undergo surface-atom rearrangements to lower surface energies and leave the facet Pb-terminated.[18] In light of the fact that different ligands are known to exhibit facet-specific binding affinities[14,27], and that oleate-capped QDs are observed to fuse primarily along the {100} faces. This leaves two possible mechanisms for QD-ligand interactions for oleate capped PbSe: (1) oleate does not sufficiently passivate the {100} facets of PbSe; or (2) oleate ligands more efficiently remove Pb atoms from the {100} surfaces. In both cases a larger {100} surface area would lend itself to greater occurrences of oriented attachment of monomer particles.

In addition to oleylamine, $Pb(oleate)_2$, was employed in the reaction in lieu of oleic acid. The TEM image analysis was supported by the absorbance spectra which showed much narrower first exciton peaks for $Pb(oleate)_2$-containing solutions as compared to

oleic acid, indicating a decrease in size dispersion (Figure 2.10). The difference in interaction for $Pb(oleate)_2$ reactions as compared to oleic acid-containing reactions is two-fold. By adding $Pb(oleate)_2$ in which there is presumably only a small excess of free oleic acid molecules, there is less free ligand available to extract Pb at the QD surface. Secondly, it is now possible that the excess $Pb(oleate)_2$ molecules bind to the PbSe {100} facets either through chemisorption or physisorption to surface Se atoms offering some steric hindrance which impedes the occurrence of oriented attachment. This experiment directly supports our ligand concentration-dependent dimer formation studies, which show that the higher the concentrations of free ligand present in the reaction mixture, the greater the dimer yields.

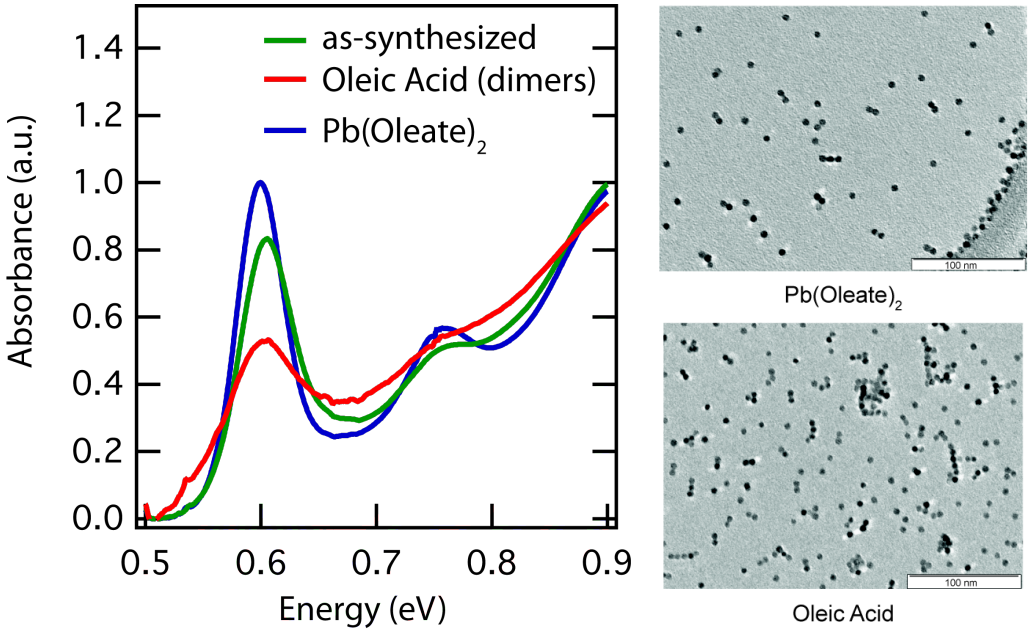

Figure 2.10. Dimers Prepared with $Pb(oleate)_2$ *vs* Oleic Acid
Absorbance spectra and resulting TEM images for dimers prepared from 7.8 nm quantum dots in the presence of either $Pb(oleate)_2$ or oleic acid. Samples were prepared by standard Schlenk techniques.

Various knobs can be tuned to affect the dimer concentration in the final reaction product, however; synthetic conditions were never optimized to the extent that quantitative dimer yields were observed. Therefore, separation techniques were utilized to achieve effective segregation of the desired dimer species from monomers and larger QD oligomers. Initially employed was the general technique of size-selective precipitation of reaction products using hexane/ethanol as the solvent/non-solvent pair. This method is commonly employed to improve size distributions in colloidal dispersions and involves measured addition of non-solvent paired with centrifugation, which causes gradual flocculation of the largest (least well-passivated) materials first. While this method was successful at removing some of the largest of QD oligomers, it did not efficiently resolve monomer and dimer species. As a result, organic density gradients were explored as a more size-sensitive method.

In addition to PbSe homodimers (dimers composed of the same size and material) PbSe heterostructures were also prepared using 4.6 and 7.8 nm PbSe QDs. Though successful addition of large and small QDs was achieved (Figure 2.11), yields for PbSe heterodimers were very low, giving only ~10% heterostructured products. In this case, there is no mechanism that precludes the formation of PbSe homodimers as well.

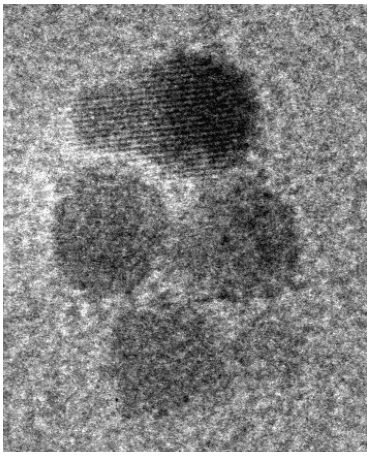

Figure 2.11. PbSe Heterodimers
TEM image showing PbSe heterodimers prepared from monomers of 2.4 and 6.4 nm. The image clearly shows continuous lattice fringes between the particles of distinct size.

2.III.a. Density Gradient Ultracentrifugation

Density gradients paired with ultracentrifugation have traditionally been employed in the carbon nanotube community to separate tubes of varying physical and electronic structures. [28] However, this technique has recently been adapted for efficient separations of Au, CdSe, and CdSe/CdS/ZnSe core/shell nanoparticles from their dimer counterparts in organic solvents. [29,30] Density gradients using ultracentrifugation separate inhomogeneous dispersions by two different mechanisms both of which require the use of two solvents with disparate densities. In the first mechanism of separation, or the "true" density gradient, solvent mixtures of varying composition are carefully layered from "heaviest" to "lightest" into a centrifuge tube and the material to be separated, dissolved in a minimal volume of the light solvent, is placed at the top. During centrifugation, particles separate

according to their different densities at different positions along the gradient. If the particle occupies a position where the gradient density is lower than it's own ($r_s<r_p$) then the particle moves downwards. If $r_s>r_p$ then the particle moves towards the meniscus. And if $r_s=r_p$ then no movement occurs, and the particle is said to have reached the isopycnic position. The second mechanism of separation involves a similar set-up to the first, however, now the materials separate strictly as a function of their sedimentation velocity. [31] In this case particles sediment according to their mass, shape, and size with no significant diffusion back into the simultaneously created density gradient. Nanoparticle separations employing organic density gradients most probably involve both of these mechanisms to some degree, though an equilibrium/isopycnic position is likely not reached.

As a proof of principle, a successful organic density gradient was prepared for separation of 5.1 nm PbSe QDs with a high starting monodispersity. The mixture was efficiently separated using graded solutions of 20-60% cyclohexane and carbon tetrachloride (CCl_4) shown below in Figure 2.12.

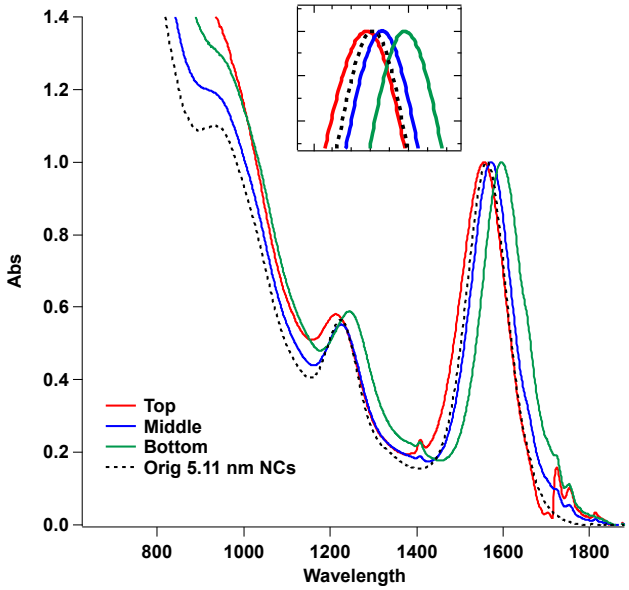

Layers	1st Exciton	Avg. QD Size (nm)*
Orig. QDs	1562	5.11
Top	1555	5.08
Middle	1571	5.16
Bottom	1596	5.29

Figure 2.12. Size-selective Separation 5.1 nm PbSe QDs
Separations show high monodispersity and sub nanometer resolution for ultracentrifugation using organic density gradients. *QD sizes were calculated from the first exciton peak position. Spectra are normalized at the first exciton peak.

Figure 2.12 shows marked shifts in the first exciton peak position as a function of gradient layer. This suggests that a sub-nanometer resolution for size-selective separations is possible using organic density gradients and ultracentrifugation. For these qausi- spherical particles, buoyancy plays a greater role than frictional forces during density gradient separation, since no equilibrium position is reached by the NPs in solution.

Following successful separations of QD monomers, dimers of 5.1 nm QDs were prepared and separated as shown in Figure 2.13.

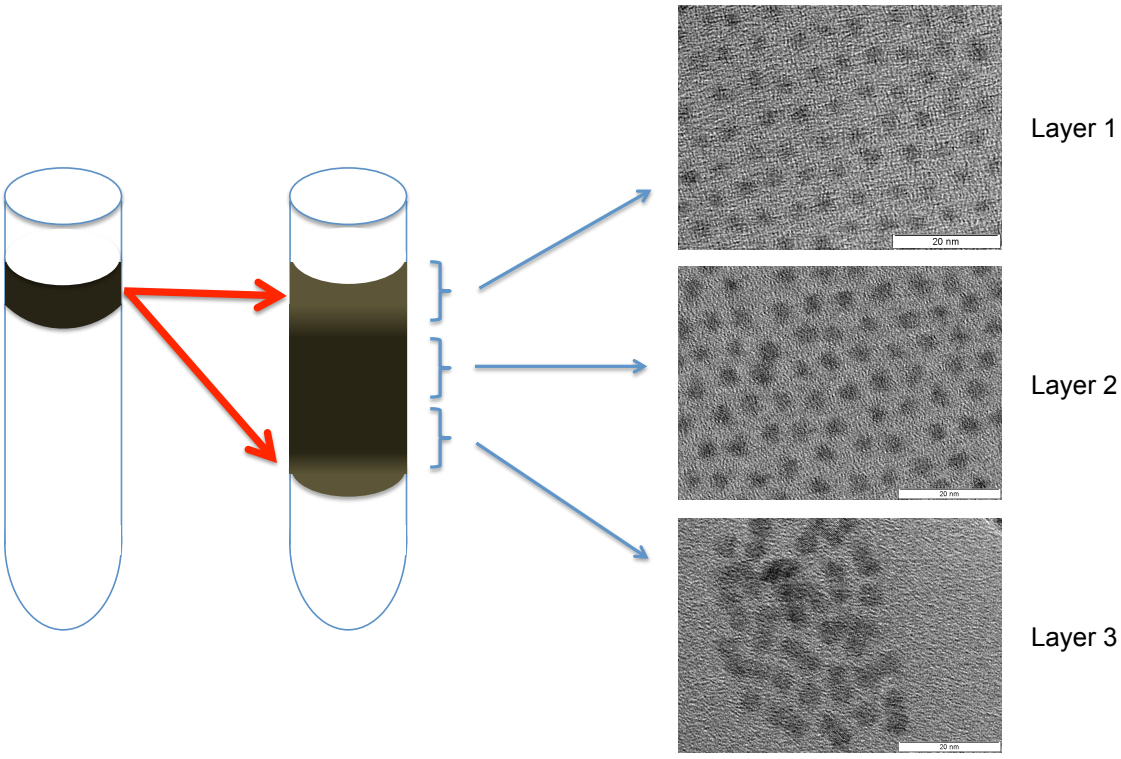

Figure 2.13. Size-Selective Separation of Dimers from 5.1 nm Monomers
The above figure shows the effective separation of 5.1 nm QD dimer reaction products using organic density gradients. TEM images show efficient segregation of QD populations from dimers and larger oligomeric material.

These separations successfully segregate sub-populations of monomers with only ~4 nm particles showing up in the first layer, ~5 nm particles and some dimer species in the second layer, and the majority of dimers and larger oligomeric materials residing in the bottom layer of the gradient. This procedure was repeated with 4.7 nm PbSe QDs and the subsequent absorption spectra following separation are shown in Figure 2.14.

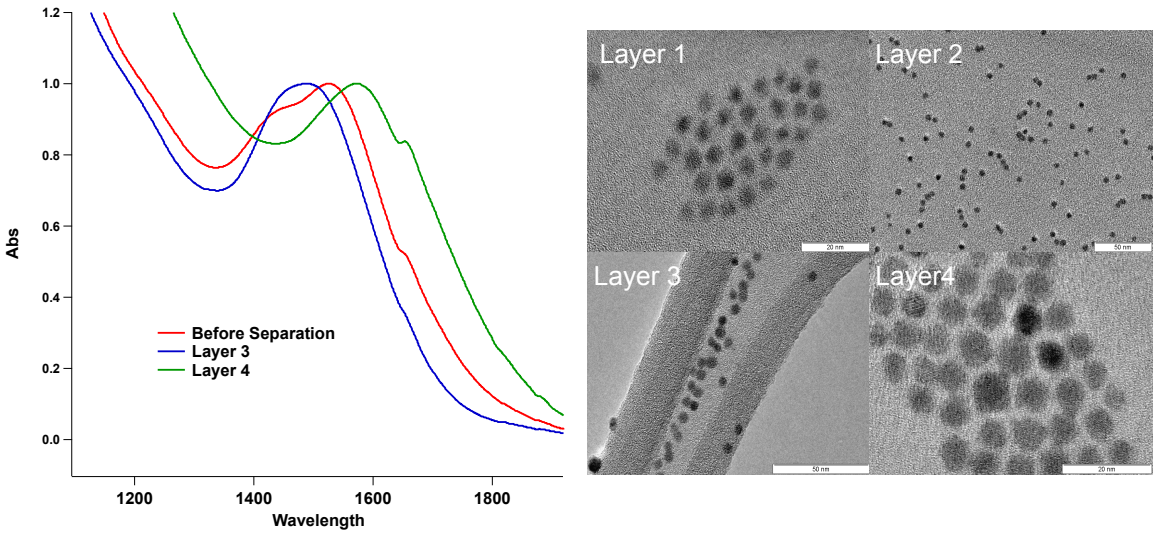

Figure 2.14. Separation of 4.7 nm QD Dimer Reaction Products Using Organic Density Gradients

(Left) Absorption spectra for post synthetic dimer reaction products, and layers 3 and 4 from the density gradient separation. (Right) TEM images showing product separations following dimer synthesis. Spectra are normalized at the first exciton peak.

TEM analysis reveals that dimer products were predominantly separated into the third layer, while the largest quasi-spheres are seen in layer four. TEM observations of these large particles are confirmed in the absorbance spectrum of layer 4 which shows a noticeable red-shift as compared to the pre-separated particles. Prior to separation, the characteristic high-energy peak is observed in the absorbance spectrum of post-synthesized dimers. Interestingly, for layer 3, where dimers have been observed by TEM, there is no double peak observed in the absorption spectrum of this layer. It is tempting to deduce that the cause of this peak therefore arises from two sub populations of QDs and is then resolved into two separate peaks following separations. However, a look at the first exciton peak width for these reactions suggests that size distributions are actually getting worse following density gradient separations. We have to conclude that an unknown side-

reaction is taking place within our QD samples during the density gradient ultracentrifugation. One possibility is that carbon tetrachloride is etching our particles via mobile chlorine atoms forming HCl in-situ during separation, and it may be necessary to find an alternative co-solvent for density gradient separations. Etching of the QDs during separations may account for the irregular particle shapes observed in Figures 2.13 and 2.14. A second caveat to both of these separations is that the product yields following density gradient separations is only a few milligrams, which was hardly enough to make a sample for further spectroscopic characterization. On the mg scale of these reactions, obtaining enough dimer products to perform further spectroscopic characterization requires multiple iterations of dimer synthesis and separation.

2.IV. Conclusions and Future Work

Both homodimers and heterodimers of PbSe were successfully synthesized via oriented attachment of as-prepared, oleate capped PbSe monomers. Dimer yields were affected by the size of the original nanoparticles, the capping ligand employed, temperature, and reaction time. Each of these reaction conditions were optimized to reduce the occurrence of large QD oligomer material and to give homodimer yields of up to 40%. A number of spectral features were observed as a result of dimer formation including broadening and a red-shift in the first exciton peak as well as the appearance of a high-energy shoulder peak to the first exciton. Organic density gradients paired with

ultracentrifugation were employed to achieve moderate segregation of dimer materials from the various reaction products, however, dimer yields following separation were low and did not allow for further spectroscopic characterization of the dimer species.

As current dimer yields are very low, future efforts to refine synthetic techniques towards higher yields should be explored. This may include employment of different capping ligands to probe how preferential binding on certain crystal surfaces may affect the appearance of nanopolar domains and in turn the degree to which the QDs fuse.

In addition to further studies with varying capping ligands, manipulation of surface composition may also lead to higher dimer yields. Especially in the case of heterodimer structures, it may be necessary to drive the process of oriented attachment by introducing two monomer QD systems with different surface polarities. For instance, by making the surface of one nanoparticle anion rich, one may drive oriented attachment to the as-prepared cation-rich particles. One of the major obstacles that will be faced while attempting to change the anion/cation ratio of PbSe NCs will be the problem of how to stabilize surface anions and keep the particle dispersed in the desired organic solvent (usually tetrachloroethylene, TCE). Thinking about new ways to deliver surface anions may be the key to the production of such anion-rich QDs.

One of the goals of this study were to present a platform for dimer formation which could be extended beyond homostructures to a variety of mixed material systems for further spectroscopic and device characterization. In order to extend the synthetic methods for producing PbSe homodimers and heterodimers to mixed material heterostructures, a

number of challenges must first be met. First and foremost, higher initial synthetic yields are desirable, which may be addressed through the surface modifications previously mentioned. Initial attempts to make PbSe/PbS heterostructures were unsuccessful, and still further challenges will arise when making heterostructures from materials with different crystal structures, as lattice mismatches will present a barrier to dimer formation. In this case it may be necessary to grow a core/shell particle first to ease lattice strain. If heterodimer attempts prove successful, larger scale separations are necessary as well as sensitive characterization techniques to confirm that the desired reaction products have been obtained. Separations of mixed materials, as was previously show will require density gradient optimization and most likely use of consecutive gradients.

References

(1) Beard, M. C.; Midgett, A. G.; Hanna, M. C.; Luther, J. M.; Hughes, B. K.; Nozik, A. J.,Comparing Multiple Exciton Generation in Quantum Dots To Impact Ionization in Bulk Semiconductors: Implications for Enhancement of Solar Energy Conversion. *Nano Letters* **2010**, *10*, 3019-3027.

(2) Ellingson, R. J.; Beard, M. C.; Johnson, J. C.; Yu, P. R.; Micic, O. I.; Nozik, A. J.; Shabaev, A.; Efros, A. L.,Highly efficient multiple exciton generation in colloidal PbSe and PbS quantum dots. *Nano Letters* **2005**, *5*, 865-871.

(3) Murphy, J. E.; Beard, M. C.; Norman, A. G.; Ahrenkiel, S. P.; Johnson, J. C.; Yu, P. R.; Micic, O. I.; Ellingson, R. J.; Nozik, A. J.,PbTe colloidal nanocrystals: Synthesis, characterization, and multiple exciton generation. *Journal of the American Chemical Society* **2006**, *128*, 3241-3247.

(4) Schaller, R. D.; Klimov, V. I.,High efficiency carrier multiplication in PbSe nanocrystals: implications for solar energy conversion. *Physical Review Letters* **2004**, *92*, 186601/186601-186604.

(5) Borys, N. J.; Walter, M. J.; Huang, J.; Talapin, D. V.; Lupton, J. M.,The Role of Particle Morphology in Interfacial Energy Transfer in CdSe/CdS Heterostructure Nanocrystals. *Science* **2010**, *330*, 1371-1374.

(6) Dooley, C. J.; Dimitrov, S. D.; Fiebig, T.,Ultrafast electron transfer dynamics in CdSe/CdTe donor-acceptor nanorods. *Journal of Physical Chemistry C* **2008**, *112*, 12074-12076.

(7) Kumar, S.; Jones, M.; Lo, S. S.; Scholes, G. D.,Nanorod Heterostructures Showing Photoinduced Charge Separation. *Small* **2007**, *3*, 1633-1639.

(8) Pandey, A.; Guyot-Sionnest, P.,Slow Electron Cooling in Colloidal Quantum Dots. *Science* **2008**, *322*, 929-932.

(9) Hines, M. A.; Guyot-Sionnest, P.,Synthesis and characterization of strongly luminescing ZnS-Capped CdSe nanocrystals. *Journal of Physical Chemistry* **1996**, *100*, 468-471.

(10) Kim, S.; Fisher, B.; Eisler, H. J.; Bawendi, M.,Type-II quantum dots: CdTe/CdSe(core/shell) and CdSe/ZinTe(core/shell) heterostructures. *Journal of the American Chemical Society* **2003**, *125*, 11466-11467.

(11) Milliron, D. J.; Hughes, S. M.; Cui, Y.; Manna, L.; Li, J. B.; Wang, L. W.; Alivisatos, A. P.,Colloidal nanocrystal heterostructures with linear and branched topology. *Nature* **2004**, *430*, 190-195.

(12) Talapin, D. V.; Koeppe, R.; Gotzinger, S.; Kornowski, A.; Lupton, J. M.; Rogach, A. L.; Benson, O.; Feldmann, J.; Weller, H.,Highly emissive colloidal CdSe/CdS heterostructures of mixed dimensionality. *Nano Letters* **2003**, *3*, 1677-1681.

(13) Talapin, D. V.; Mekis, I.; Gotzinger, S.; Kornowski, A.; Benson, O.; Weller, H.,CdSe/CdS/ZnS and CdSe/ZnSe/ZnS core-shell-shell nanocrystals. *Journal of Physical Chemistry B* **2004**, *108*, 18826-18831.

(14) Cho, K. S.; Talapin, D. V.; Gaschler, W.; Murray, C. B.,Designing PbSe Nanowires and Nanorings Through Oriented Attachment of Nanoparticles. *Journal of the American Chemical Society* **2005**, *127*, 7140-7147.

(15) Moreels, I.; Lambert, K.; De Muynck, D.; Vanhaecke, F.; Poelman, D.; Martins, J. C.; Allan, G.; Hens, Z.,Composition and size-dependent extinction coefficient of colloidal PbSe quantum dots. *Chem Mater* **2007**, *19*, 6101-6106.

(16) Schapotschnikow, P.; van Huis, M. A.; Zandbergen, H. W.; Vanmaekelbergh, D.; Vlugt, T. J. H.,Morphological Transformations and Fusion of PbSe Nanocrystals Studied Using Atomistic Simulations. *Nano Letters* **2010**, *10*, 3966-3971.

(17) Smith, D. K.; Luther, J. M.; Semonin, O. E.; Nozik, A. J.; Beard, M. C.,Tuning the Synthesis of Ternary Lead Chalcogenide Quantum Dots by Balancing Precursor Reactivity. *Acs Nano* **2011**, *5*, 183-190.

(18) Fang, C.; van Huis, M. A.; Vanmaekelbergh, D.; Zandbergen, H. W.,Energetics of Polar and Nonpolar Facets of PbSe Nanocrystals from Theory and Experiment. *Acs Nano* **2010**, *4*, 211-218.

(19) Murphy, J. E.; Beard, M. C.; Nozik, A. J.,Time-resolved photoconductivity of PbSe nanocrystal arrays. *Journal of Physical Chemistry B* **2006**, *110*, 25455-25461.

(20) Hanrath, T.; Veldman, D.; Choi, J. J.; Christova, C. G.; Wienk, M. M.; Janssen, R. A. J.,PbSe Nanocrystal Network Formation during Pyridine Ligand Displacement. *Acs Applied Materials & Interfaces* **2009**, *1*, 244-250.

(21) Bartnik, A. C.; Efros, A. L.; Koh, W. K.; Murray, C. B.; Wise, F. W.,Electronic states and optical properties of PbSe nanorods and nanowires. *Physical Review B* **2010**, *82*.

(22) Tudury, G. E.; Marquezini, M. V.; Ferreira, L. G.; Barbosa, L. C.; Cesar, C. L.,Effect of band anisotropy on electronic structure of PbS, PbSe, and PbTe quantum dots. *Physical Review B* **2000**, *62*, 7357-7364.

(23) An, J. M.; Franceschetti, A.; Zunger, A.,Pauli blocking versus electrostatic attenuation of optical transition intensities in charged PbSe quantum dots. *Physical Review B* **2007**, *76*.

(24) Allan, G.; Delerue, C.,Confinement effects in PbSe quantum wells and nanocrystals. *Physical Review B* **2004**, *70*.

(25) Koh, W.-k.; Bartnik, A. C.; Wise, F. W.; Murray, C. B.,Synthesis of Monodisperse PbSe Nanorods: A Case for Oriented Attachment. *Journal of the American Chemical Society* **2010**, *132*, 3909-3913.

(26) Moreels, I.; Fritzinger, B.; Martins, J. C.; Hens, Z.,Surface Chemistry of Colloidal PbSe Nanocrystals. *Journal of the American Chemical Society* **2008**, *130*, 15081-15086.

(27) Bealing, C. R.; Baumgardner, W. J.; Choi, J. J.; Hanrath, T.; Hennig, R. G.,Predicting Nanocrystal Shape through Consideration of Surface-Ligand Interactions. *Acs Nano* **2012**, *6*, 2118-2127.

(28) Arnold, M. S.; Green, A. A.; Hulvat, J. F.; Stupp, S. I.; Hersam, M. C.,Sorting carbon nanotubes by electronic structure using density differentiation. *Nature Nanotechnology* **2006**, *1*, 60-65.

(29) Bai, L.; Ma, X.; Liu, J.; Sun, X.; Zhao, D.; Evans, D. G.,Rapid Separation and Purification of Nanoparticles in Organic Density Gradients. *Journal of the American Chemical Society* **2010**, *132*, 2333-2337.

(30) Xu, X.; Stoettinger, S.; Battagliarin, G.; Hinze, G.; Mugnaioli, E.; Li, C.; Muellen, K.; Basche, T.,Assembly and Separation of Semiconductor Quantum Dot Dimers and Trimers. *Journal of the American Chemical Society* **2011**, *133*, 18062-18065.

(31) W., M.; Borger, L. *Analytical Ultracentrifugation of Polymers and Nanoparticles* Heidelberg: Heidelberg, 2006.

Chapter 3:

Control of PbSe Quantum Dot Surface Chemistry and Photophysics Using an Alkylselenide Ligand

---

Abstract

We have synthesized alkylselenide reagents to replace the native oleate ligand on PbSe quantum dots (QDs) in order to investigate the effect of surface modification on their stoichiometry, photophysics, and air stability. The alkylselenide reagent removes all of the oleate on the QD surface and results in Se addition; however, complete Se-enrichment does not occur, achieving a 53% decrease in the amount of excess Pb for 2 nm diameter QDs and a 23% decrease for 10 nm QDs. Our analysis suggests that the Se-ligand preferentially binds to the {111} faces, which are more prevalent in smaller QDs. We find that attachment of the alkylselenide ligand to the QD surface enhances oxidative resistance, likely resulting from a more stable bond between surface Pb atoms and the alkylselenide ligand compared to Pb-oleate. However, binding of the alkylselenide ligand produces a separate non-radiative relaxation route that partially quenches PL suggesting the formation of a dark hole-trap.

3.I. Introduction

Precise control over quantum dot (QD) surfaces is an ongoing research challenge that if solved should lead to a broader impact of QDs in many technological areas. Recent studies have demonstrated that photophysical properties such as photoluminescence (PL)[1,2], carrier mobility[3,4], and multiple-exciton generation (MEG)[5,6], can depend on the QD surface composition. A better understanding of the QD-ligand interactions and its relation to surface chemistry will enable greater control of photophysical properties. As an example, modifying QD surface chemistry by employing surface treatments to lead chalcogenide (PbX, X=S,Se) QDs has produced QD-films for use in next-generation photovoltaic structures that have achieved power conversion efficiencies greater than 5%.[7] Quantum confined semiconductors offer numerous advantages over bulk semiconductors for the design of novel opto-electronic applications such as low-cost solution processing[8] and enhanced multiple exciton generation. Further advances will necessarily involve better control over the surface defect states and their passivation.[9]

Though PbSe QDs are often modeled as quasi-spheres, their surfaces are in fact multifaceted, and the relative contribution of different facets changes with particle size and synthetic conditions. The {111} and {100} faces of the PbX rock salt crystal structure are usually assumed to dominate the QD surface. Under this assumption, the faceted nature follows that of a truncated-cube as shown in Figure 3.1.

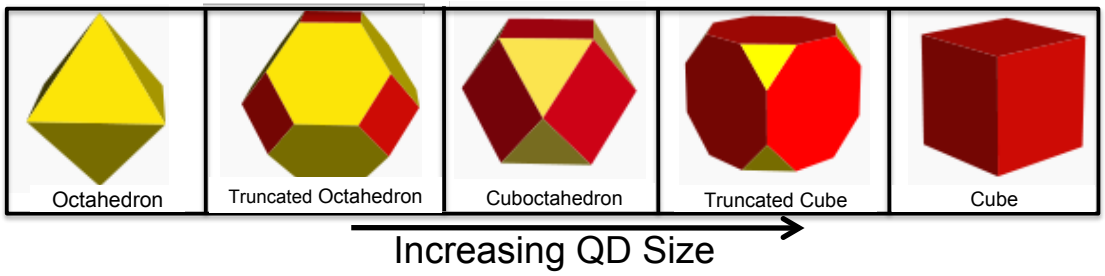

Figure 3.1. Size Dependent Morphology for the Pb-Chalcogenides
The shape evolution followed by Pb-Chalcogenide QDs can be understood in the simplified view of shape evolution of a truncated-cube.

The smallest QDs (~1-3 nm) exhibit the most spherical nature, and are likely truncated octahedra dominated by 8-{111} faces. As the QDs continue to grow into a size regime between ~3-8 nm, the interplay between growth along the <111> and <100> directions favor the lower surface energy {100} face over the higher energy {111} faces and a cuboctahedron results in crystal termination with roughly equal contributions from the {100} and {111} faces. Other faces such as the {110} may also be present and recently were postulated to be responsible for oriented growth of Pb-chalcogenide quantum sheets.[10] In the QD core, (111) planes alternate between all Pb and all Se atoms, while the (100) and (110) planes are stoichiometric. The actual structure of the QDs likely deviates from this simple picture, especially for smaller QDs with a larger number of exposed facets leading to reconstructed lattice planes, as recently observed in CdSe QDs[11] and calculated for PbSe QDs[12,13]. Atomistic calculations show that the surface energies of the various facets can vary depending on Pb *versus* Se termination, how the atoms are arranged on the surface (*i.e.*, atomically flat *vs.* nano-faceted regions on the larger faces), and the ligand that terminates the QD.[14] Assuming that surface atoms are mobile at room temperature, the particle faces will rearrange to achieve the lowest possible surface free energy, with the

stoichiometric {100} face having the lowest surface energy. At the largest sizes, PbSe QDs are known to undergo a sphere-to-cube transition in which all faces are terminated by {100} surfaces.[12,13,15-17] The quasi-sphere-to-cube transition depends upon the growth conditions along the <100> and <111> directions and should reflect the relative reactivity of the anion precursor. While the precise contribution of different facets is difficult to determine interesting studies have shown that the interplay between ligand-ligand and ligand-solvent interactions along with the underlying QD morphology can be employed to tune different QD superlattice configurations.[18]

Several research groups have found that as-made PbSe QDs are significantly cation-rich.[15,19,20] Moreels *et al.* introduced a model of a typical PbSe QD where the core is stoichiometric while all surface Se atoms are terminated by Pb, resulting in a Pb-rich QD where the calculated Pb:Se ratios match the values measured using analytical techniques.[19] Moreels *et al.* further measured a Pb_{excess}:oleate ratio of ~ 1, and when accounting for all surface Pb, this results in two surface Pb atoms per one oleate ligand.[21] Therefore, excess Pb-surface atoms are not compensated by the -1 charge assigned to the oleate ligand assuming each Pb has a +2 charge and each Se a -2 charge. Recent DFT calculations support this 2:1 $Pb_{surface}$:acid anion ratio for both the {100} and {111} faces as the most stable Pb-carboxylic acid bonding configuration.[16-18,22]

Altering the anion/cation ratio at the QD surface has been shown to affect both photophysical and electrical properties and may influence QD film performance. For instance, PbSe QD films treated with ethanedithiol (EDT) exhibit *p*-type transport behavior while hydrazine-treated films exhibit *n*-type behavior.[23] EDT treatment of films produces

an anion-rich environment while hydrazine treated films retain the cation-rich nature of the as-prepared QDs. (see Figure 3.3 for details). This is consistent with the behavior of bulk PbSe where Pb-vacancies lead to *p*-type behavior while Se-vacancies exhibit *n*-type behavior.[24] Mid-gap surface states that could serve as carrier trap sites are also highly dependent on the QD-ligand structure. Stoichiometric ligand-free QDs do not have mid-gap states.[12,17,25] However, non-stoichiometric QDs and those with ligands could have mid-gap surface states that serve as carrier trap sites, which would be highly dependent on the QD-ligand structure.[12,17] A better understanding of QD-ligand interactions and control over QD surfaces will enable a greater control of the electrical properties of these functional QD-solids.

Here we report the successful addition of Se atoms to the surface of PbSe QDs and the resulting changes to the photophysical properties that arise from shifting away from Pb-oleate termination. Se atoms are attached to the QD surface with sufficient passivation in the form of an alkylselenide ligand. The alkylselenide reagents can be used directly in the preparation of PbSe QDs or as a post-synthetic treatment to exchange surface oleate ligands (See Figure 3.2).

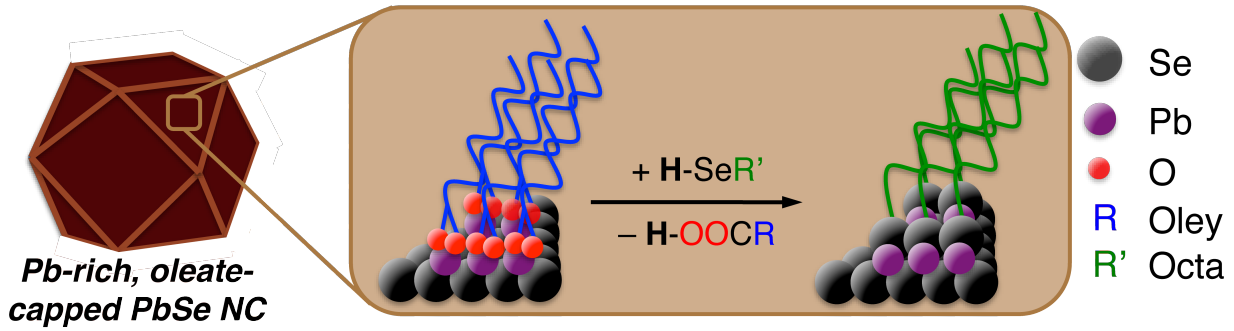

Figure 3.2. Mechanism of Surface Exchange from Oleate to Alkylselenide
The surface exchange of Pb-oleate-capped QDs for a Se-terminated surface occurs *via* proton transfer from the alkylselenol to produce free oleic acid.

Low-temperature PL spectroscopy reveals that addition of the alkylselenide ligand significantly reduces non-radiative surface trap sites associated with oxidation, presumably through a strong, relatively stable Pb_{surf}–$SeC_{18}H_{37}$ interaction. We demonstrate that the oxidation rate of PbSe films is reduced by the addition of the alkylselenide ligand. In addition, a new Se-related trap state arises following treatment, as evidenced by a decrease in photoluminescence quantum yields (PLQYs).

3.II. Results and Discussion

3.II.a. Aklyselenide Synthesis and QD Addition

Similarly to work by Jasieniak *et al.* [26] on Se-treated CdSe, we successfully prepared anion-rich PbSe QDs with an overall Pb/Se ratio of 0.96 through the addition of TOP-Se to oleate-capped QDs. The resulting QDs were stable in excess TOP-Se and a layer of Pb could be added to the QD surface by introduction of $Pb(oleate)_2$. However, in this case the PL

properties continually degraded upon successive addition of Pb and Se. In contrast to CdSe QDs, excess TOP leads to vibrational signatures that mask the optical excitonic signatures of the PbSe QDs and therefore removing excess TOP is important. However, after several washes to remove excess TOP-Se, the resulting QDs precipitated presumably due to non-ligated surface Se. In order to increase the anion/cation ratio of PbSe and retain colloidal stability, we found it necessary to develop a methodology that incorporates a solubilizing group with the large Se anion at the particle surface, that unlike TOP, will not leave as a neutral molecule upon washing.

Two alkylselenide reagents were prepared from adapted literature procedures, dioctadecyl diselenide, $[CH_3(CH_2)_{17}Se]_2$ (**1**), and octadecylselenol, $CH_3(CH_2)_{17}SeH$ (**2**).[27] The selenol **2** was determined to be the active species for Pb_{surf}–oleate exchange *via* proton transfer from **2** to form free oleic acid and a Pb_{surf}–$SeC_{18}H_{37}$ group (Figure 3.2). The diselenide **1** is easily transformed *in-situ* to **2** through the use of 1 equiv of diphenylphosphine (DPP) as a reductant, analogous to the well-known reaction of secondary phosphines with disulfides.[28] Although **2** exhibited fast ligand exchange reactivity (1-2 min), due to its potential instability towards air and moisture, the air-stable diselenide **1** was used for the bulk of the surface chemistry reported here, and is convenient in the procedures developed here due to the presence of DPP (or other secondary phosphines) in PbSe QD preparations.

Alkylselenide-terminated QDs are produced using two methods. The first method utilizes an *in-situ* selenide termination *via* a two-injection synthesis procedure beginning with a solution of $Pb(oleate)_2$ (from lead oxide and oleic acid). The first injection solution is

the commonly employed trioctylphosphine selenide (TOP-Se) with 0.08 equiv of DPP *vs* Se to nucleate and grow oleate-capped PbSe QDs at 160 °C. After the desired growth time is reached, a second injection of **1** in chloroform is added. After 20 seconds the solution is rapidly cooled, and the alkylselenide-capped PbSe QDs are isolated *via* repeated precipitations from hexane with ethanol. Alternatively, traditionally prepared and isolated oleate-capped PbSe QDs can be treated with **1** (plus 1 equiv of DPP) or **2** in hexane at room temperature. Treatment with **1**/DPP takes 1-2 days to reach completion, at which point the alkylselenide-capped QDs precipitate. The product is isolated *via* centrifugation, redispersed in chloroform, and stored in a glovebox.

Treatment with **2** in hexane occurs rapidly, and the QDs precipitate from solution in less than 5 min. Excess **1** and **2** are both highly soluble in hexane, and remain in the supernatant following isolation of the solid product (confirmed by ^{1}H NMR spectroscopy). The ratio of Pb:Se was determined by ICP methods in order to quantify the extent to which alkylselenide was added to the QD surface. Compositional analysis for as-prepared and alkylselenide-treated QDs is shown in Figure 3.3.

3.II.b. QD -Ligand Structure

The Pb:Se ratios were measured *via* ICP-AES (Figure 3.3) for the as-prepared (red circles) and alkylselenide (black circles) treated QDs.

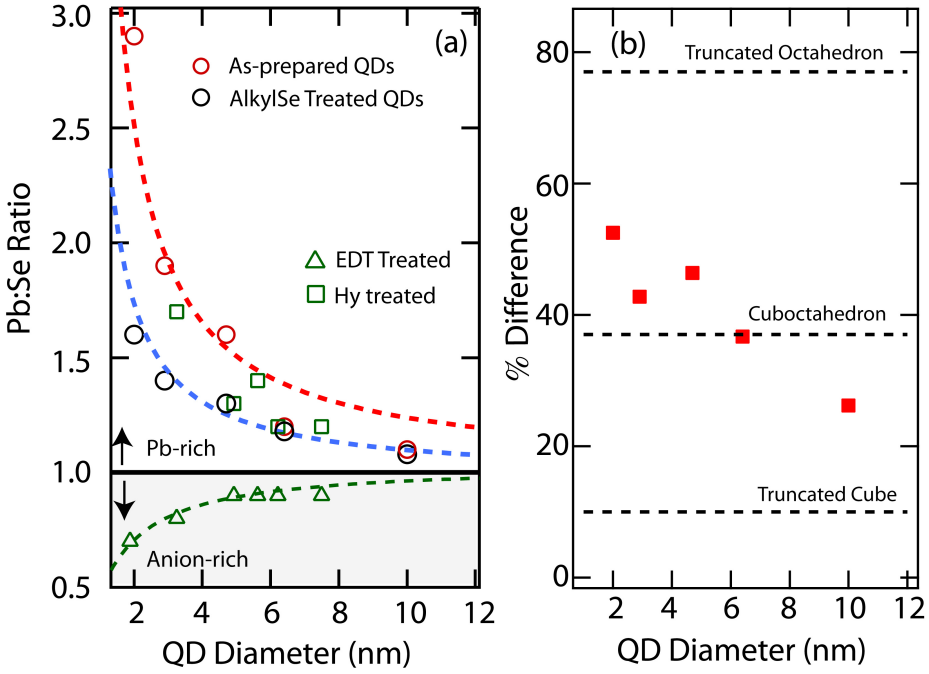

Figure 3.3. Change in PbSe Ration as a Function of Diameter/Morphology
(a) Pb:Se ratios from elemental analysis for as-prepared (red circles) and corresponding alkylselenide-treated QDs (black circles) as a function of QD size. The red dashed line is a model assuming only Pb-terminated surfaces. The dashed blue line is a model with ~40% Se addition. We also show Pb:X ratios for conductive PbSe films prepared by EDT treatment (green triangles) or hydrazine treatment (green squares) **(b)** Percent decrease in the excess Pb after alkylselenide treatment, dashed lines are for a cuboctahedron and truncated cube model.

The as-prepared QDs exhibit Pb:Se ratios ranging from 2.9 for the 2 nm QDs to 1.1 for the 10 nm diameter QDs. We compare our Pb:Se ratio of as-prepared QDs to those reported by Moreels *et al.*[19], Smith *et al.*[20], and Dai *et al.*[29] (see Figure 3.4) and find reasonable agreement despite dissimilar reaction conditions. Deviations of literature values from our measured Pb:Se ratios are expected in light of sample-to-sample variations and significant differences in synthetic methods, especially those employed by Moreels *et al.*

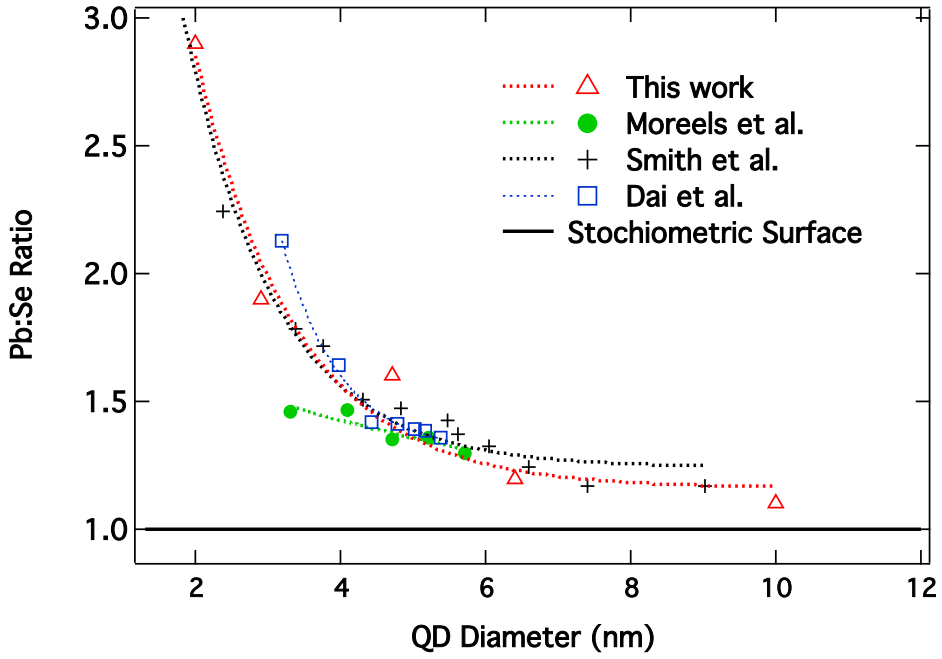

Figure 3.4. Size-Dependent Elemental Analysis for PbSe QDs
Pb:Se ratios from elemental analysis for as-prepared and alkylselenide treated PbSe of various diameters as compared to literature values for Smith *et al.*[20], Moreels *et al.*[19], and Dai *et al.*[29]

After the ligand exchange the Pb:Se ratio decreases from 2.9 to 1.6 for the 2 nm QDs resulting in a 53% decrease in the excess Pb, while for the 10 nm diameter QDs we observed a 23% decrease in the excess Pb. Figure 3.3b displays the % decrease in the excess Pb as a function of QD size. As a comparison to the treated PbSe QD films studied for electrooptical applications such as absorber layers in QD-based solar cells we plot the Pb:Se ratios for hydrazine (green squares) and EDT (green triangles) treated PbSe QD films. We find that the Pb:Se ratio for the hydrazine treated films is about the same as for untreated QDs, but upon treatment with EDT, the Pb:X (X=Se + S) ratio for the resulting film becomes anion rich.

For a given morphology the Pb:Se ratio can be estimated by determining the number of excess Pb atoms (N_{excess}^{Pb}) and comparing that to the total number of atoms within the stoichiometric core (N_{core}) by the following, $Pb{:}Se = 1 + (2N_{excess}^{Pb}/N_{core})$. N_{excess}^{Pb} is found by calculating the number of Pb atoms in one monolayer and dividing by 2 to account for the ½ Pb surface coverage of a stoichiometric QD. This expression can be reduced to the following for any of the proposed morphologies, Pb:Se = $(d + a)^3 \,/d^3$, where d is the quantum dot diameter, and where a is the PbSe lattice constant (0.61 nm) which corresponds to twice the average outer layer thickness of 0.3 nm. More explicitly, to find that the Pb to Se ratio is $Pb{:}Se = 1 + 2N_{excess}^{Pb}/N_{core}$ where N_{excess}^{Pb} is the number of Pb atoms in of a stoichiometric core, and N_{core} is the number of total atoms in the stoichiometric core. We note that since within the stoichiometric core $N_{Pb} = N_{Se}$ the total number of Pb atoms is $N_{Pb} = 0.5N_{core} + N_{Excess}^{Pb}$ and the total number of Se atoms is $N_{Se} = 0.5N_{core}$. Therefore,

$$N_{Pb}/N_{Se} = 1 + 2N_{excess}^{Pb}/N_{core} \qquad [3.1]$$

as noted above. So to calculate the Pb:Se ratio we need only find N_{excess}^{Pb} the amount of Pb added to the stoichiometric core. In the core half, of the surface atoms are Pb, therefore; to find N_{excess}^{Pb}, we can calculate the amount of Pb in a one monolayer shell and divide by 2. However, we need to calculate $2N_{excess}^{Pb}$ therefore we simply find the number of Pb atoms in a shell around the given morphology. The number of atoms in a giving morphology is equal to $N_{core} = V/V_0$ where $V_0 = a^3/8$ is the volume occupied by one atom. For each morphology model we calculate $2N_{excess}^{Pb}$ as the volume of a shell divided by the volume of each atom, so $2N_{excess}^{Pb} = V_{shell}/V_0$. Substituting into Eq. 2.1 we find

$$N_{Pb}/N_{Se} = 1 + V_{Shell}/V_{core} \qquad [3.2]$$

The volume of a shell can be calculated by subtracting the volume of the core by the volume of the core plus the shell. So $V_{Shell} = V(d+a) - V(d)$ where $V(d) = V_{core}$. Eq. 2.2 can then be expressed as

$$N_{Pb}/N_{Se} = V(d+a)/V(d) \qquad [3.3]$$

We have considered the following morphologies, sphere, cube, octahedron, cuboctahedron, and truncated cubes. The volumes can be found in standard geometry tables but always take the form $V(d) = A \cdot d^3$ where d is the diameter and A is some proportionality constant, for example, $A = \pi/6$ for a sphere. We find that for any of the morphologies Eq. 2.3 can be written as

$$N_{Pb}/N_{Se} = (d+a)^3/d^3 \qquad [3.4]$$

We can account for addition of Se by introducing a parameter *f* that represents the degree of Pb- or Se-termination (*f* = 1 is complete Pb-termination and *f* = 0 is complete Se-termination) by the following, $Pb{:}Se = (1-f) + f \cdot (d+a)^3/d^3$. The value of f can be estimated by considering the faceted nature of the QDs and how the Pb:Se ratio would change for the following shapes; octahedron, truncated octahedron, cuboctahedron, and truncated cube. All morphologies predict the same Pb:Se ratio of the untreated or completely Pb-enriched surfaces as noted above. But the Se-enriched QDs will show differences if we assume that the alkylselenide ligand preferentially binds to one face because the ratio of the {111} and {100} faces depends on the morphology. We tentatively conclude that the alkylselenide ligand binds preferentially to the {111} faces by the

following observation. When the alkylselenide ligand is used as the sole Se-source during PbSe QD synthesis, large hexapods result. (See Figure 3.5 below)

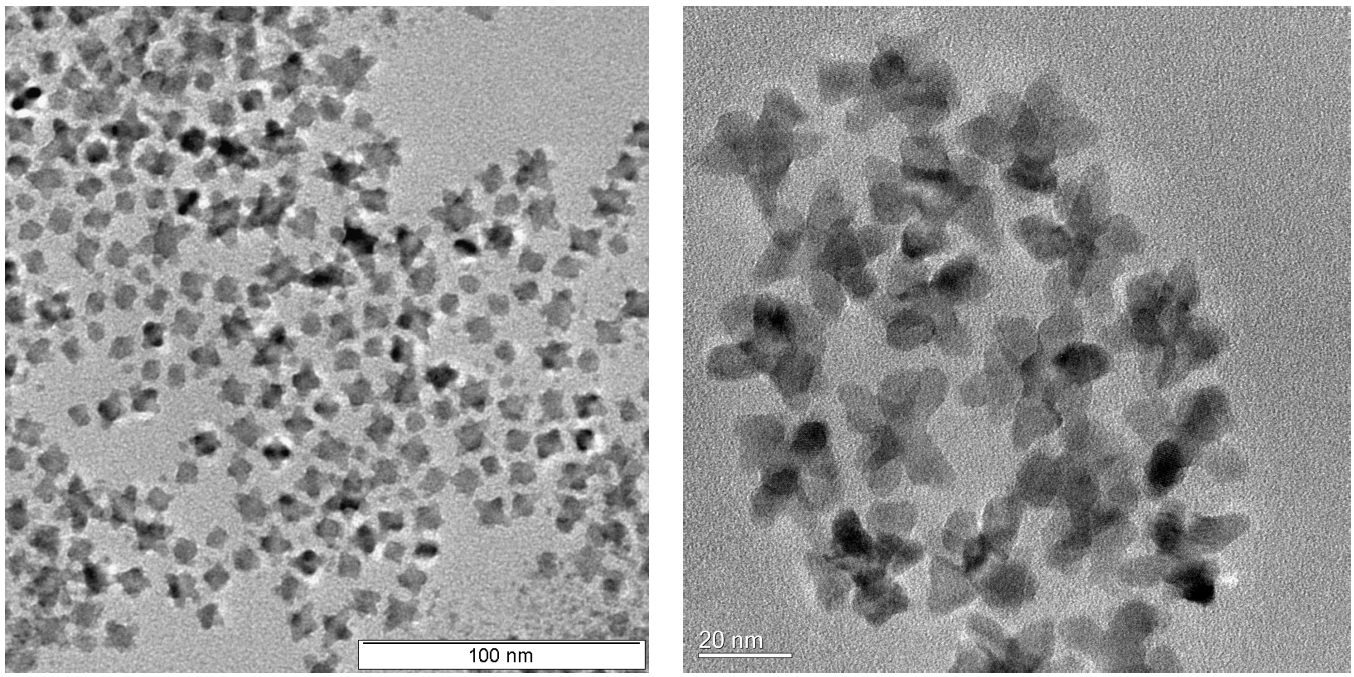

Figure 3.5. TEM of Hexapodal PbSe
Hexapodal nanoparticles were grown using dioctadecyl diselenide as the sole source of Se as well as the capping ligand. Hexapods result from surface-selective passivation of the 8-{111} facets allowing the 6-{100} facets to grow faster.

Hexapods result from continued growth along the 6-{100} faces and hindered growth along the 8-{111} faces. We propose that this hindered growth is due to preferential alkylselenide ligand binding on the {111} faces. The resulting hexapod morphology is in contrast to the growth dynamics observed under normal synthesis conditions (using TOP-Se) for Pb-oleate-terminated QDs, where TEM analysis consistently finds that smaller QDs are quasi-spherical, while larger QDs are cubic. Cubes result because the {111} faces are favored during growth over the {100} faces. We, therefore, assume in the following that alkylselenide addition to oleate-terminated QDs adds Se primarily to the {111} faces. Since

complete alkylselenide surface coverage does not occur, the Pb-enriched {100} faces must dominate the underlying QD-morphology and this is consistent with the cuboctahedron and truncated cube shapes. For example, a QD morphology resembling a truncated octahedron would result in a Se-rich QD after ligand exchange along the {111} face, which is not observed. These tentative conclusions are consistent with the findings of Bian et. al who explain that there is a natural tendency of intermediate-sized QDs prepared by conventional synthesis conditions towards an underlying bcc superlattice structure due to the characteristic structural properties of cuboctahedron QDs.[29] An exact calculation of f can be done but involves a laborious geometry exercise and is not necessary for our conclusions. Instead we estimate f by calculating the percent surface area for the {100} surface for the different morphologies, $f = S_{100}/(S_{100} + S_{111})$ and find $f = 0.90$ for the truncated cube, $f = 0.63$ for the cuboctahedron, and $f = 0.23$ for a truncated octahedron. When f = 0.6 (dashed blue line) the model reproduces our data, suggesting that following treatment, ~40% of the QD surface becomes alkylselenide terminated by primarily adding Se to the {111} face. The percent change in Pb-enrichment can be estimated as $(1 - f)$ and is plotted as dashed lines in Figure. 3.3b for the three morphologies. We also show the % Pb decrease for the ICP data (Figure 3.3b, red squares). For smaller diameters, the cuboctahedron model approximately reproduces our data, while at larger sizes the measured data are significantly lower and begin to approach the truncated cube. These observations can be explained by a sphere-to-cube transition that PbSe QDs are known to undergo and that the exact morphology of the QDs likely deviates from any of the these model shapes. Finally, we can also analyze the EDT-treated PbSe QD films in a similar

manner and find that f = 0.25 (green dashed line) suggesting an 75% anion enrichment of the QD surfaces.

Following exchange with alkylselenol, ^{1}H NMR spectroscopy was performed to determine the efficacy of exchange. NMR spectra of as-prepared PbSe QDs show three characteristic resonances (Figure 3.6a).

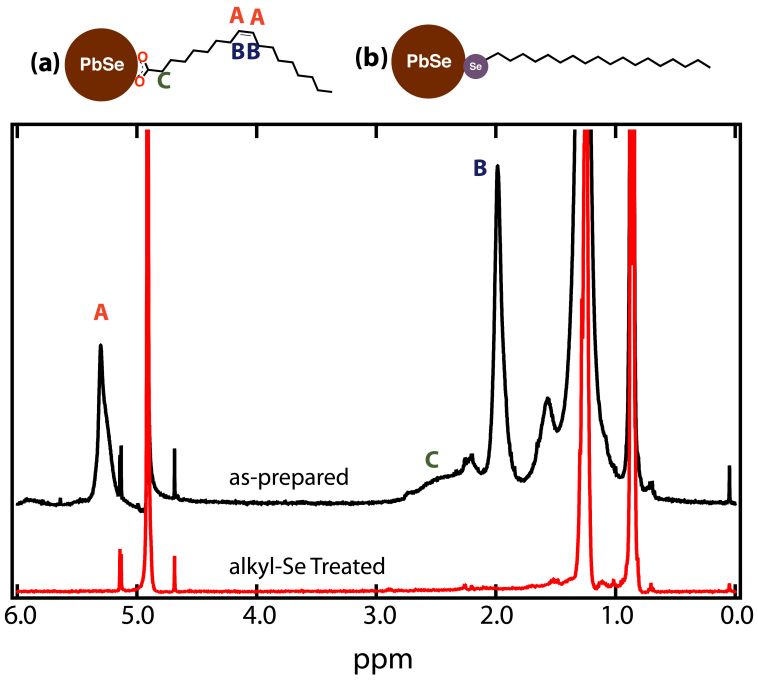

Figure 3.6. NMR Before and After Alkylselenide Treatment
NMR spectra of as-prepared and alkylselenide treated 4.7 nm PbSe; taken in $CDCl_3$ with dibromomethane (~4.9 ppm) as an internal standard.

The most distinctive peak, indicating the presence of oleate, has a chemical shift of 5.34 ppm, which corresponds to the olefinic protons on the internal C-C double bond (Figure 3.6a, region A). The second characteristic oleate resonance is at 2.3 ppm, corresponding to the methylene groups adjacent to the C-C double bond (Figure 3.6a, region B). Finally a broad resonance between 2-3 ppm is observed corresponding to the 2 protons closest to

the carboxylic acid group of oleic acid (Figure 3.6a, region C). Full assignment of the free oleic acid peaks are shown below in Figure 3.7.

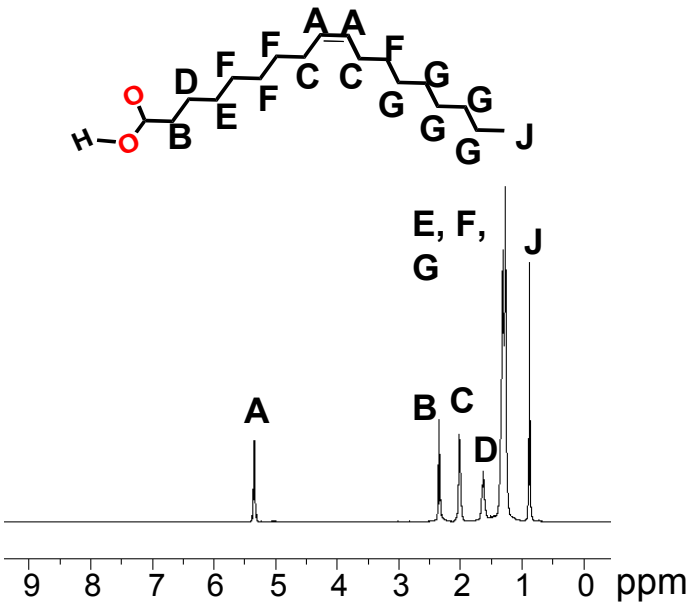

Figure 3.7. ^{1}H NMR for Oleic Acid
The ^{1}H NMR spectrum above is for free oleic acid in $CDCl_3$ along with a peak assignment.[30] The signature peak for oleic acid lies at ~5.4 ppm for the olefinic protons.

It is worth noting here that there is significant broadening in the oleate resonances for QD samples as compared to the free oleic acid spectrum shown in Figure 3.7. Broadened resonance peaks in the NMR spectrum are characteristic features of oleate that is bound to the QD surface. High Resolution Magic Angle Spinning (HRMAS) experiments, give evidence that this broadening is due to the similar but distinct conditions of individual oleic acid molecules on different surfaces of the multifaceted QDs, rather than from an average signal arising from fast exchange of free (oleic acid) and surface-bound (oleate) ligand. Figure 3.8 (red) shows ^{1}H NMR for oleate-capped QDs in toluene-d_8 with free

Pb(oleate)$_2$ producing a resonance at ~5.5 ppm for the olefinic protons and the resonance for olefinic protons of QD-bound ligands downfield at ~5.7 ppm.

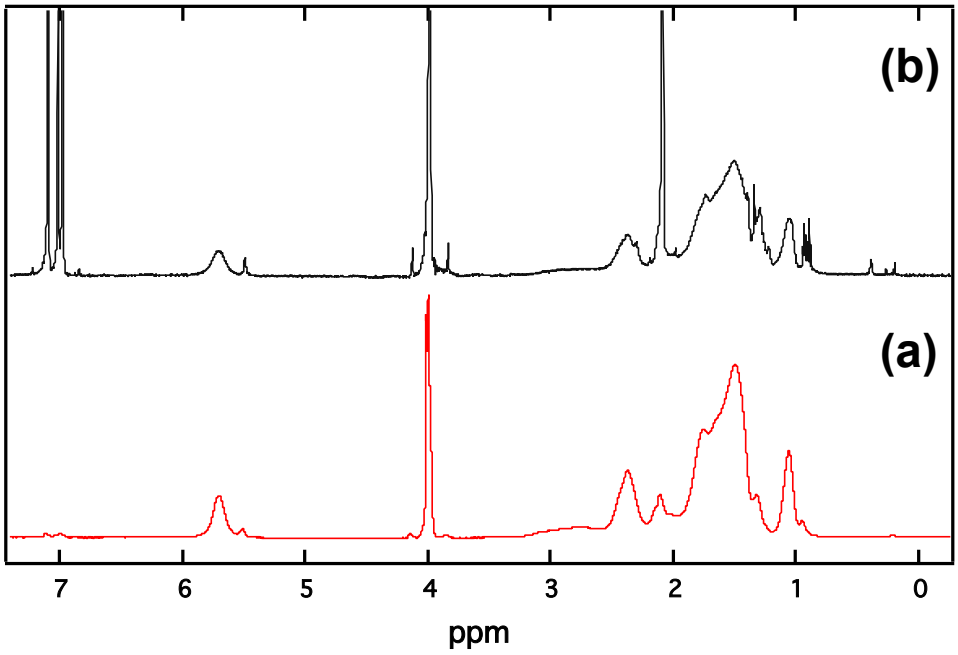

Figure 3.8. Comparing Standard ^{1}H NMR to HR-MAS of Oleate Capped PbSe QDs
(a) ^{1}H NMR spectra of PbSe QDs in toluene-d_8 (red) showing free and bound ligand. **(b)** HR-MAS ^{1}H NMR (black) showing decreased broadening for free oleic acid (~5.5 ppm) and toluene-d_8 (~2 ppm and 7 ppm) while broad resonances are maintained for bound oleate. Ferrocene (~4 ppm) is employed as an internal standard

By spinning at the magic angle, broadening effects due to chemical shift anisotropy are reduced, thereby increasing the spectrum resolution; i.e., differences in chemical shift due to variable molecular orientations are reduced. Figure 3.8 (black) clearly shows that upon spinning at the magic angle resonance for toluene-d_8 as well as those for free oleic acid are in fact sharpened. For bound oleate, however, the resonance corresponding to the olefinic protons (~5.7 ppm) remains broad indicating these molecules are in fact seeing multiple

chemical environments and are not just broadened due to an average between free and surface bound states.

The ^{1}H NMR spectrum recorded following treatment and washing of 4.7 nm QDs indicates a quantitative exchange of oleate for the alkylselenide ligand. The characteristic oleate resonances due to the unsaturation of the alkyl chain (5.34 ppm) are now absent and the only remaining peaks are those in the region between 1-3 ppm, corresponding to the saturated alkyl chains of the bound alkylselenide (Figure 3.6b). Similar investigation of two additional alkylselenide-treated QD samples (7.9 and 2.3 nm) exhibited the same result: absence of the olefinic proton peaks.

In addition to NMR evidence, IR spectroscopy also confirmed the removal of oleate from the QD surface and binding of the alkylselenide ligand. In Figure 3.9 we compare the IR spectra for free oleic acid (a), oleate-capped QDs (b), alkyl-Se-capped QDs (c), free dialkyldiselenide (d), and free alkylselenol (e). Dialkyldiselenide can be distinguished from the alkylselenol by the H-Se stretch (~2300 cm^{-1}) highlighted in Figure 3.10.

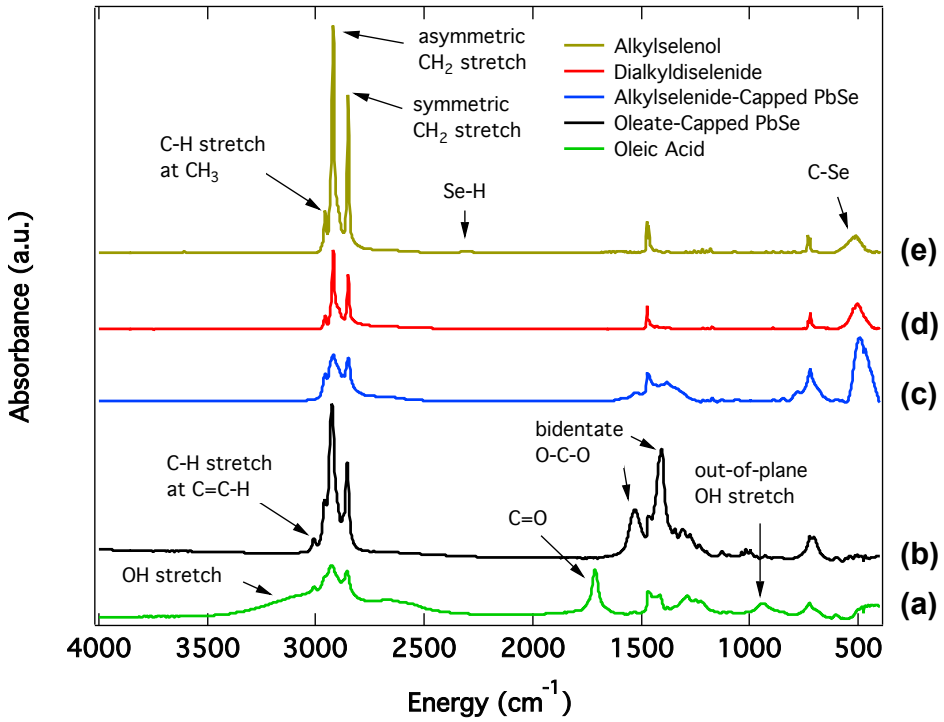

Figure 3.9. FTIR of PbSe QDs and Surface Ligands
FTIR of **(a)** oleic acid, **(b)**oleate-capped 5.7 nm QDs, **(c)** alkylselenide-capped 5.7 nm QDs, **(d)** dialkyldiselenide, and **(e)** alkylselenol.

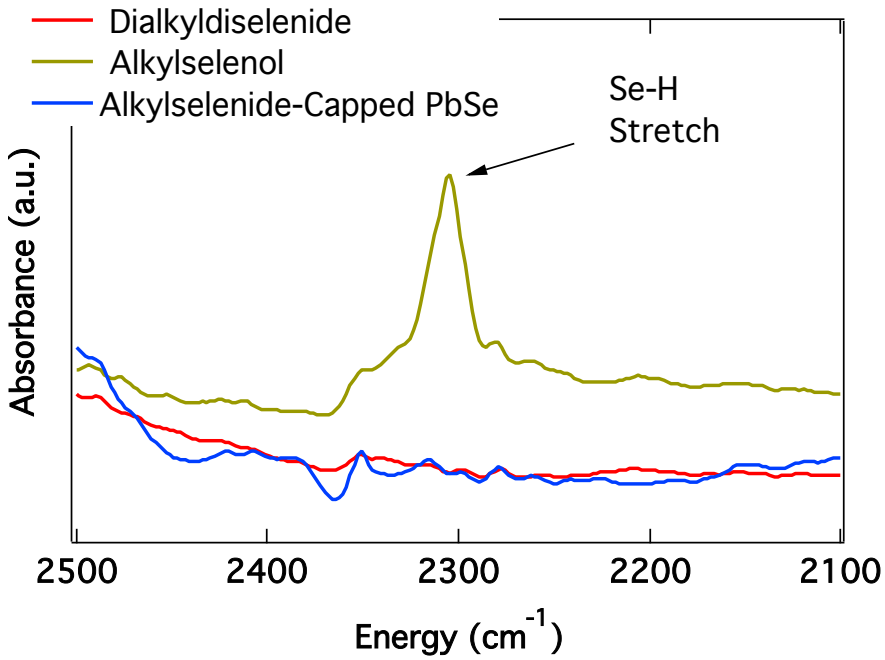

Figure 3.10. FTIR of Free and QD-Bound Se-Ligands on PbSe QDs
FTIR spectra zoomed in for the region between 2500-2100 cm^{-1} to show the characteristic Se-H stretch present only for the alkylselenol ligand.

For each of the Se-ligands, a new absorption is revealed at ~500 cm^{-1} indicative of a Se-C bond[27], which is confirmed in the spectrum for alkyl-Se-capped QDs. It is also notable that the spectrum for alkyl-Se-capped QDs is without the characteristic olefinic C-H stretch seen in oleate-capped QDs, indicating the absence of both oleate at the QD surface and free oleic acid following ligand exchange.

The alkylselenol ligand should react in a 1:1 fashion *via* proton exchange with the existing bound oleate ligands on the QD surface. Therefore, the increase in overall Se content in the QDs following treatment with alkylselenol indicates that we need to more carefully consider the QD-oleate interaction. DFT calculations demonstrated that weakly binding carboxylic acid can bind to the stoichiometric {100} facets while oleate anion

predominates on the {111} surfaces.[16] It is reasonable to suggest that these weakly adsorbed, but not chemically bound, neutral oleic acid ligands would dissociate from the {100} surface in the presence of excess alkylselenol. In this manner, only the {111} surfaces undergo true ligand exchange, and yet all of the surface oleate is removed following exchange. Further, a surface Se anion in the form of the alkylselenide ligand could potentially passivate up to 3 surface Pb atoms, depending on the QD surface facet. This 3-fold bridging is especially applicable to a surface such as the {111} where Pb atoms are more prevalent, while there may be bonding to only 1 or 2 Pb atoms on a {100} surface. Crystal edges, with multiple exposed Pb bonding sites may be even more likely to have single Se anions bridging multiple Pb atoms. Quantitative NMR experiments show 2.97×10^{-6} moles of capping ligand per mg of QDs for as-prepared samples and 2.30×10^{-6} moles/mg for alkylselenide treated QDs. This 22% decrease in surface ligand coverage following exchange from oleate to alkylselenide supports our above hypotheses that neutral oleic acid may also be adsorbed to the QD surface. Experiments to further explore these propositions are ongoing.

3.II.c. Optical Properties and Reduced Oxidation Rate

QD films for spectroscopic studies are dropcast from chloroform solution onto a sapphire substrate, and sealed under inert atmosphere. For the alkylselenide-capped QDs, the absorbance spectrum shows an initial red-shift in the first excitonic peak of approximately 30 meV compared with films of as-prepared QDs (Figure 3.11), suggesting

an increase in QD diameter of not more than 0.3 nm, less than a monolayer for the QD sizes investigated (1-10 nm).[19,20]

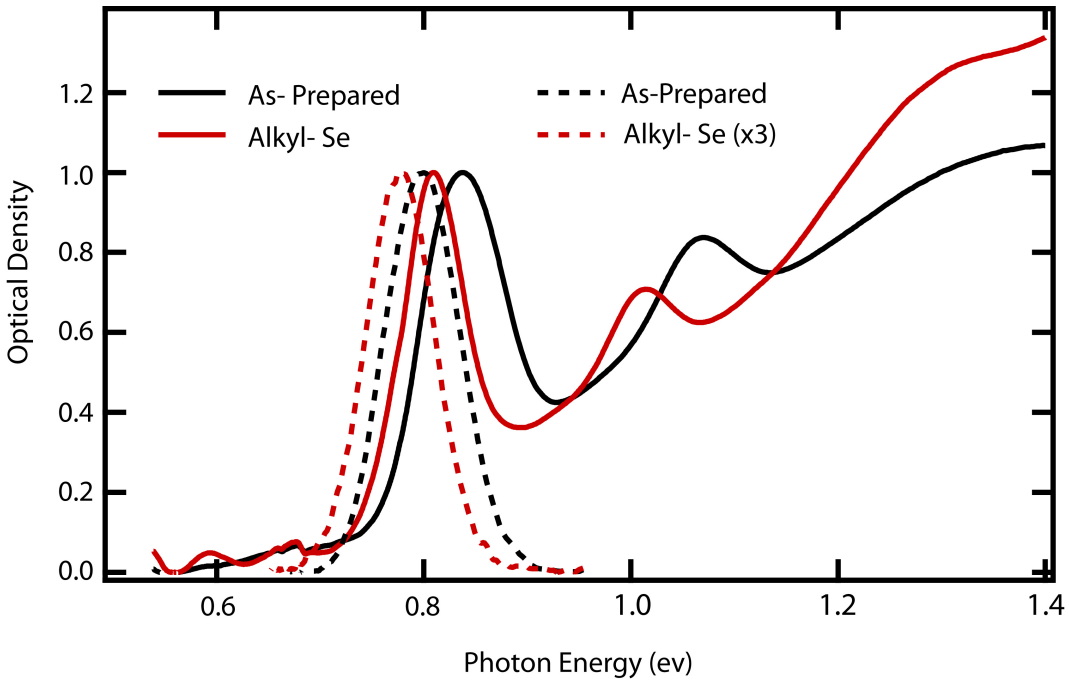

Figure 3.11. Absorption and Emission for Treated and Untreated PbSe QDs
Absorption spectra of as-prepared QDs with diameter of 4.7 nm before and after alkylselenide treatment. The solid lines are for the absorption while the dashed lines are for emission. After treatment the emission efficiency decreases by ~ 3.

For our spectroscopic study, we focused on QDs of intermediate size (4 – 5 nm), which allows for direct comparison to a recent report describing trends in the PL *versus* temperature that exhibited sensitivity to QD surface composition and quality.[1]

The temperature-dependent PL spectra for as-prepared and alkylselenide-treated QDs before (A,D) and after (B,E) exposure to oxygen are presented in Figure 3.12.

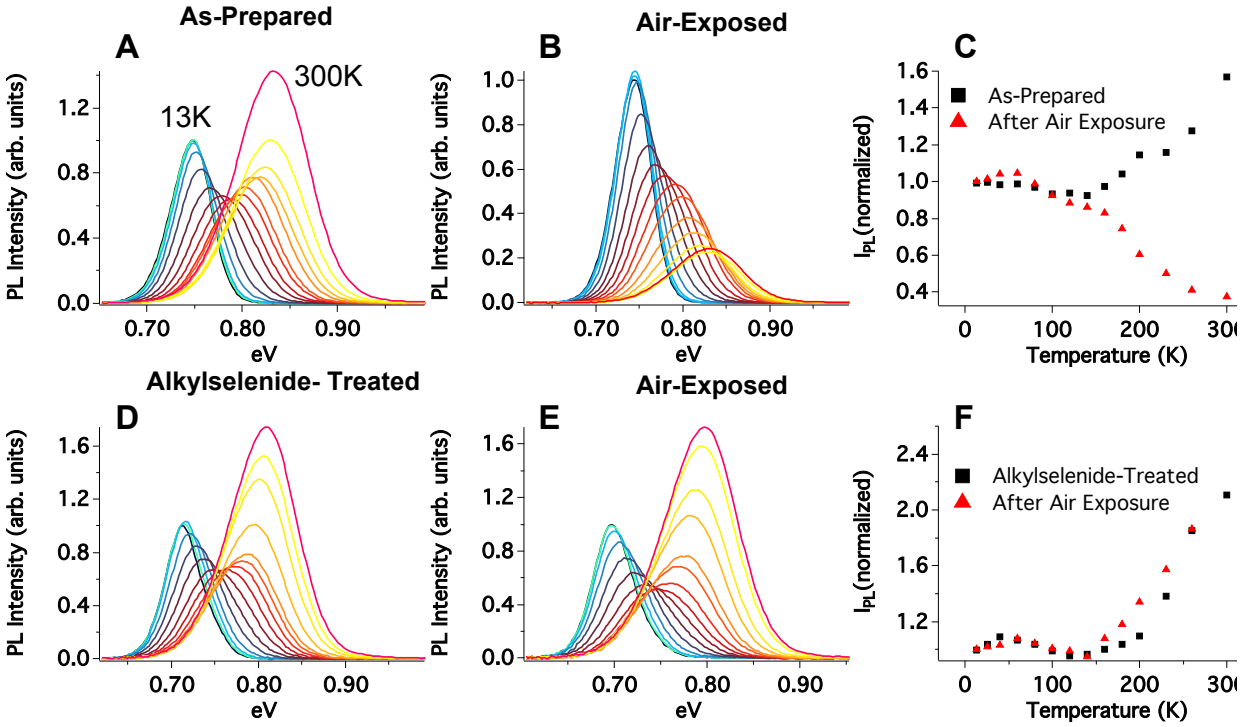

Figure 3.12. Temperature Dependent Photoluminescence of 4.7 nm PbSe
(A-B, D-E) Temperature-dependent photoluminescence data for as-prepared and alkylselenide-treated 4.7 nm PbSe QDs before and after oxygen exposure. **(C)** Integrated PL intensity *vs.* temperature plot for pristine and air-exposed 4.7 nm QDs. **(F)** Integrated PL intensity *vs.* temperature plot for alkylselenide-treated and air-exposed alkylselenide-treated 4.7 nm QDs.

PbSe has a temperature dependent bandgap reported in Figure 3.13. For this size regime the shift of the absorbance peak for the first exciton peak is on the order of 0.01 eV towards higher energy from 13K - 300K. (See Figure 3.13)

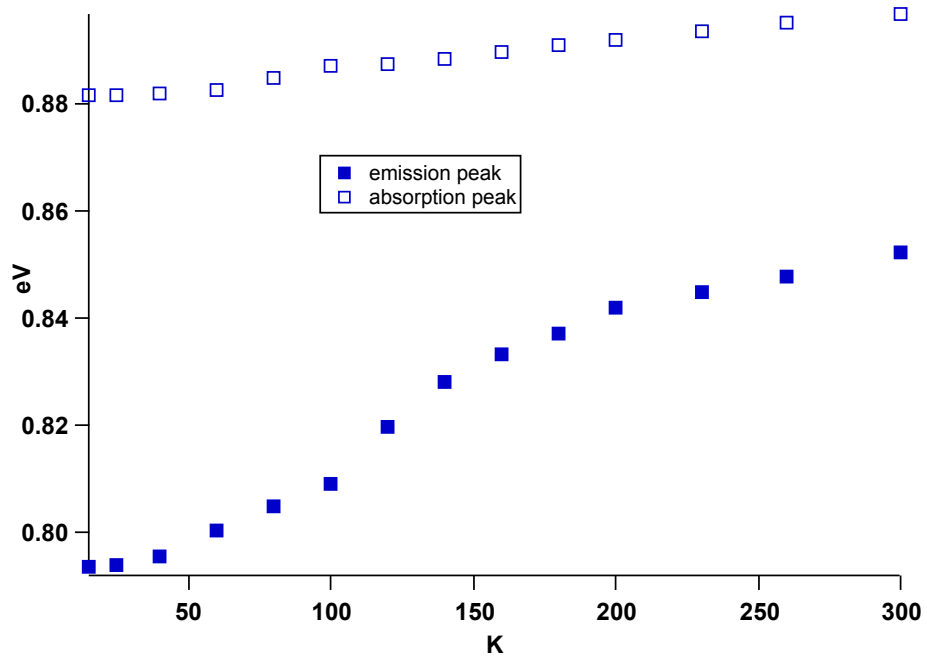

Figure 3.13. **Temperature Dependent Absorption/Emission**
Temperature dependent absorption (open squares) and emission (closed squares) for ~4.5 nm PbSe QDs.

The spectra for as-prepared QDs exhibit a temperature-dependent emission peak shift of 0.1 eV through this temperature range. Since the PL shift is much larger than the absorbance shift, we implement a model invoking two distinct but interacting emitting species. The excited states are denoted **A** and **B**, respectively, and are depicted in the energy band diagrams in Figure 3.14, where **B** is the 8-fold degenerate conduction band and **A** is a lower energy electron trap with the degeneracy of a trap level typically being 2 (with spin up and spin down). Emission from **A** occurs at low temperature, and the population of carriers gradually flows into state **B** as the temperature is increased. Luminescence lifetimes as well as relaxation rates of states **A** and **B** have been reported in the literature. [31] For states **A** and **B** the luminescence lifetimes are ~10.5 μs and 1.36 μs

respectively, while the radiative rates of **A** and **B** are ~0.06 μs^{-1} and 0.279 μs^{-1}. Qualitatively, both of these observations of shorter luminescence lifetimes and faster relaxation times for state **B** likely contribute to the fact that state **B** gives rise to the predominantly observed luminescence at room temperature. At low T (13-100 K), this is not the case only because state **B** is not yet populated, and therefore no luminescence is observed from **B** .

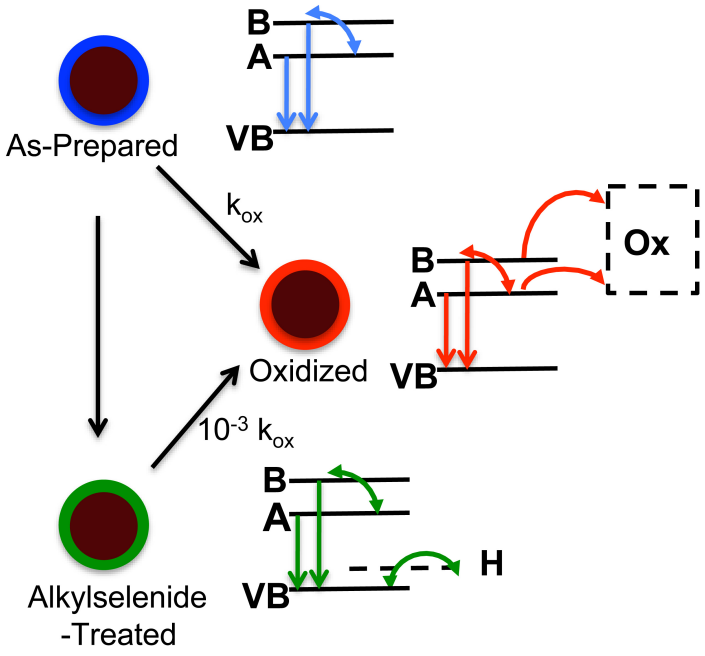

Figure 3.14. Relaxation Pathways for As-Prepared and Treated PbSe QDs
Relaxation pathways for excited populations are shown for as-prepared, oxidized, and alkylselenide-treated QDs. Solid lines indicate bright states, while dashed lines signify dark states. Each QD-type exhibits population flow between states **B** and **A**, as well as radiative decay from bands **A** and **B** to the VB.

A recent investigation of oleate-capped PbSe QDs studied the thermal equilibrium between states **A** and **B** for various QD sizes and developed a phenomenological model to describe the kinetics of the various relaxation pathways.[1] The effect of oxidation was also included

in this model, and it was demonstrated that upon oxidation of as-prepared QDs, an additional relaxation pathway is introduced and is depicted by pathway **Ox** as shown in Figure 3.14. Upon ligand exchange of as-made QDs with alkylselenide, emission from states **A** and **B** are still observed, and we deduce the formation of a new nonradiative decay pathway identified as a hole-trap level, **H**, which we propose to lie near the valence band.

A plot of the integrated PL intensity (I_{PL}(T)), which is proportional to the PLQY, *versus* temperature is given for each sample (Figure 3.12 C,F). Prior to air exposure, I_{PL}(T) plots for as-prepared and alkylselenide-capped QDs are quite similar, though measureable decreases in the room temperature PLQYs (ranging between a factor of 0.3 and 0.5) are observed for alkylselenide-treated particles. This decrease in PLQY at room temperature is attributed to the creation of a low-lying intrinsically dark state associated with the addition of surface selenium as was shown in similar work in CdSe. [26] According to our model, some photoexcited holes become trapped in **H** leading to the significant reduction in the overall PLQY at room temperature compared to as-prepared QDs. Partial alkylselenide termination at the surface may introduce acceptor-like states near the valence band intrinsic to the large, electron-rich Se_{surf} groups. This is similar to P_{surf}-based traps in InP and Se_{surf}-based traps in CdSe.[26,32]

Alongside the previously mentioned decreases in the PLQY observed by the Mulvaney group upon Se termination, we have seen similar effects in our lab for sulfur treatments as well. Treatment of PbSe QDs with sulfur containing ligands such as ethanedithiol and dodecanethiol also show a quenching effect on room temperature emission indicative of hole-related traps due to anion enrichment at the QD surface. There

are literature reports of the addition of sulfur complexes to the surface of very small (< 3 nm) CdSe QDs, which shows an increase in the PLQYs, however, this enhancement only occurs following UV irradiation of these sulfur-treated QDs. [30] Since the effects of UV irradiation on the elemental sulfur (S_8 rings) were not determined definitively, and the resultant surface termination of these CdSe QDs is not known by the authors, a clear comparison cannot be made between this study and our own. It should also be noted that following treatment with S_8, the PLQY remains unchanged begging the question of whether the S_8 ring is only physisorbed or truly chemically bound to the QD surface. Following ring-opening (radical) reactions of S_8 initiated by UV irradiation, the CdSe surface chemistry is certainly more complicated than in our PbSe system.

Although the I_{PL}(T) curves for as-prepared and alkyselenide-capped QDs are similar, noticeable qualitative differences in the shape support the expected change in surface-influenced photophysics. For example, a small rise in I_{PL}(T) occurs at low temperature in alkylselenide QDs but not in as-prepared QD samples (Figure 3.15).

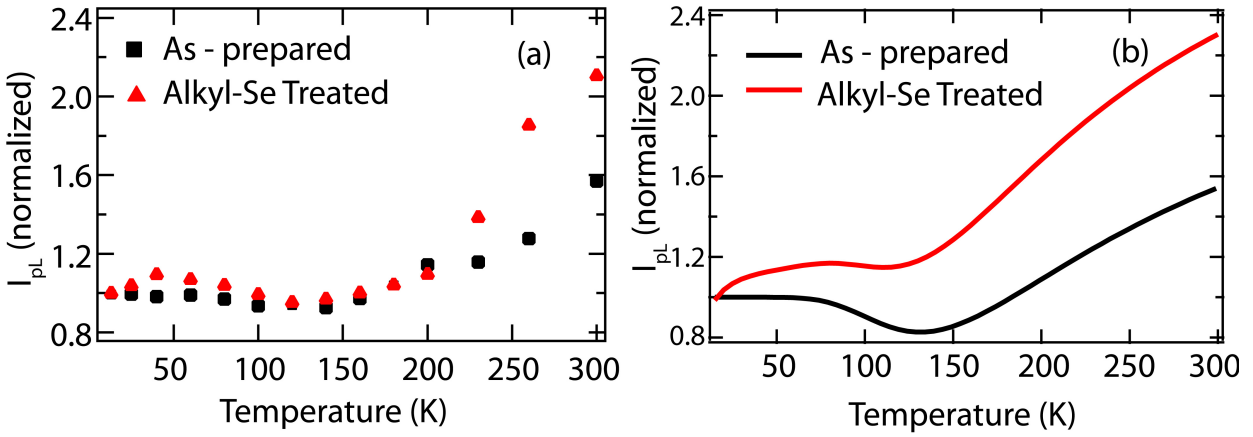

Figure 3.15. Experimental and Simulated Data for I_{PL} *vs* T for 4.7 nm PbSe QDs
(a) Integrated PL intensity *vs.* temperature plot for as prepared and alkylselenide-treated 4.7 nm QDs, showing characteristic rise in I_{PL} at low T for alkylselenide-treated QDs and steeper slope above 150 K. **(b)** Simulated data set that qualitatively matches the measured data, the simulation is described in the text. The red curve was scaled by a factor of 2.5.

This rise is consistent with the thermal activation of holes from the dark state **H** to the **VB** where the radiative transition **A→VB** can occur.[1] This characteristic rise in I_{PL} at low temperatures is also apparent in QDs treated only with elemental Se *via* TOP-Se (data not shown), and the rise is more pronounced for smaller QDs (2-3 nm) as shown in Figure 3.16.

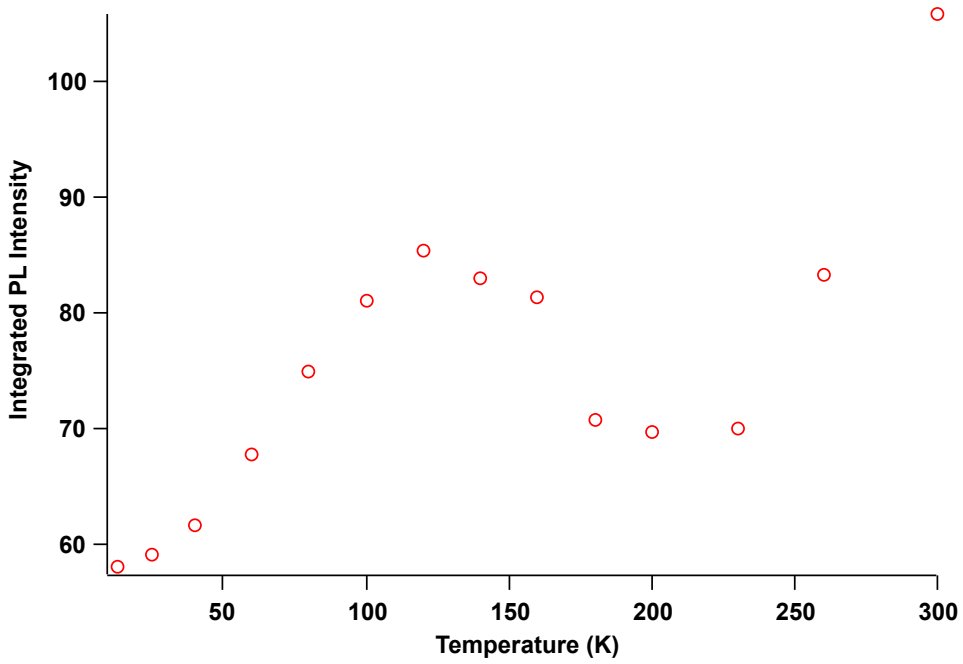

Figure 3.16. Integrated PL *vs.* Temperature for 3.3 nm PbSe QDs
The I_{PL} *vs* T plot of 3.3 nm PbSe shows a more pronounced rise in the data at low temperatures when compared to larger QDs indicative of an increase in the amount of surface Se.

The more pronounced rise for smaller QDs can be correlated with the amount of Se added to the surface (see Figure 3.3a). In addition to a rise in I_{PL}, the steeper slope observed in the I_{PL}(T) above 150K for alkylselenide QDs *vs.* as-prepared samples is indicative of a lower density of **A** states (identified with excess surface Pb) pushing the **A**→**B** equilibrium more strongly toward **B** with increased temperature. A quantitative estimate of state density changes would rely on a more detailed model beyond the scope of this study; however, the qualitative trends strongly suggest that the photophysics is altered by the replacement of Pb-oleate with alkylselenide.

To further support the validity of our hypotheses regarding the normalized I_{PL}(T) curves, we employ here a simulation which is based on the general phenomenological

model presented by Chappell *et al.* In our case, the relatively subtle trends prevented an accurate least-squares fit to the data without significant parameter covariance. Thus this simulation depicts how the relevant trends in our data arise as a function of varying those parameters related to surface trap states. The integrated PL is calculated from

$$I_{PL}(T) = \frac{1}{(1+h\,\exp(-E_h/kT))}\left\{\frac{1}{(1+c\,\exp(\Delta G/kT))\left(1+s\left(\exp\left(E_{ph}/kT\right)-1\right)^{-m}\right)} + \Phi_b\left(1-\frac{1}{1+c\,\exp(\Delta G/kT)}\right)\right\},$$

where F_b is the ratio of the radiative efficiency of state **B** to state **A**, DG is the energy gap between states **A** and **B,** and E_h is the energy of activation between the hole trap **H** and the valence band. E_{ph}, s, and m are parameters relating to carrier-phonon coupling[33], which are floated to fit I_{PL} curves for untreated QDs and then are fixed at the same values for alkylselenide treated QDs, upon the expectation that these terms are independent of surface treatment. We tentatively assign **H** to a hole trap level based upon the consideration discussed below. c represents a statistical weighting of **A** and **B** states, and h is related to the statistical distribution of VB and hole trap states **H**. The higher the values of h, the stronger the influence of hole traps. With all other parameters remaining approximately equal, an increase in h leads to the rise in I_{PL}(T) at low temperature and also the overall smaller value of I_{PL}(T) at room temperature as evidenced in the simulated data in Figure 3.15b. How each of these parameters changes in our simulation is shown in 3.1.

Table 3.1. Fit Parameters As They Vary with Changing Surface Chemistry

	m	F_B	c	$DG(meV)$	s	$E_{ph}(meV)$	h	$E_h(meV)$
As-Prepared	4	4	2	-30.3	0.18	5.2	0	0
Alkylselenide-Treated	4	4	3	-30.3	.18	5.2	2.5	0.35

Besides increasing the values of hole trap parameters h and E_h, a higher value of c for alkylselenide-treated QDs is also needed to produce the larger slope in I_{PL} at higher temperatures as seen in the experimental data. This is indicative of a lower relative ratio of **A**:**B** concentrations, presumably from passivating some fraction of the electron traps **A** that arise from excess Pb.

As-prepared and alkylselenide-capped QD films react very differently following 1 min of air exposure. As-prepared samples exhibit quenching of PL intensity at temperatures above 150 K due to the introduction of oxygen-based non-radiative trap states, as depicted in our model as **Ox** (Figure 3.14).[1] This characteristic quenching of PL intensity for oleate-capped Pb salts is not observed for alkylselenide-capped QDs, even after exposure times of 90 min. This result is most likely due to the formation of a more stable Pb_{surf}-Se bond, which passivates Pb_{surf} sites and impedes oxidation over timescales in which as-prepared QDs undergo oxidative damage. Upon air exposure for multiple hours, the characteristic decay in PL intensity at T > 150 K is observed, signifying surface

oxidation. Nevertheless, the rate of PL quenching is slowed by at least two orders of magnitude for alkylselenide-capped QDs.

3.III. Conclusions

Following treatment with the alkylselenide ligand, QDs exhibit two new properties: (1) they resist short-term oxidation and (2) they adopt the expected photophysical properties of a more stoichiometric QD. The former is an interesting practical result that may allow for short-term processing or characterizing of PbSe QDs in the presence of oxygen, while the latter suggests that controlling the surface composition allows for engineering of specific dynamical behavior. Surface composition naturally changes with QD size and thus surface chemistry is usually an uncontrolled variable in size-dependent studies. Trends for various properties that are believed to be dependent on QD size, such as PLQY[34] and electron/hole mobilities[4], may at least in part be dictated more definitively with surface composition. Since surface effects can dominate both the photophysical and electrical properties of QDs, tailoring of the surface to enhance beneficial properties, such as improved transport, is a potentially powerful tool.

The surface exchanges presented here can easily be translated to other Pb-chalcogenide systems and to various Pb-chalcogenide nanostructures, with the end goal of a more robust QD surface. This type of surface passivation holds promise to enable further exploration of the effects of surface modification on photophysical and materials properties, including carrier dynamics. Consequences of this surface treatment

methodology for carrier mobility and doping in electronically-coupled QD films will be investigated employing similar alkylchalcogenide compounds with tunable ligand lengths.

3.IV. Materials and Methods

All chemicals were used as received without further purification. Selenium (99.99%), sodium borohydride (99.99%), oleic acid (90%), 1-iodooctadecane (90%) diphenylphosphine(DPP, 98%), trioctylphosphine (TOP 90%), anhydrous ethanol, hexane, and tetrachloroethylene (TCE 99.9%) were purchased from Aldrich and used as received Lead oxide (99.999%) was purchased from Alfa Aesar. The diselenide and selenol reagents were prepared using dry and/or degassed solvents and standard Schlenk techniques under a nitrogen atmosphere. *Warning*: A small amount of H_2Se is released in the early stages of these reactions. Due to the high toxicity of this volatile compound, all manipulations should be performed in a fume hood with adequate ventilation. In addition, excess nitrogen flow from these reactions was bubbled through a 5 wt% aqueous lead acetate solution to trap the volatile H_2Se as solid PbSe.

3.IV.a. Synthesis of dioctadecyl diselenide (1): $\mathbf{H_{37}C_{18}Se - SeC_{18}H_{37}}$

This preparation was adapted from a literature procedure of similar dialkyl diselenides.[27] Cooled, degassed absolute ethanol (50 mL) was added via cannula to a cooled (0 °C) solid mixture of Se metal (1.0 g, 12.7 mmol) and sodium borohydride (0.34 g, 8.9

mmol) under nitrogen. The reaction bubbled vigorously for about 1 min (releasing a small amount of H_2Se), and changed to dark red in color, indicative of the formation of Na_2Se_2. After 15 min at 0 °C, the dark red solution was heated at reflux for 30 min to complete the formation of Na_2Se_2. After cooling to room temperature, a solution of 1-iodooctadecane (3.4 g, 8.9 mmol) in THF (15 mL) was added dropwise via syringe. After 15 min at room temperature, the reaction was heated at lux for 2 hours. The reaction was then cooled and acidified via the addition of ca. 2 mL of acetic acid. The yellow product began to precipitate from the solution, but was redissolved with chloroform (40 mL). To ensure that any trace H_2Se was fully expelled from the reaction flask, nitrogen was bubbled directly through the reaction mixture for 15 min. The solution was then extracted with water (2 x 30 mL), dried over $MgSO_4$, and filtered. The solvent was removed *in vacuo*, leaving analytically pure, solid yellow product (2.43 g, 82%). ^{1}H NMR (400 MHz, chloroform-*d*, 20 °C) d 2.91 (t, 2H), 1.72 (pent, 2H), 1.26 (m, 30H), 0.88 (t, 3H). ^{13}C{^{1}H} NMR (100 MHz, chloroform-*d* , 20 °C) d 31.9, 31.0, 30.3, 29.7, 29.6, 29.5, 29.4, 29.1, 22.7, 14.1. Anal. Calcd for $C_{36}H_{74}Se_2$: C, 65.03; H, 11.22. Found: C, 64.63; H, 10.91.

3.IV.b. Synthesis of octadecylselenol (2) : $\mathbf{HSeC_{18}H_{37}}$

Cooled, degassed absolute ethanol (20 mL) was added via cannula to a cooled (0 °C) solid mixture of Se metal (0.60 g, 7.6 mmol) and sodium borohydride (0.32 g, 8.4 mmol) under nitrogen. A pale orange-red color develops over ca. 15 min at 0 °C. The reaction was allowed to warm to room temperature and stirred for 30 min. A solution of 1-

iodooctadecane (2.9 g, 7.6 mmol) in THF (15 mL) was added dropwise via syringe. The reaction was stirred at 30 °C for 90 min, followed by cooling to 0 °C, and quenching with dilute aqueous HCl. Chloroform (15 mL) was added, and nitrogen was bubbled through the solution to remove any trace H_2Se. The solution was extracted with water (2 x 30 mL), dried over $MgSO_4$, and filtered. The solvent was removed in vacuo, and the off-white product was stored in a glovebox. The crude product (2.0 g, 79%) is 85% pure by ^1H NMR analysis. Analytically pure, colorless product (1.3 g, 51%) can be isolated via sublimation (120 °C, 0.005 mmHg). ^1H NMR (400 MHz, chloroform-*d*, 20 °C) d 2.58 (q, 2H), 1.70 (pent, 2H), 1.26 (m, 30H), 0.88 (t, 3H), -0.69 (t, 1H, Se-*H*). $^{13}C\{^1H\}$ NMR (100 MHz, chloroform-*d*, 20 °C) d 34.0, 31.9, 29.7, 29.6, 29.5, 29.4, 29.0, 22.7, 17.7, 14.1. Anal. Calcd for $C_{18}H_{38}Se$: C, 64.83; H, 11.49. Found: C, 65.13; H, 11.23.

3.IV.c. Synthesis of alkylselenide-capped PbSe QDs via two-injection method

A solution of $Pb(oleate)_2$ was prepared by heating PbO (0.25 g, 1.12 mmol) with oleic acid (0.633g, 2.24 mmol) in 1-octadecene (8 mL). This solution was heated to 100 °C under vacuum for 10 min before being degassing under N_2 for 30 min. The reaction temperature was increased to 160 °C before first injection of 1 M TOP-Se (2.24 mL) containing diphenyl phosphine (0.035g, 0.188 mmol). A second solution containing dioctadecyl diselenide (0.037g .025 mmol) in a minimum amount of $CHCl_3$ was injected 25 sec after the first injection. The reaction was heated continuously for another 20 sec following the second injection, at which point the reaction was removed from heating and

quenched with 10 mL hexane. The resulting particles were washed twice by precipitation with EtOH and isolated by centrifugation.

3.IV.d. Synthesis of alkylselenide-capped PbSe QDs via ligand exchange

PbSe QDs were prepared according to previously reported methods.[23] [35] For exchange using **1**, 250 mg of QDs were dispersed in 7 mL hexane, followed by the addition of **1** (0.035 g, 0.048 mmol) and DPP (0.003g, 0.016 mmol). This solution was allowed to stir for 2-days, after which the QDs were observed to precipitate from solution. The particles were washed twice with hexane, isolated by centrifugation, and redispersed in $CHCl_3$. Similarly, for exchange using **2**, the QDs (0.250 g) were dispersed in 7 mL hexane and **2** (0.009 g, 0.027 mmol) was added. Upon gentle stirring, the QDs precipitated from solution within minutes. The particles were washed twice with hexane, isolated by centrifugation, and redispersed in $CHCl_3$.

3.IV.e. Synthesis of Hexapods

A solution of $Pb(oleate)_2$ in 1-octadecene was heated to 180 °C in the presence of 0.035 g of **1**. To this solution 1 mL of trioctylphosphine with 0.020 g DPP was quickly injected. The reaction was heated continuously for 40 seconds following injection. The resulting particles were precipitated with EtOH and redispersed in $CHCl_3$.

3.IV.d Film Preparation

Films were dropcast onto a sapphire substrate from a solution of ~5-10 mg/mL of QDs in a 4:1 hexane/octane solution. The resulting films were macroscopically uniform, essentially opaque at the excitation wavelength (488 nm), and were estimated to be greater than 100 nm thick. Films were sealed in a copper gasket with an o-ring between a second sapphire window. For air exposure studies, the airtight seal on the sample holder was broken and the films were exposed to ambient air in the dark. The films were resealed in the glove box before PL was measured again.

3.IV.e Characterization

Elemental analyses for treated QDs were performed by Galbraith Laboratories (Knoxville, TN) using inductively-coupled plasma optical emission spectroscopy (ICP-OES). Elemental analyses for compounds 1 and 2 were performed by Huffman Laboratories in Golden, CO. NMR experiments were performed on a Varian Inova 400 MHz Spectrometer. Prior to ligand exchange, NMR spectra were recorded using toluene-d_8 as solvent, which allowed us to distinguish between free and bound OA. High Resolution Magic Angle Spinning (HRAS) experiments were performed on a Bruker Avrance III NMR Spectrometer 600 MHz using toluene-d_8 as the solvent. All spectra of exchanged QDs were taken in chloroform-*d* due to their insolubility in toluene. High-resolution transmission electron microscopy (HR-TEM) was carried out using a Philips CM 200 at 120 kV. Fourier transform

infrared (FTIR) absorbance spectra were recorded on a Thermo-Nicolet 6700 FTIR spectrometer in transmission mode with a resolution of 4 cm^{-1}. For photoluminescence films were left stationary in the PL system during the measurement of a sample across the entire temperature range, which was always collected beginning at 13 K and warming up to 325 K. No significant difference was noted for data collected while cooling from 325 K to 13 K. The sample was allowed to fully equilibrate at each temperature (i.e. until the PL spectrum remained constant, about 5-10 minutes). PL spectra were recorded under vacuum ($<10^{-5}$ Torr) in a closed-loop He cryostat. Films were excited with 10–20 mW Ar ion laser excitation at 488 nm, mechanically chopped at 1 kHz, and unfocused (spot size roughly 3 mm diameter). The resulting PL spectra were detected with an amplified InSb photodiode routed to a lock-in amplifier. Spectra were corrected for monochromator and detector efficiencies using a calibrated lamp. Representative temperature-dependent PL spectra were reported for each sample set and these spectra were reproducible within 7% error. This error is most probably due to inhomogeneities in film surfaces between samples.

References

(1) Chappell, H. E.; Hughes, B. K.; Beard, M. C.; Nozik, A. J.; Johnson, J. C.,Emission Quenching in PbSe Quantum Dot Arrays by Short-Term Air Exposure. *J. Phys. Chem. Lett.* **2011**, *2*, 889-893.

(2) Lingley, Z.; Lu, S.; Madhukar, A.,A High Quantum Efficiency Preserving Approach to Ligand Exchange on Lead Sulfide Quantum Dots and Interdot Resonant Energy Transfer. *Nano Lett.* **2011**, *11*, 2887-2891.

(3) Tang, J.; Brzozowski, L.; Barkhouse, D. A. R.; Wang, X.; Debnath, R.; Wolowiec, R.; Palmiano, E.; Levina, L.; Pattantyus-Abraham, A. G.; Jamakosmanovic, D.*et al.*,Quantum Dot Photovoltaics in the Extreme Quantum Confinement Regime: The Surface-Chemical Origins of Exceptional Air- and Light-Stability. *ACS Nano* **2010**, *4*, 869-878.

(4) Liu, Y.; Gibbs, M.; Puthussery, J.; Gaik, S.; Ihly, R.; Hillhouse, H. W.; Law, M.,Dependence of Carrier Mobility on Nanocrystal Size and Ligand Length in PbSe Nanocrystal Solids. *Nano Lett.* **2010**, *10*, 1960-1969.

(5) Midgett, A. G.; Hillhouse, H. W.; Hughes, B. K.; Nozik, A. J.; Beard, M. C.,Flowing versus Static Conditions for Measuring Multiple Exciton Generation in PbSe Quantum Dots. *J. Phys. Chem. B* **2010**, *114*, 17486-17500.

(6) Sykora, M.; Koposov, A. Y.; McGuire, J. A.; Schulze, R. K.; Tretiak, O.; Pietryga, J. M.; Klimov, V. I.,Effect of Air Exposure on Surface Properties, Electronic Structure, and Carrier Relaxation in PbSe Nanocrystals. *ACS Nano* **2010**, *4*, 2021-2034.

(7) Semonin, O. E.; Luther, J. M.; Choi, S.; Chen, H.-Y.; Gao, J.; Nozik, A. J.; Beard, M. C.,Peak External Photocurrent Quantum Efficiency Exceeding 100% via MEG in a Quantum Dot Solar Cell. *Science* **2011**, *334*, 1530-1533.

(8) Hillhouse, H. W.; Beard, M. C.,Solar cells from colloidal nanocrystals: Fundamentals, materials, devices, and economics. *Curr. Opin. Colloid Interface Sci.* **2009**, *14*, 245-259.

(9) Kramer, I. J.; Sargent, E. H.,Colloidal Quantum Dot Photovoltaics: A Path Forward. *ACS Nano* **2011**, *5*, 8506-8514.

(10) Schliehe, C.; Juarez, B. H.; Pelletier, M.; Jander, S.; Greshnykh, D.; Nagel, M.; Meyer, A.; Foerster, S.; Kornowski, A.; Klinke, C.*et al.*,Ultrathin PbS Sheets by Two-Dimensional Oriented Attachment. *Science* **2010**, *329*, 550-553.

(11) Lovingood, D. D.; Achey, R.; Paravastu, A. K.; Strouse, G. F.,Size- and Site-Dependent Reconstruction in CdSe QDs Evidenced by 77Se{1H} CP-MAS NMR Spectroscopy. *J. Am. Chem. Soc.* **2010**, *132*, 3344-3354.

(12) Gai, Y.; Peng, H.; Li, J.,Electronic Properties of Nonstoichiometric PbSe Quantum Dots from First Principles. *J. Phys. Chem. B* **2009**, *113*, 21506-21511.

(13) Petkov, V.; Moreels, I.; Hens, Z.; Ren, Y.,PbSe quantum dots: Finite, off-stoichiometric, and structurally distorted. *Phys. Rev. B* **2010**, *81*.

(14) Fang, C.; van Huis, M. A.; Vanmaekelbergh, D.; Zandbergen, H. W.,Energetics of Polar and Nonpolar Facets of PbSe Nanocrystals from Theory and Experiment. *ACS Nano* **2010**, *4*, 211-218.

(15) Dai, Q.; Wang, Y.; Li, X.; Zhang, Y.; Pellegrino, D. J.; Zhao, M.; Zou, B.; Seo, J.; Wang, Y.; Yu, W. W.,Size-Dependent Composition and Molar Extinction Coefficient of PbSe Semiconductor Nanocrystals. *ACS Nano* **2009**, *3*, 1518-1524.

(16) Argeri, M.; Fraccarollo, A.; Grassi, F.; Marchese, L.; Cossi, M.,Density Functional Theory Modeling of PbSe Nanoclusters: Effect of Surface Passivation on Shape and Composition. *J. Phys. Chem. B* **2011**, *115*, 11382-11389.

(17) Voznyy, O.,Mobile Surface Traps in CdSe Nanocrystals with Carboxylic Acid Ligands. *J. Phys. Chem. B* **2011**, *115*, 15927-15932.

(18) Choi, J. J.; Bealing, C. R.; Bian, K.; Hughes, K. J.; Zhang, W.; Smilgies, D.-M.; Hennig, R. G.; Engstrom, J. R.; Hanrath, T.,Controlling Nanocrystal Superlattice Symmetry and Shape-Anisotropic Interactions through Variable Ligand Surface Coverage. *J. Am. Chem. Soc.* **2011**, *133*, 3131-3138.

(19) Moreels, I.; Lambert, K.; De Muynck, D.; Vanhaecke, F.; Poelman, D.; Martins, J. C.; Allan, G.; Hens, Z.,Composition and size-dependent extinction coefficient of colloidal PbSe quantum dots. *Chem. Mater.* **2007**, *19*, 6101-6106.

(20) Smith, D. S., D. K.; Luther, J. M.; Semonin, O. E.; Nozik, A. J.; Beard, M. C.,Tuning the Synthesis of Ternary Lead Chalcogenide Quantum Dots by Balancing Precursor Reactivity. *ACS Nano* **2011**, *5*, 183-190.

(21) Moreels, I.; Fritzinger, B.; Martins, J. C.; Hens, Z.,Surface Chemistry of Colloidal PbSe Nanocrystals. *J. Am. Chem. Soc.* **2008**, *130*, 15081-15086.

(22) Bealing, C. R.; Baumgardner, W. J.; Choi, J. J.; Hanrath, T.; Hennig, R. G.,Predicting Nanocrystal Shape through Consideration of Surface-Ligand Interactions. *ACS Nano* **2012**, *6*, 2118-2127.

(23) Law, M.; Luther, J. M.; Song, O.; Hughes, B. K.; Perkins, C. L.; Nozik, A. J.,Structural, optical, and electrical properties of PbSe nanocrystal solids treated thermally or with simple amines. *J. Am. Chem. Soc.* **2008**, *130*, 5974-5985.

(24) Allgaier, R. S.; Scanlon, W. W.,Mobility of Electrons and Holes in PbS, PbSe and PbTe between Room Temperature and 4.2 K. *Phys. Rev.* **1958**, *111*, 1029-1037.

(25) Franceschetti, A.,Structural and electronic properties of PbSe nanocrystals from first principles. *Phys. Rev. B* **2008**, *78*.

(26) Mulvaney, P.; Jasieniak, J.,From Cd-rich to Se-rich - The manipulation of CdSe nanocrystal surface stoichiometry. *J. Am. Chem. Soc.* **2007**, *129*, 2841-2848.

(27) Klayman, D. L.; Griffin, T. S.,Reaction of Selenium with Sodium-Borohydride in Protic Solvents-Facile Method for Introduction of Selenium into Organic Molecules. *J. Am. Chem. Soc.* **1973**, *95*, 197-200.

(28) Koval, I. V.,Chemistry of Disulfides *Usp. Khim.* **1994**, *63*, 776-792.

(29) Bian, K.; Choi, J. J.; Kaushik, A.; Clancy, P.; Smilgies, D.-M.; Hanrath, T.,Shape-Anisotropy Driven Symmetry Transformations in Nanocrystal Superlattice Polymorphs. *ACS Nano* **2011**, *5*, 2815-2823.

(30) Rene-Boisneuf, L.; Scaiano, J. C.,Sensitivity versus Stability: Making Quantum Dots More Luminescent by Sulfur Photocuring without Compromising Sensor Response. *Chem. Mater.* **2008**, *20*, 6638-6642.

(31) Kigel, A.; Brumer, M.; Maikov, G. I.; Sashchiuk, A.; Lifshitz, E.,Thermally Activated Photoluminescence in Lead Selenide Colloidal Quantum Dots. *Small* **2009**, *5*, 1675-1681.

(32) Poles, E.; Selmarten, D. C.; Micic, O. I.; Nozik, A. J.,Anti-Stokes photoluminescence in colloidal semiconductor quantum dots. *Appl. Phys. Lett.* **1999**, *75*, 971-973.

(33) Morello, G.; De Giorgi, M.; Kudera, S.; Manna, L.; Cingolani, R.; Anni, M.,Temperature and size dependence of nonradiative relaxation and exciton-phonon coupling in colloidal CdTe quantum dots. *J. Phys. Chem. B* **2007**, *111*, 5846-5849.

(34) Semonin, O. E.; Johnson, J. C.; Luther, J. M.; Midgett, A. G.; Nozik, A. J.; Beard, M. C.,Absolute Photoluminescence Quantum Yields of IR-26 Dye, PbS, and PbSe Quantum Dots. *J. Phys. Chem. Lett.* **2010**, *1*, 2445-2450.

(35) Bawendi, M. G.; Steckel, J. S.; Yen, B. K. H.; Oertel, D. C.,On the mechanism of lead chalcogenide nanocrystal formation. *J. Am. Chem. Soc.* **2006**, *128*, 13032-13033.

Chapter 4

Electronic Impurity Doping of PbSe QDs

Abstract

Intentional impurity doping of colloidal PbSe quantum dots (QDs) could lead to better control over many desirable electrical and optical properties such as photoluminescence quantum yields, charge-carrier mobilities for QD-films, and enhanced multiple exciton generation. Impurity doping can be tailored by modulating the concentration of the desired dopant or surface atoms post-synthetically. We have investigated a method of chemically doping PbSe QDs through the introduction of low levels of impurity metals such as Cu^{+}, Ag^{+}, and In^{3+}, which may add to the surface and/or intercalate the QDs, and we have studied the resulting effects on photophysical properties including the appearance of a low-energy intraband transition and a 1^{st} exciton bleach. Substitutional doping of PbSe QDs with aliovalent metal cations allows for modulation of the dominant carrier type and its density without the need for harsh chemical treatments.

4.I. Introduction

The intentional introduction of impurity atoms into semiconductors has been employed for a number of years in order to enhance/modulate electrical, optical and magnetic properties and effect materials performance in technologies such as solar cells, LEDs, thermoelectrics and other optoelectronics. Materials can be doped either n-type (adding extra electrons) or p-type (adding extra holes.) The effect of doping a semiconductor is a change in the materials electronic structure. Dopants can effect the position of the Fermi level as well as create acceptor/donor levels above the valence and below the conduction band levels respectively. The addition of extra charge carriers serves to enhance electrical transport through materials with poor conductivity. Chemical doping in bulk semiconductors such as Si and Ge has been performed for over half a decade in order to produce a p-n junction, which lies at the heart of most modern electronics.

4.I.a. p-n junction

A prototypical p-n junction is shown in Figure 4.1a. A p-n junction is a semiconductor architecture in which a single crystalline semiconductor (bulk) is doped so that it maintains an n-type and a p-type region without grain boundaries between them. The interface between these two regions is known as a p-n junction. When these two regions first come into contact, equilibrium is reached and a space charge region (depletion region) forms between them as electrons move towards the p-type material leaving behind positively charged vacancies, and likewise holes move towards the n-type material. With a non-neutral region at the junction, an electric field results from the separation of charges.

This field prevents further diffusion of carriers into opposing regions. With this architecture, carriers are allowed to flow in only one direction (a diode). The energy bands for a p-n junction in a photo-excited semiconductor are shown below in Figure 4.1b, which illustrates how the electrons and holes move in opposite directions allowing carriers to be collected independently following photon absorption. The carrier concentration can be manipulated by changing the doping levels on either side of the junction. These ideas that have been used to successfully create bulk heterojunctions would ideally be employed when building QD solar cells in which a heterojunction can then be created using the same QD materials with different doping levels.

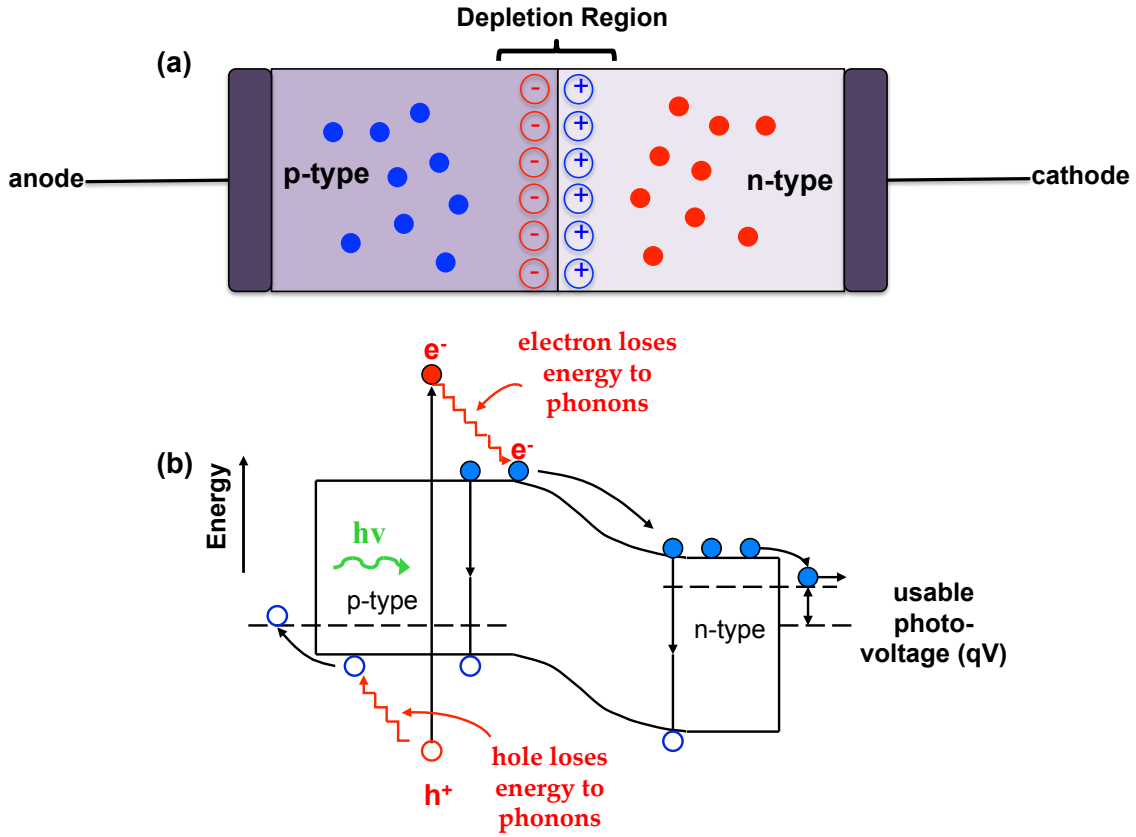

Figure 4.1. P-N Junction
(a) Typical p-n junction for a semiconductor material showing the depletion region at the junction where electrons from the n-type region that have reached the conduction band have diffused across the junction and combined with holes to form negative ions and leaving behind positive ions. **(b)** Energy bands at a p-n junction following absorption of a photon, showing the creation of "hot carriers" and the flow of current in only one direction, with electrons moving towards the cathode and holes moving towards the anode. Excitons may also recombine before the effective collection of charge.

4.I.b. Nanocrystal Doping: Mechanisms and Challenges

The traditional methods for doping bulk semiconductors (introduction during growth or diffusion of impurities at high temperatures) do not carry over precisely to the nanoscale. Traditionally it has been difficult to successfully introduce dopants to nanocrystals with some early assessments being that nanoparticles were "undopable." [1] A

number of different theories have been proposed with regard to the mechanism of impurity doping in nanocrystals and explanations as to why this endeavor has proven to be so challenging. Three models to explain doping in semiconductor nanocrystals have been presented in the literature. [2] The first of which is derived from Turnbull et al. on the nature of introducing impurities to very small crystals or crystallites. [3] Turnbull argues that while the doping mechanism (or dopant solubility) for bulk and nanocrystalline material is the same, the presence of fewer atoms in a nanocrystalline material should lead to a lower probability of incorporation into the crystal lattice. The underlying idea here being that upon doping nanocrystal QDs, even with a single dopant atom per nanocrystal, would exceed the solubility limit for that impurity in the semiconductor, thus leading to a thermodynamic barrier to further doping in the QD material. A second, very popular, model for doping, or the difficulty therein, relies on the idea of self-purification. [4,5] According to this mechanism, in order to reach a thermodynamic minimum in energy, semiconductor nanocrystals expel impurities to their surface if introduced during growth. The self-purification model also purports that impurity diffusion through nanocrystals is less than that in bulk, and there is, therefore, a minimum reaction temperature required for the successful introduction of dopants. Impurity doping is then incompatible with the relatively low reaction temperatures (~100-300 C) employed for colloidally grown nanocrystals. A final mechanism for semiconductor nanocrystal doping has been proposed that invokes a kinetic argument for dopant addition during nanocrystal growth. [6,7] Here doping efficiency is determined by the ease with which a dopant atom can bind to the nanoparticle surface before then being over-coated with additional semiconductor

materials. This argument makes both the composition and faceted nature of the nanoparticle surface key factors.

4.I.c. Doping in Semiconductor QDs

Despite initial difficulties, doping of semiconductor nanoparticles has been achieved successfully for a number of QD systems. To date there are three key strategies in the literature that have traditionally been employed for doping QDs: remote doping, electrochemical doping, and electronic impurity doping. During remote doping, a molecule with an electron withdrawing or donating group is placed in the vicinity of the QD surface either chemically bound or physisorbed. This molecule then undergoes redox chemistry at the QD surface doping either n-type (electron-donating molecule) or p-type (electron-withdrawing molecule). Remote chemical doping has been observed for PbSe QD films exposed to buffer solutions containing the ferrocene/ferrocenium redox pair to control the dominate carrier type[8], while n-type doping of CdSe QDs has been observed upon addition of sodium biphenyl to QD solutions. [9] Electrochemical doping is achieved through the application of an external electric field to QD films and has also been observed in samples of both PbSe[10] and CdSe.[11] The latter two methods of QD-doping, while effective and useful for performing spectroscopic measurements and observing the resulting properties of doped QDs, become less conventional for applications such as building QD solar cells or any optoelectronic device where a p-n junction must be present. One such spectroscopic property that has been observed upon doping QDs using the latter two methods is an

intraband absorption from the $1S_e$-$1P_e$ or conversely from the $1S_h$-$1P_h$. This transition results from the presence of extra carriers injected into the $1S_e/1S_h$ levels causing a bleach of the first exciton transition upon excitation and the subsequent intraband absorption ($1S_e$-$1P_e$). In comparison to electronic impurity doping these two methods can be considered relatively clean experiments due to the lack of changes to the QD composition.

The final doping strategy, electronic impurity doping, involves the addition of impurity atoms (typically heterovalent) either substitutionally or interstitially into the QD lattice. This doping method has the added flexibility of achieving QD doping by manipulation of the QD composition at either the surface or interior positions. There are at least four approaches towards electronic impurity doping: single source precursors, nucleation doping, surface treatments, and cation diffusion. A multitude of semiconductor QDs have been impurity doped in this manner[12-16]; though this method has been problematic on a number of fronts for reasons discussed previously for doping nanoparticles. Electronic impurity doping, while more complex and difficult to characterize, has been shown to affect both optical and electronic properties. For example, at low doping levels (<5 impurity atoms/NC), the addition of Ag^+ to CdSe shows enhancement in PLQYs as well as increased film conductivity.[12] Similar Ag+ doping studies for PbSe indicated lowering of the Fermi level and lead to films with a lower charge-transport activation energy (E_A). [13] Magneto-optical properties have been observed for core/shell particles of ZnSe/CdSe doped with paramagnetic impurities like Co^{2+} [17], and the addition of Mn^{2+} to CdS/ZnS core/shell QDs shows impurity position-dependent emission properties. [15]

While electronic impurity doping in semiconductor QDs has been achieved for a multitude of systems, with appreciable effort going into studies involving CdSe; relatively little effort has been directed towards the Pb-chalcogenides. Electrical measurements have been made on films of PbSe lightly-doped with Ag^+ to determine that Ag+ is in fact an electronically active impurity[13], however, optical properties have not been explored in any depth. In this study we report intentionally electronic impurity doping of PbSe QDs with a variety of heterovalent cations and the resulting changes to the semiconductor optical properties. We observe the efficiency of select cations to diffuse and become incorporated into (or onto) the nanocrystal lattice both in solution as well as in QD films. Subsequent absorbance measurements show a characteristic bleach of the 1^{st} exciton transition for the incorporation of heterovalent cations and a concurrent size-dependent low-energy absorbance (in the case of Ag^+ doping), which we believe can be attributed to the intraband transition seen previously only in electrochemically- and remotely-doped QD samples.

4.II. Materials and Methods

All chemicals were used as received without further purification. Selenium (99.99%), silver nitrate (99+%), teterakis(acetonitrile)copper(I)hexafluorophosphate, indium(III) acetylacetonate, (99.99+%), potassium nitrate(99.999%), iron nitrate nonohydrate (99.999%), sodium nitrate (99.0+%), aluminum nitrate nonahydrate (99.997%), gold chloride, oleic acid (90%), diphenylphosphine (DPP, 98%), trioctylphosphine (TOP, 90%), anhydrous ethanol, methanol, hexane and

tetrachloroethylene (TCE 99.9%) were purchased from Aldrich and used as received. Lead oxide(99.999%) was purchased from Alfa Aesar.

PbSe QDs were prepared following previously published procedures. [18] QDs were washed 2X using hexane/ethanol as the solvent/non-solvent pair, and were stored in a glovebox as a dry powder. Subsequently, all work was performed under air-free conditions.

4.II.a. Solution Doping of PbSe QDs

For solution doping of PbSe QDs, the concentration of dopant atoms added was based on an estimation of the total starting Pb content. As an estimate of the Pb content per solution, PbSe QDs were treated as perfectly spherical and completely stoichiometric. Since we know PbSe QDs to be Pb-rich [19-21], the values for Pb content obtained using this approximation will be artificially low. QD diameters were determined using absorption spectroscopy. [22] In order to calculate the total number of atoms/QD for a spherical nanoparticle, the volume of the QD $\left(\frac{4}{3}\pi r^3\right)$ should be divided by the volume of a unit cell for a rocksalt crystal structure, a^3, (where a is the lattice constant) and multiplied by the number of atoms/unit cell (8). [20] The total number of QDs is determined using Beer's law and a known molar extinction coefficient for PbSe at 400 nm where the absorption cross-section shows no size or shape dependence. [22] Given an average QD size from the absorption spectrum, an approximate number of Pb atoms/sample was determined. Typically dopant atoms were added at concentrations between 1% and 25% (in some

extreme cases up to 50%) of the estimated total of Pb, though the true amount of dopant atom incorporated into the sample is always much less than half of this estimation as confirmed by elemental analysis. For a typical treatment, a minimum volume of cation precursor solution (10-20 μL dissolved in ethanol or methanol) is added to QDs dispersed in hexane (~5mL) under vigorous stirring. Treated nanoparticles are allowed to sit in dopant-containing solution for ~10 min and are then precipitated using ethanol to remove any excess dopant, and the QDs are resuspended in hexane.

4.II.b. Doping Films of PbSe QDs

QD films were prepared by dropcasting PbSe nanoparticles from hexane solution (~5-10 mg/mL) onto 1 inch round 1 mm thick Si substrates, which are silent in the IR regions of interest. Films were subsequently treated in a 2mM solution of ethanedithiol (EDT) in acetonitrile to remove oleic acid surface ligands, which have broad peaks in the IR. Films were sealed in a copper gasket with an O-ring between a second Si window. Doping was performed by preparing solutions of a given dopant precursor containing up to 100% impurity atoms (as estimated from the amount of QDs added to the film) in either methanol or ethanol. Films were then allowed to soak for increasing time intervals typically starting at a single dip and proceeding at small steps as the 1st exciton transition begins to bleach.

4.II.c. Characterization

Optical absorption data was collected on a Shimadzu UV-3600 spectrophotometer. High-resolution transmission electron microscopy (TEM) characterization was performed on a Philips CM200 Transmission Electron Microscope at 120 kV. Fourier transform infrared (FTIR) absorbance spectra were recorded on a Thermo-Nicolet 6700 FTIR spectrometer in transmission mode with a resolution of 4 cm^{-1}. Photoluminescence quantum yields (PLQYs) were measured on solution-QD samples dispersed in TCE using a LabSphere integrating sphere, with excitation provided by NIR-LEDs (emitting at 950). The emission and excitation spectra were fiber coupled to the emission monochromator of the fluorescence spectrometer and measured with a two-stage thermocouple-cooled InGaAs photodiode. The excitation LED is driven by a 15V square wave at 25 Hz using a Stanford Research Systems (SRS) DS335 function generator. The resulting InGaAs signal was amplified using a SRS SR530 lock-in amplifier, and spectra were corrected for detector efficiencies using a calibrated lamp. Solid-state ^{77}Se NMR experiments were performed on a 200 MHz Bruker DSX NMR Spectrometer, and electron paramagnetic resonance experiments were performed on a Bruker ESR. Elemental analysis on doped QDs was performed using inductively coupled plasma mass spectrometry on an Agilent 7700 ICP-MS.

4.III. Results and Discussion

4.III.a. Doping with Cu^+, Ag^+, and In^{3+}

Cu^{+}, Ag^{+}, and In^{3+} dopants were chosen for a first pass at doping PbSe QDs. There is already precedence in the literature for effective doping of PbSe by Ag^{+} [13], and Cu^{+} is known to readily undergo cation exchange with Pb^{2+} in PbSe QDs. [23] If one envisions atoms within the PbSe NC as being neutral, then both Cu and Ag, with one less valence electron than Pb, would be expected to dope PbSe QDs p-type (providing for an acceptor level near the PbSe valence band) if the atoms dope PbSe substitutionally. If the atoms dope PbSe interstitially, then the addition of their single valence electron into the crystal lattice would render Ag and Cu n-type dopants (providing a donor level near the conduction band.) Early studies of Ag doping of CdSe QDs show that at low concentrations, Ag behaves as an interstitial dopant (n-type), while heavy doping results in substitution of Ag for Pb in the lattice (p-type). [12]

PbSe QDs were first doped using a solution containing Cu^{+}. Upon varying the doping concentration for 5.6 nm PbSe QDs a marked change was first observed in the absorption spectrum. As the dopant concentration is increased, the 1^{st} exciton absorption undergoes a noticeable bleaching affect as shown in Figure 4.2.

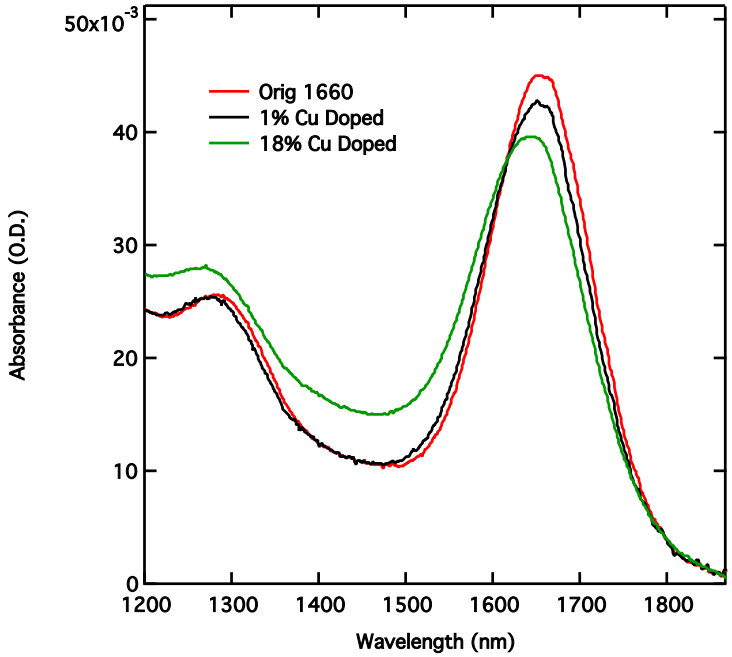

Figure 4.2. Absorbance Spectra for Cu(I)-Doped 5.6 nm PbSe QDs
Absorbance spectra for PbSe QDs doped at 1% and 18% from solutions of methanolic Cu(I) showing an increasing 1st exciton bleach as a function of the amount of dopant solution added. A small blue shift is also observed at the highest dopant concentration.

Alongside the decrease in absorption intensity there is also a small but noticeable blue shift in the 1st exciton peak of ~5 nm for the 1% doped sample and 12 nm for the 18% doped sample. As these particles were not exposed to oxygen at any point during processing, oxidation was ruled out as a cause for the observed blue shift. Mocatta et al. modeled the effects of impurity doping on the electronic properties of strongly confined dopants in QDs. [14] They predict shifts in the QD-bandgap based on phenomena observed upon doping bulk semiconductors. For both n- and p-type doping, shifts in the bandgap of bulk semiconductors are observed due to appearance of tail states (Urbach tails) in the bandgap. These tail states arise from the introduction of disorder in the crystal structure with addition of dopant atoms. Their calculations predict that a red-shift should be observed at

low dopant concentrations, with a turnover to a high energy blue-shift with increasing impurity density. Their model predicts that the turnover concentration is dependent on the ratio of the range of impurity interactions a and the QD size R. As the ratio of a/R increases, the earlier the onset of this blue-shift is observed, predicting in the case of Cu-doped InAs QDs (p-type dopant), a red-shift would not be observed at all. Finally the absolute PLQY for 1% and 10% Cu addition were measured, resulting in a drop in PLQY up to 84% for the 10% doped samples as compared to the original QDs. This drop in PLQY is indicative of some surface addition of Cu to the PbSe QDs creating new traps that preclude efficient exciton recombination. TEM images of Cu-doped PbSe nanoparticles (Figure 4.3) show significant flocculation of the particles, which is suggestive of surface addition of Cu without sufficient passivation from oleic acid.

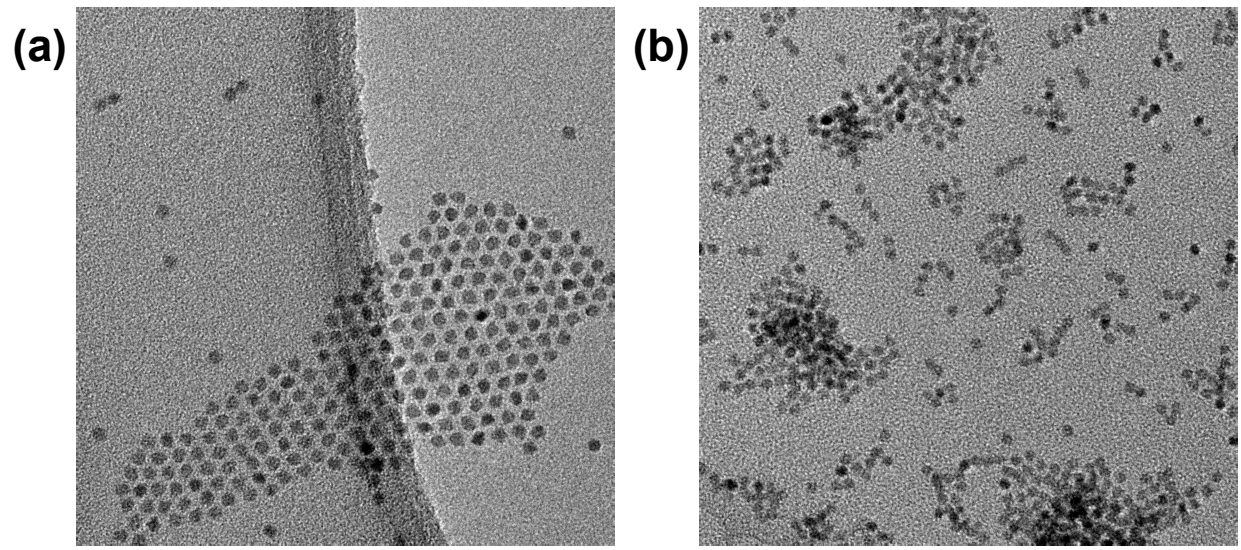

Figure 4.3. TEM of 20% Cu(I) Doped PbSe QDs
(a) PbSe QDs before undergoing electronic impurity doping with Cu(I) appear well passivated in an ordered array. **(b)** Following treatment with methanolic Cu(I) solution, while the QDs maintain their overall quasi-spherical shapes, changes to the QD surface upon treatment has lead to aggregation on the TEM grid.

In order to investigate the a/R dependence proposed by Mocatta et al., a QD size-dependent experiment was performed for Cu-doped PbSe. Both 4.1 nm and 5.6 nm QDs were doped from 1-50% as shown in Figure 4.4. In these spectra the absorbance shifts observed in the 1st exciton peak, however slight, appear to exhibit the opposite behavior as a function of size. The smaller 4.1 nm QDs shift red as a function of dopant concentration, while the larger 5.6 nm QDs shift to the blue. Discrepancies in our data with the models predicted by Mocatta et al. suggest that alternative explanations lie at the heart of the observed spectral shifts in our system, which will be discussed in further detail later in this chapter.

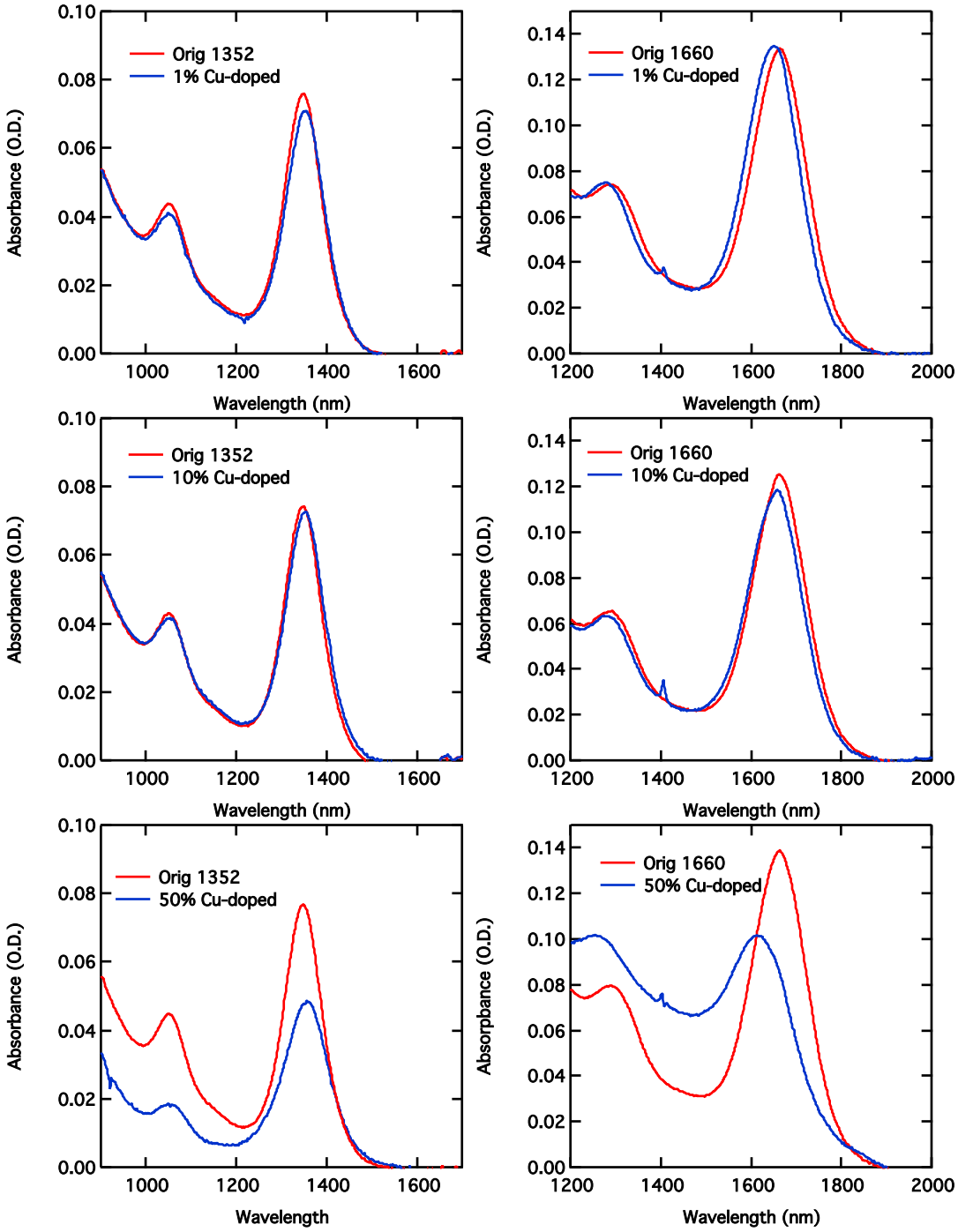

Figure 4.4. Size Dependent Cu(I)-Doping of PbSe QDs
Absorbance spectra for systematic doping of two sizes of PbSe QDs: 4.1 nm (1352 nm 1st exciton) and 5.6 nm (1660 nm 1st exciton). As the amount of dopant input into the system increases, both a bleach and a shift in the 1st exciton peak are observed. 4.1 nm QDs experience a red shift while 5.6 nm QDs undergo a blue shift of the 1st exciton peak.

Similar decreases in the 1st exciton transition for Ag-doped QDs was also observed as shown in Figure 4.5.

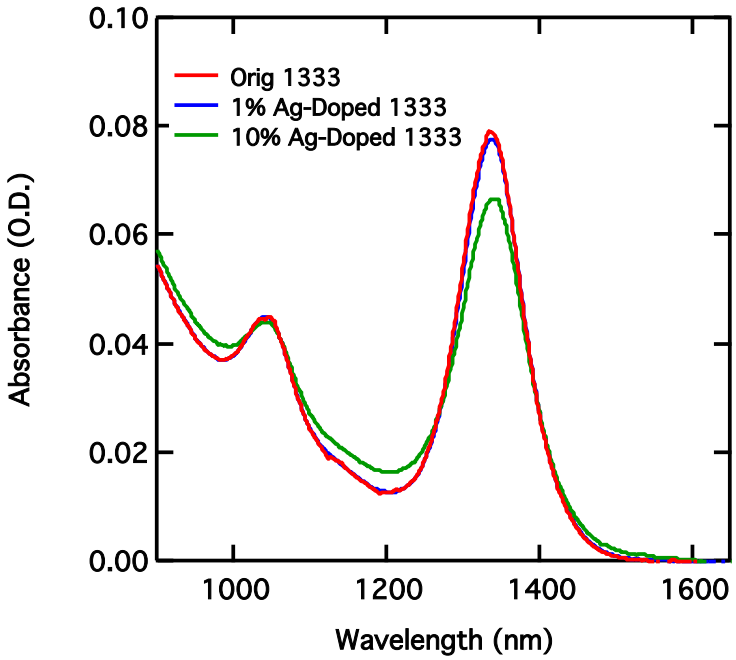

Figure 4.5. Absorbance spectra for Ag(I)-doped 4 nm PbSe QDs
Absorbance spectra for PbSe QDs doped at 1% and 10% from solutions of ethanolic Ag(I) showing an increasing 1st exciton bleach as a function of the amount of dopant solution added. The 1st exciton transition remains centered at 1333 nm.

In contrast to the Cu doping experiments presented in Figure 4.2, significant decreases in the first exciton for Ag doping are not observed until the number of Ag dopants added reaches 10% (of the estimated number of Pb atoms). This could speak to the relative ease with which Ag diffuses into PbSe QDs as compared to Cu, under the same time constraints, or it may suggest that the QDs reach a thermodynamic equilibrium with the surrounding Ag-containing solution. ICP data presented later in the chapter may provide support for

the former supposition. 10% doping with Ag atoms gives rise to a 42% decrease in the absolute PLQY, again suggesting that some percentage of the dopant are adding to the QD surface and contributing trap states. A shift in the 1st exciton peak is not observed for the addition of Ag atoms to PbSe QDs. It is worth noting here, that in the lightly-doped regime, Sahu et al. observed neither spectral shifts nor a decrease in the absorbance of the 1st exciton peak upon addition of Ag dopants to CdSe, though elemental analysis did confirm the presence of Ag.[12]

Finally, for the addition of an In^{3+} precursor, no significant changes are observed to the absorbance spectrum (Figure 4.6). For In, doping levels as high as 25% failed to show a significant spectral response for the 1st exciton transition. The absolute PLQY for In doped QDs showed only a 15% decrease for 10% doped QDs. Comparing these values to those obtained for the addition of both Ag and Cu atoms, this suggests that neither diffusion of In atoms into PbSe nor surface addition are as efficient for this cation as it is for the previous two.

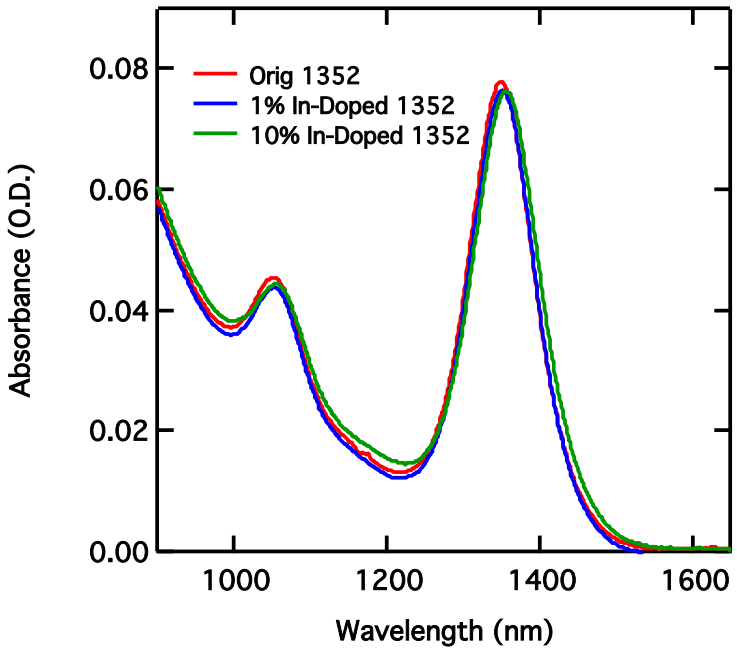

Figure 4.6 Absorbance Spectra for In-Doped 4.1 nm PbSe QDs
Absorbance spectra for PbSe QDs doped at 1% and 10% from solutions of ethanolic In(III) showing no discernable bleach of the 1st exciton peak as a function of dopant atom input.

To confirm our suspicions regarding cation diffusion, elemental analysis data was collected for the 3 cations under study. A plot of cation input vs. actual cation percentage as measured by ICP is shown in Figure 4.7.

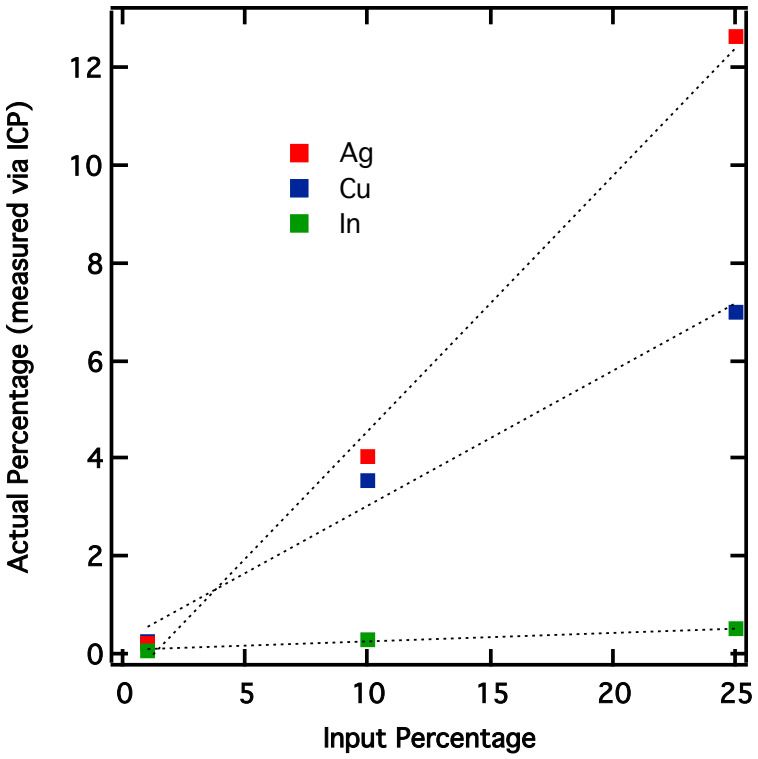

Figure 4.7 Doping Efficiency for Ag, Cu, and In impurities
A plot of the dopant content *vs* the actual input percentage are shown at 3 different input concentrations (1%, 10%, and 25%) for 5.7 nm PbSe QDs. Ag(I) impurities are most affective at incorporating into the QD lattice while In(III) was least likely to either diffuse or adhere to the QD surface.

Interestingly it appears that Ag is the most efficient at adding to our PbSe QDs. Recalling that the PLQYs obtained for 10% addition of Ag and Cu atoms showed decreases of 42% and 84% respectively, this data, in conjunction with the elemental analysis, suggests that Ag is actually penetrating the interior of the QD more efficiently than Cu as well. It should be noted that for each of these cases, the amount of impurity atom input into the system is always higher than that which actually incorporates into the QD. At most, the doping efficiency observed is about 50%, as seen for Ag. It is not surprising that In appears to diffuse almost not at all into the QD. In light of the 15% decrease in the absolute PLQY at

10% dopant addition, what little In does incorporate, is most probably only sitting at the QD surface.

In order to further probe the origin of both the 1st exciton bleach as well as the spectral shifts to lower energies, observed for the case of Cu doping, a control experiment was performed using an isovalent cation, Cd^{2+}. As shown in Figure 4.8, addition of methanolic solutions of Cd^{2+} at 10% and 25% doping levels does not return a 1st exciton bleach.

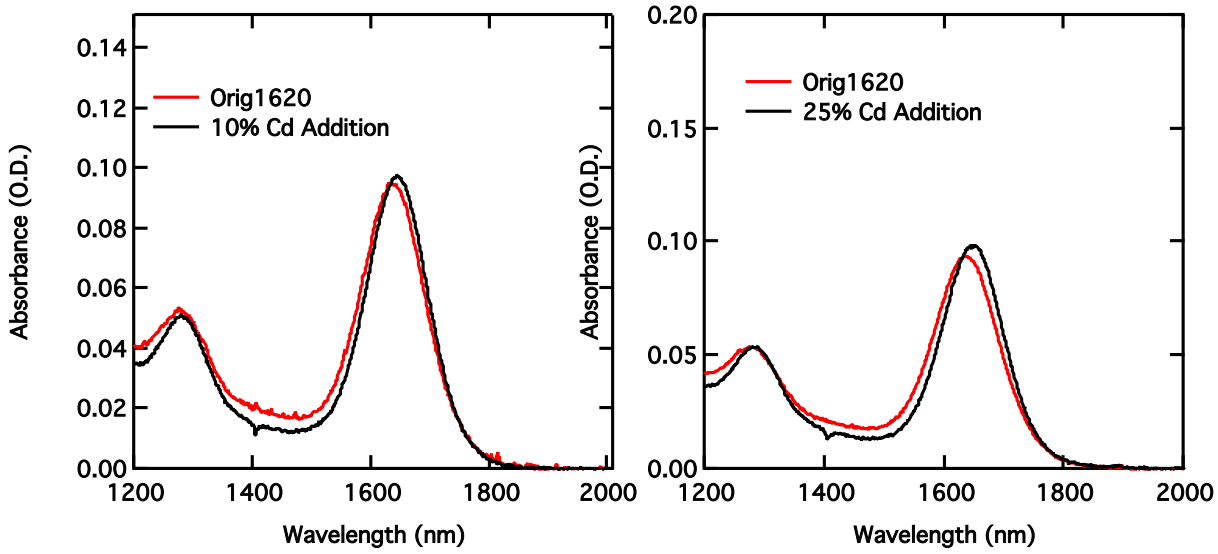

Figure 4.8. Doping Control Experiment Using Isovalent Cd(II)
Minimum volumes of 10% and 25% methanolic Cd(II) are injected into solutions containing to 5.4 nm PbSe QDs in TCE, and the subsequent absorption spectra show no bleach of the 1st transition, though a slight blue shift is observed. (Equivolume solutions containing only TCE and the corresponding amounts of methanol were subtracted from each spectrum.)

In this case the doped samples appear to have a slightly higher absorbance at the 1st exciton peak than the undoped samples, however, integration shows the peak areas to be

the same. These experiments were performed by in-situ injection of Cd^{2+} dopants in a minimal volume of methanol to the cuvette used for measurement. This ensures that changes to the first exciton peak are not a result of incomplete transfer of QD solution, and absorption artifacts due to μL additions of methanol were removed from the background. To this point, therefore, a change in the 1st exciton peak intensity is only seen as a result of successful addition of heterovalent impurities. A small shift in the 1st exciton is observed, however, following addition of the methanolic Cd^{2+} solution. Using the same method of in-situ addition and measurement, kinetics experiments allowed us to see the gradual red-shift in this peak over time. In light of the Mocatta predictions, we concluded that this shift could either be due to the introduction of disorder into the system (causing Urbach tailing) or it occurs as a result of methanol addition. Control experiments using only methanol in the absence of impurity atoms suggest that the solvent alone is responsible for the red shifts observed in these spectra, though the possibility remains that the blue shift initially observed for Cu^{+} doping may be a result of band tailing effects. We also attempted to reverse the doping process by reintroduction of a Pb^{2+} precursor to our system following Cu^{+} doping. Upon addition of an excess of $Pb(oleate)_2$, the 1st exciton peak recovers completely suggesting that the bleach observed for our doped QDs is in fact a direct result of introducing impurity atoms (Figure 4.9). However, after the initial decrease following doping, the PLQY does not recover upon $Pb(oleate)_2$ treatment.

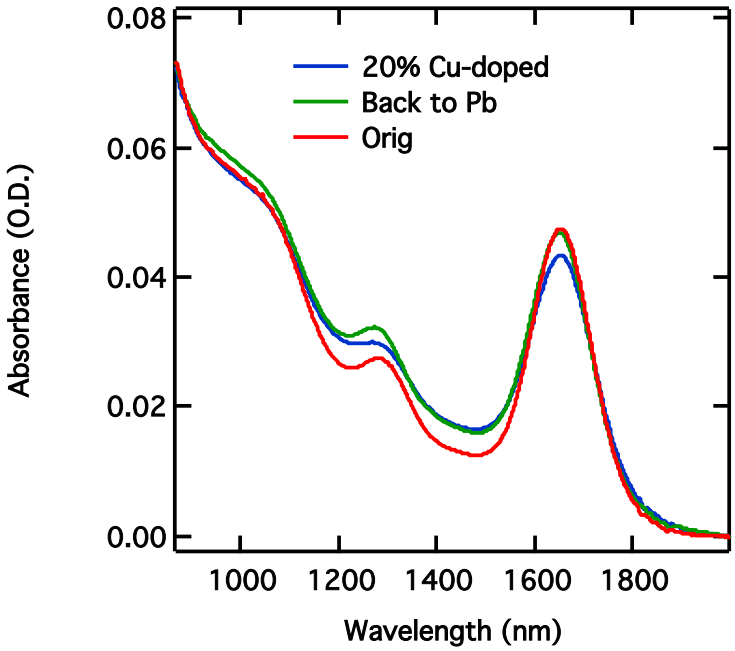

Figure 4.9. Reversible Cu(I) Doping of 5.7 nm PbSe QDs
Following 20% Cu(I) input to 5.7 nm PbSe QDs, an excess of $Pb(oleate)_2$ results in a return to the original, pre-doping optical density of the 1st exciton peak, presumably displacing all impurity Cu(I) atoms with Pb(II) by mass action.

4.III.b. FT-IR

Infrared absorption spectroscopy was employed to probe the origin of the observed 1st exciton bleach. Previous studies using both electrochemical and remote doping[8,9] techniques have reported a similar bleach to the 1st exciton transition as those observed in this study. These literature reports have found, however, that the 1st exciton bleach is concurrent with a broad absorption in the IR corresponding to an intraband transition within the QDs. The bleach of the 1st exciton transition arises as a result of introducing additional carriers from dopant impurities into the conduction or valence band, which then prevents some absorption into the first excited state. The intraband absorption is then the absorption of these additional carriers from $1S_e$ to $1P_e$ state in the case of an n-type dopant,

or from the $1S_h$ to the $1P_h$ for a p-type dopant. A rough estimate of the predicted intraband absorption energies plotted as a function of bandgap is shown in Figure 4.10 where it is approximated that the $m_e \approx m_h$ in PbSe, so that these transitions would occur at nearly the same energies for electron and hole. [18]

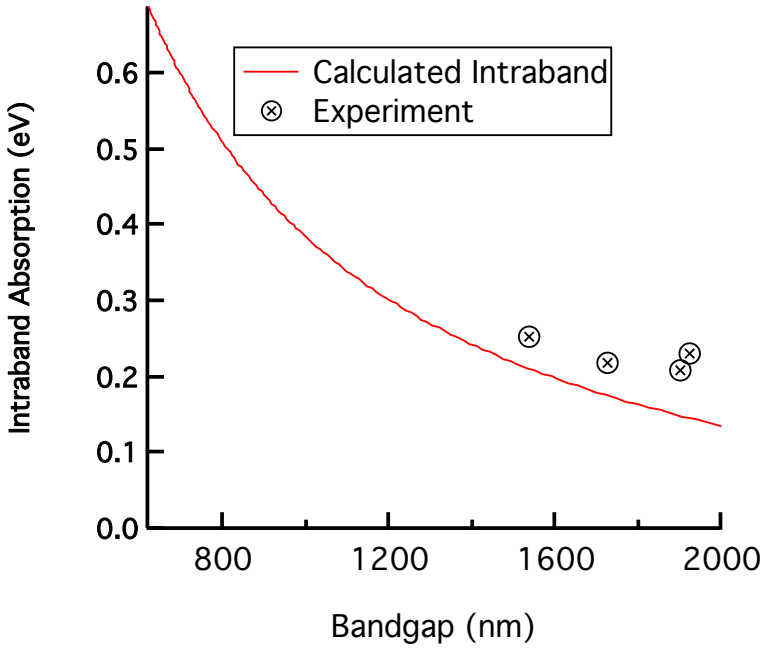

Figure 4.10. Calculated and Experimental Intraband Absorption
The calculated intraband absorption as a function of bandgap is plotted alongside the experimental data for Ag(I) doped PbSe QDs at various sizes. The experimental data trend is offset to higher values for the intraband absorption than the values approximated in the calculated spectrum.

The IR spectrum of 6 nm Ag-doped PbSe QDs is shown below in Figure 4.11a. A clear but broad absorbance is observed to grow in around 2000 cm^{-1} or 0.25 eV as a function of time spent in the dopant solution. We assign this absorption to our intraband transition, which becomes more pronounced as the impurity concentration in the film

increases. Simultaneously, the 1st exciton transition undergoes bleaching, which appears to occur in a 1:1 fashion with the new absorption feature (see Figure 4.11b).

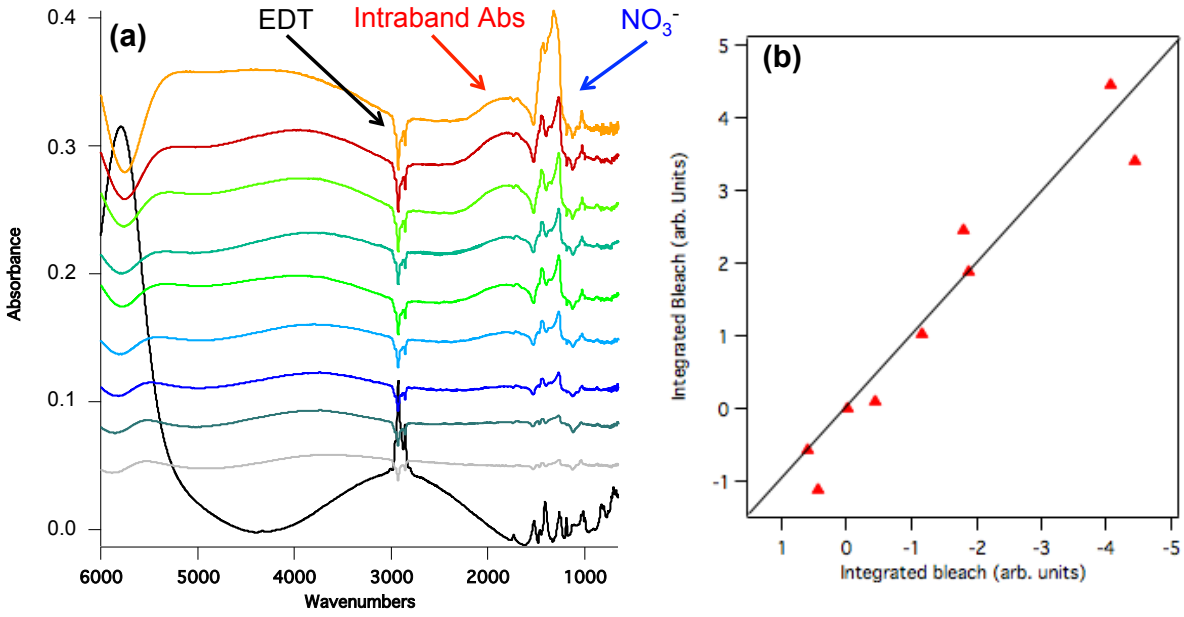

Figure 4.11. Intraband Absorption and 1st Exciton Bleach for 6 nm PbSe QDs
(a) The FTIR spectra for 6 nm PbSe QDs doped with Ag(I) shows the gradual appearance of a low-energy, intraband absorption peak. **(b)** The integrated area of this peak matches that of the apparent 1st exciton bleach in a 1:1 fashion.

Since our first data point does not fall exactly on the curve for the estimated intraband (Figure 4.10), additional QD sizes were also probed. Our experimental data points appear to follow a similar shape trend as the curve for the calculated intraband, and a size dependence was revealed for its appearance. Note that as the QD diameter is increased, the exact position of the intraband absorption peak becomes difficult to discern due to the presence of the counterion (NO^{3-}) absorption stretches. The intraband, while present in all samples studied above 5 nm, is no longer observed for samples smaller than 4.6 to 5 nm. The size-dependent appearance of the intraband transition, while unclear, does serve to

dismiss some uncertainties about the source of this broad infrared absorbance for Ag-doped PbSe nanoparticles. Literature reports the size-dependent absorbance spectrum for Ag_2Se to be in the general region where we have observed our intraband. [24] While the 1st energy transitions of Ag_2Se give rise to sharper excitonic features than our broad absorbance at 0.25 eV, the disappearance of this absorption entirely at a QD diameter of ~5 nm further supports our hypotheses that we are in fact seeing an intraband absorption and not simply converting our particles to Ag_2Se via cation exchange. XRD data for treated films (not shown here) reveals peaks for both PbSe and the $AgNO_3$ precursor, but it is without clear signatures for crystalline Ag_2Se in either it's tetrahedral or orthorhombic phases.

Subsequent IR studies with Cu^+ and In^{3+} failed to show evidence for an intraband transition at any QD size. This did not come as a surprise in the case of In^{3+} as no significant bleach of the 1st exciton transition was observed. The lack of an intraband for samples doped with Cu was less clear, and this system required further investigation.

4.III.c Magnetic Resonance Spectroscopy on Cu-Doped Samples

In order to further investigate properties of samples doped with Cu impurities, both nuclear magnetic resonance (NMR) and electron paramagnetic resonance (EPR) spectroscopies were employed. Both of these techniques have the potential for probing different aspects of our doped nanocrystals. Solid-state ^{77}Se NMR can give important information about the chemical environment surrounding our native Se atoms in PbSe QDs, and EPR can help us to probe the oxidation state and position of the added impurity atoms.

There is precedence for utilizing EPR spectroscopy to discern surface impurities from impurities encapsulated within the QD for the addition of paramagnetic atoms. [25] Additionally, any changes to the observed magnetic resonance spectra as a result of changing the electron density within our nanoparticles was also of interest. The EPR spectrum for 5.4 nm Cu doped PbSe is shown in Figure 4.12.

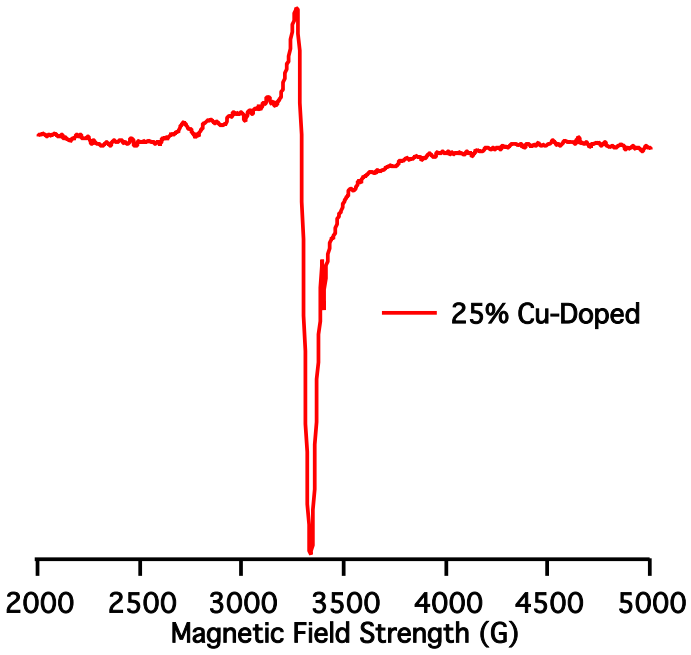

Figure 4.12. EPR Spectrum for Cu(I) Doped PbSe QDs
The EPR spectrum of 5.4nm QDs doped with Cu(I), an EPR silent dopant atom, indicate the presence of Cu(II) species. The presence of Cu(II) points towards low levels of oxidation, or in-situ redox chemistry taking place at the QD/dopant interface.

The EPR spectrum closely resembles the signature spectrum of Cu^{2+} indicating one of two possibilities: (1) Cu^{+} is undergoing redox chemistry with the QD by donating electron density into the nanoparticle to become Cu^{2+}, or (2) this may suggest that even slight oxygen exposure of the doped QDs results in oxidation of Cu^{+} to Cu^{2+}. The latter would

result in Cu entering the QD as an isovalent impurity and may be a contributing factor for the lack of an observed intraband transition. Solid-state ^{77}Se NMR was performed in order to determine if a change in the electronic environment of Se atoms could be discerned following effective cation exchange with the Pb. Due to very slow T_1 relaxation times, solid state ^{77}Se NMR experiments were run for several days at a time, with the resulting signal-to-noise still appearing very large. Representative NMR spectra are shown in Figure 4.13 for undoped and doped 5.4 nm PbSe QDs. The undoped QDs exhibit a double peak most probably due to the two chemically distinct Se atoms, at both the surface and in the interior of the QD. While the signal to noise makes any line broadening due to a change in electron density impossible to discern, it is apparent that as a result of Cu doping, the ^{77}Se signal goes from a split peak or a doublet to what appears to be a singlet with even less resolution. This result is likely due to Cu passivation of Se sites near the QD surface. Interior Se atoms still feel nearest neighbor Pb atoms, though this signal is presumably lower as a result of Se atoms that now see Cu dopants in the lattice.

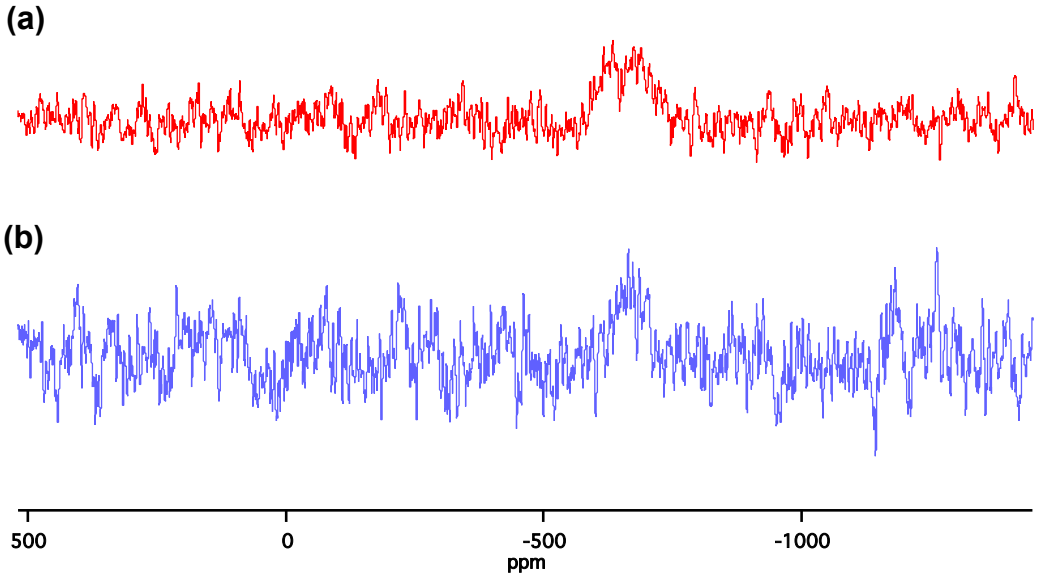

Figure 4.13. ^{77}Se NMR Spectra for Undoped and Cu(I)-Doped PbSe QDs
The solid-state ^{77}Se NMR spectra for 5.4 nm PbSe QDs shows **(a)** a doublet in the undoped sample becoming **(b)** a singlet in the Cu-doped nanoparticles. If two separate populations gave rise to the doublet Se signal in the undoped QDs, then the singlet observed following Cu doping suggests a decrease in one of these subpopulations.

4.III.d. Doping with other cations

Subsequent doping experiments were performed with a number of additional heterovalent cations including: K^+, Fe^{3+}, Na^+, Al^{3+} and Au^{3+}. Though some of these cations exhibit a decrease in the magnitude of the 1st energy transition, as of yet, few exhibit a clearly visible intraband absorption peak. Representative spectra for those that effectively bleach the 1st exciton transition but do not show an intraband absorption are shown in Figure 4.14.

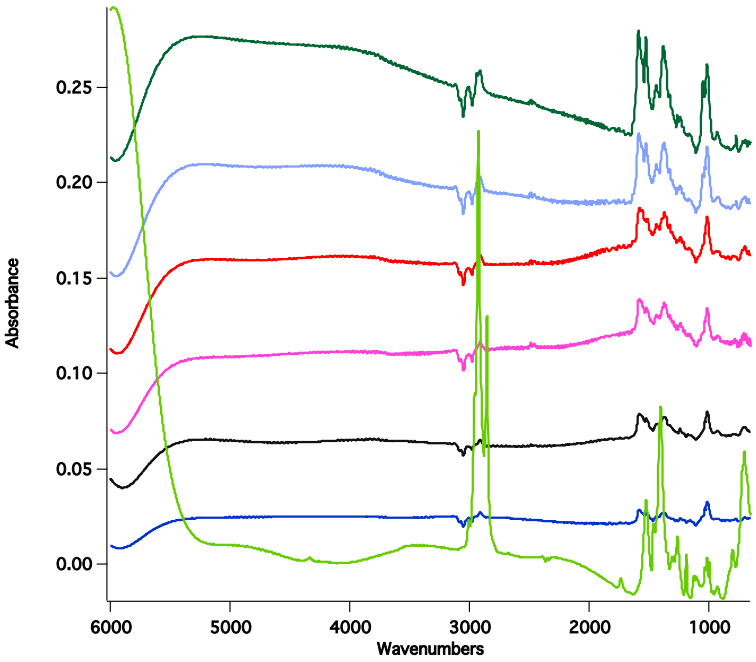

Figure 4.14. FT-IR Spectra for In(III)-Doped PbSe QDs
Representative data for a cation that did not show a significant intraband absorption. It should be noted that long soak times in saturated solutions of ethanolic In(III) precursor were necessary to induce decreases in the 1st exciton peak.

4.IV. Conclusions

PbSe QDs have been doped with a serial of different impurity cations, many of which have resulted in an effective bleach of the 1st exciton transition. For Ag impurities, this bleach is concurrent with a low energy absorbance (intraband absorption) indicative of additional carriers in the 1S state. The size dependent occurrence of this intraband transition, and the lack thereof for additional dopants, leaves some uncertainty regarding the mechanism of doping in PbSe QDs and will require further study particularly of how the electronic properties are affected by impurity doping. Following addition of heterovalent impurities, values for the absolute PLQYs decrease indicating that the addition of dopant

cations is, at least in part, to the QD surface, producing surface related defects/trap levels. In the case of Cu impurities this effect seems to be amplified as TEM analysis shows that the QDs begin to aggregate due to insufficient surface passivation, and the drops in the PLQY are most significant for these samples. For samples in which an insignificant amount of dopant diffuses into the QD, no subsequent changes were observed spectroscopically at low doping levels.

References

(1) Buonsanti, R.; Milliron, D. J.,Chemistry of Doped Colloidal Nanocrystals. *Chemistry of Materials* **2013**, *25*, 1305-1317.

(2) Norris, D. J.; Efros, A. L.; Erwin, S. C.,Doped nanocrystals. *Science* **2008**, *319*, 1776-1779.

(3) Turnbull, D.,Formation of Crystal Nuclei in Liquid Metals. *Journal of Applied Physics* **1950**, *21*, 7.

(4) Mikulec, F. V.; Kuno, M.; Bennati, M.; Hall, D. A.; Griffin, R. G.; Bawendi, M. G.,Organometallic synthesis and spectroscopic characterization of manganese-doped CdSe nanocrystals. *Journal of the American Chemical Society* **2000**, *122*, 2532-2540.

(5) Dalpian, G. M.; Chelikowsky, J. R.,Self-purification in semiconductor nanocrystals. *Physical Review Letters* **2006**, *96*.

(6) J.D., B.; Gamelin, D. R. *Doped Semiconductor Nanocrysatals: Synthesis, Characterization, Physcial Properties and Applications*, 2005; Vol. 47.

(7) Erwin, S. C.; Zu, L. J.; Haftel, M. I.; Efros, A. L.; Kennedy, T. A.; Norris, D. J.,Doping semiconductor nanocrystals. *Nature* **2005**, *436*, 91-94.

(8) Engel, J. H.; Surendranath, Y.; Alivisatos, A. P.,Controlled Chemical Doping of Semiconductor Nanocrystals Using Redox Buffers. *Journal of the American Chemical Society* **2012**, *134*, 13200-13203.

(9) Shim, M.; Guyot-Sionnest, P.,N-type colloidal semiconductor nanocrystals. *Nature* **2000**, *407*, 981-983.

(10) Wehrenberg, B. L.; Yu, D.; Ma, J. S.; Guyot-Sionnest, P.,Conduction in charged PbSe nanocrystal films. *Journal of Physical Chemistry B* **2005**, *109*, 20192-20199.

(11) Yu, D.; Wang, C. J.; Guyot-Sionnest, P.,n-type conducting CdSe nanocrystal solids. *Science* **2003**, *300*, 1277-1280.

(12) Sahu, A.; Kang, M. S.; Kompch, A.; Notthoff, C.; Wills, A. W.; Deng, D.; Winterer, M.; Frisbie, C. D.; Norris, D. J.,Electronic Impurity Doping in CdSe Nanocrystals. *Nano Letters* **2012**, *12*, 2587-2594.

(13) Kang, M. S.; Sahu, A.; Frisbie, C. D.; Norris, D. J.,Influence of Silver Doping on Electron Transport in Thin Films of PbSe Nanocrystals. *Advanced Materials* **2013**, *25*, 725-731.

(14) Mocatta, D.; Cohen, G.; Schattner, J.; Millo, O.; Rabani, E.; Banin, U.,Heavily Doped Semiconductor Nanocrystal Quantum Dots. *Science* **2011**, *332*, 77-81.

(15) Yang, Y.; Chen, O.; Angerhofer, A.; Cao, Y. C.,Radial-position-controlled doping in CdS/ZnS core/shell nanocrystals. *Journal of the American Chemical Society* **2006**, *128*, 12428-12429.

(16) Chen, D.; Viswanatha, R.; Ong, G. L.; Xie, R.; Balasubramaninan, M.; Peng, X.,Temperature Dependence of "Elementary Processes" in Doping Semiconductor Nanocrystals. *Journal of the American Chemical Society* **2009**, *131*, 9333-9339.

(17) Pandey, A.; Brovelli, S.; Viswanatha, R.; Li, L.; Pietryga, J. M.; Klimov, V. I.; Crooker, S. A.,Long-lived photoinduced magnetization in copper-doped ZnSe-CdSe core-shell nanocrystals. *Nature Nanotechnology* **2012**, *7*, 792-797.

(18) Murphy, J. E.; Beard, M. C.; Norman, A. G.; Ahrenkiel, S. P.; Johnson, J. C.; Yu, P. R.; Micic, O. I.; Ellingson, R. J.; Nozik, A. J.,PbTe colloidal nanocrystals: Synthesis, characterization, and multiple exciton generation. *Journal of the American Chemical Society* **2006**, *128*, 3241-3247.

(19) Hughes, B. K.; Ruddy, D. A.; Blackburn, J. L.; Smith, D. K.; Bergren, M. R.; Nozik, A. J.; Johnson, J. C.; Beard, M. C.,Control of PbSe Quantum Dot Surface Chemistry and Photophysics Using an Alkylselenide Ligand. *ACS Nano* **2012**, *6*, 5498-5506.

(20) Moreels, I.; Lambert, K.; De Muynck, D.; Vanhaecke, F.; Poelman, D.; Martins, J. C.; Allan, G.; Hens, Z.,Composition and size-dependent extinction coefficient of colloidal PbSe quantum dots. *Chemistry of Materials* **2007**, *19*, 6101-6106.

(21) Smith, D. K.; Luther, J. M.; Semonin, O. E.; Nozik, A. J.; Beard, M. C.,Tuning the Synthesis of Ternary Lead Chalcogenide Quantum Dots by Balancing Precursor Reactivity. *ACS Nano* **2011**, *5*, 183-190.

(22) Dai, Q.; Wang, Y.; Li, X.; Zhang, Y.; Pellegrino, D. J.; Zhao, M.; Zou, B.; Seo, J.; Wang, Y.; Yu, W. W.,Size-Dependent Composition and Molar Extinction Coefficient of PbSe Semiconductor Nanocrystals. *ACS Nano* **2009**, *3*, 1518-1524.

(23) Luther, J. M.; Zheng, H.; Sadtler, B.; Alivisatos, A. P.,Synthesis of PbS Nanorods and Other Ionic Nanocrystals of Complex Morphology by Sequential Cation Exchange Reactions. *Journal of the American Chemical Society* **2009**, *131*, 16851-16857.

(24) Sahu, A.; Khare, A.; Deng, D. D.; Norris, D. J.,Quantum confinement in silver selenide semiconductor nanocrystals. *Chemical Communications* **2012**, *48*, 5458-5460.

(25) Kennedy, T. A.; Glaser, E. R.; Klein, P. B.; Bhargava, R. N.,Symmetry and Electronic-Structue of the Mn Impurity in ZNS Nanocrystals. *Physical Review B* **1995**, *52*, 14356-14359.

Chapter 5:
Conclusions

5.I. Manipulating Composition, Morphology and Surface Chemistry of Semiconductor Quantum Dots

Over the course of this research project, we have set out to enhance our understanding of the intricacies of QD growth, composition and surface chemistry. In this thesis it has been shown that the complex chemistry of semiconductor QDs lends itself to a great deal of tunable parameter space that allows for directed synthesis of interesting structures with unique photophysical properties. In Chapter 2, through manipulation of QD morphology, dimer structures have been prepared, which show spectroscopic features that have previously only been predicted in the literature, and never discussed in light of the absorption spectra for elongated quantum-confined structures. Mixed dimer systems have implications for studying light harvesting systems, and may prove an interesting material for both QD solar cells as well as find use in catalysis reactions.

Chapters 3 and 4 illustrate how changes to the morphology and chemical environment at the QD surface can play a role, not only in enhanced oxygen stability, but it also defines both doping levels and defect states present at the QD surface. A greater understanding of how to manipulate the QD composition, whether through surface

modifications or through the introduction of impurity atoms, will allow for tailoring of QD electrical properties, which will facilitate the use of semiconductor QDs in systems requiring p-n junctions. The consequence of increasing QD stability through directed surface modifications is that QDs become a more viable resource for use in a multitude of fields including solar photoconversion.

5.II. Outlook and Future Challenges

As the nanoscience field continues to grow, the bank of potential uses for these materials increases, and studies like those contained within this thesis become imperative for future understanding of how to maximize the efficiencies of semiconductor QDs for specific technologies. Each week brings new insights into the chemistry of semiconductor nanocrystals, new material combinations, and finer control over morphology, surface composition and structure. Nanocrystal syntheses are generally performed with simple, safe, and solution-phase procedures that can be widely replicated by a diverse set of scientists. The ability to incorporate these structures into novel functional solids is increasing at an encouraging rate and is a testament to the growing knowledge base of nanocrystal synthesis. In order for quantum-confined nanostructures to have the largest technological impact, we must continually seek to move beyond the basic challenges of reproducibility and growth mechanisms to a deeper understanding of obtaining precise control over nanocrystal formation that will enable further engineering of nanostructures with unique and desirable properties. In conclusion, with persistent ingenuity, imagination,

and dedication from researchers worldwide, the field of quantum-confined semiconductors will continue to have a bright and exciting future.